

ALMA MATER STUDIORUM - UNIVERSITÀ DI BOLOGNA

SCUOLA DI INGEGNERIA E ARCHITETTURA

DIPARTIMENTO DI INGEGNERIA INDUSTRIALE - DIN

CORSO DI LAUREA MAGISTRALE IN INGEGNERIA MECCANICA

TESI DI LAUREA

in

MECCANICA DELLE MACCHINE

**MECHATRONIC DESIGN SOLUTION
FOR PLANAR OVERCONSTRAINED
CABLE-DRIVEN PARALLEL ROBOT**

CANDIDATO:
Andrea Lucarini

RELATORE:
Prof. Ing. Edoardo Idà

CORRELATORI:
Prof. Ing. Marco Carricato
Ing. Federico Zaccaria

Anno accademico 2022/2023

Sessione II

Abstract

Cable-driven parallel robots (*CDPRs* in short) combine the successful features of parallel manipulators with the benefits of cable transmissions. The payload is divided among light extendable cables, resulting in an energy-efficient system that can achieve high end-effector acceleration over a huge workspace. From a structural point of view, a CDPR is formed by a set of actuation units, and a mobile platform, working as an end-effector (*EE* in short). The cables, driven by the actuation units, are guided inside the robot workspace using a guidance system and then connected to the mobile platform. The variation of cable lengths is responsible for the EE displacement throughout the robot workspace. These features result in easily reconfigurable systems where the workspace can be modified by relocating the actuation and guidance units. Nevertheless, the use of CDPRs in industrial environments is still limited, mainly due to the drawbacks of employing flexible cables. Indeed, cables impose unilateral constraints that can only exert tensile forces and, consequently, the EE cannot withstand any arbitrary external action. The highly non-linear behaviour of the cables complicates the control of the robot and the determination of the platform pose through direct kinematics. To enhance the robot's controllability, CDPRs can be overconstrained by employing a number of cables higher than the degrees of freedom of the EE. This allows cables to pull one against the other and to keep the overall system controllable over a wide range of externally applied loads.

In this thesis, an eight-cable, planar, overconstrained CDPR is designed: the robot should have the deployable and reconfigurable features required by the performing task. In particular, this CDPR has its actuation units directly installed into the EE mobile platform, and the frame anchor points can be rearranged in different ways to obtain a discrete reconfiguration. The cable arrangement, location of anchor points and mechanical design will be studied, by implementing a hybrid optimisation procedure able to find a suitable optimum design point. The genetic algorithm is combined with a local minimum optimiser, maximizing the CDPR volume index and deriving a mechanical design for the prototype that will be built inside the university laboratory.

The final objective of this thesis is to derive an optimal mechatronic design, suitable for a planar overconstrained CDPR. To this purpose, the first chapter will depict a general overview of CDPRs, describing their main advantages and disadvantages compared to other manipulators and the major fields of application, focusing in particular on the construction sector. Then, in the second chapter, the state of the art of reconfigurable and deployable CDPRs will be described to better highlight the main advantages of the proposed architecture. In the third section, a morphological matrix with possible actuation solutions will be presented and analyzed to choose the optimal design solution for the CDPR architecture, taking into account the cost constraint. In conclusion, the hybrid optimisation method will be evaluated: the cost function is obtained by implementing a wrench-feasible workspace computation, including advanced cable interference checks.

Contents

| | |
|--|-----------|
| Abstract | 3 |
| 1 Cable-Driven Parallel Robots | 7 |
| 1.1 Classification | 8 |
| 1.2 Fields of Applications | 10 |
| 1.2.1 Production Engineering | 11 |
| 1.2.2 Handling and Logistics | 11 |
| 1.2.3 Robotics in Construction | 12 |
| 1.2.3.1 Cleaning Task | 14 |
| 1.2.3.2 Painting Task | 16 |
| 1.2.3.3 Maintenance Inspection Task | 17 |
| 1.2.3.4 Modules Installation Task | 18 |
| 2 Design Peculiarities for CDPRs | 23 |
| 2.1 Reconfigurable CDPRs | 23 |
| 2.2 Deployable CDPRs | 27 |
| 3 Conceptual Design | 33 |
| 3.1 Actuation Unit for CDPR | 34 |
| 3.1.1 Rototranslating Winch | 35 |
| 3.1.2 Spooling-helper Winch | 36 |
| 3.1.3 Spline Winch | 36 |
| 3.2 Task Requirements | 37 |
| 3.3 Design solutions | 39 |
| 3.3.1 Frame Traslating Motor | 39 |
| 3.3.2 EE Spooling-helper Motor | 41 |
| 3.3.3 Eight EE Motors | 42 |
| 3.4 Morphological Decision Matrix | 43 |
| 4 Optimisation Algorithms for Mechanical Design | 47 |
| 4.1 Optimisation Algorithms | 48 |
| 4.1.1 Basic Optimisation Problem | 49 |
| 4.1.2 Local Optimum Algoirthm | 51 |
| 4.1.3 Genetic Algorithm | 53 |
| 4.2 Cost Function Definition | 55 |
| 4.2.1 Workspace Computation | 56 |
| 4.2.2 Cable Interference | 58 |
| 4.3 Optimisation Results | 60 |

| | |
|--|-----------|
| 5 Conclusions | 67 |
| Appendices | 71 |
| A In-depth Analysis of Robotics in Construction | 73 |
| A.1 Additive Manufacturing | 76 |
| B MATLAB Code for Cable Interference | 79 |
| C Details for the Workspace Solutions | 81 |
| C.1 First <i>ga</i> Design | 81 |
| C.2 Second <i>ga</i> Design | 82 |
| C.3 Third <i>ga</i> Design | 83 |
| C.4 Fourth <i>ga</i> Design | 84 |
| C.5 Final Optimal Design | 85 |
| D Mechanical Transmission Design | 87 |
| D.1 Drum and Servo-motor Design | 87 |
| Greetings | 91 |

Chapter 1

Cable-Driven Parallel Robots

Cable-driven parallel robots (*CDPRs*) belong to the large group of multi-body systems. This includes, besides robots, also other mechanisms with coupled motion of their bodies. Within the multi-body system, robots or manipulators are a subgroup designed to generate motion that a program can define. The norm ISO 8373 defining industrial robots states that a robot has at least three degrees of freedom, the motion generated by the robot is programmable, and the robot is universal concerning the application. Disregarding variants of kinematically redundant, over-, or under-actuated robots, the degree of freedom of the end-effector (*EE*) motion is equal to the number of actuators. In other words, in a nonsingular configuration, each actuator contributes a mostly unique part to generating the motion at the EE. Based on the topology, robots are subdivided into serial and parallel manipulators. Serial manipulators consist of joints and links where every articulated joint is actuated. Such mechanical structures are called open kinematic chains. If one connects more than one kinematic chain to the EE, the resulting mechanism is called a parallel robot. The robot is called fully parallel if the number of chains equals the number of actuators. *CDPRs* are a special kind of parallel kinematic machines or parallel robots.

A cable robot (Fig. 1.1) can be decomposed into a mobile platform (*MP*), a fixed machine frame, m cables attached to the MP on their distal end and attached to the machine frame on their proximal end. The lengths of the cables (and sometimes also

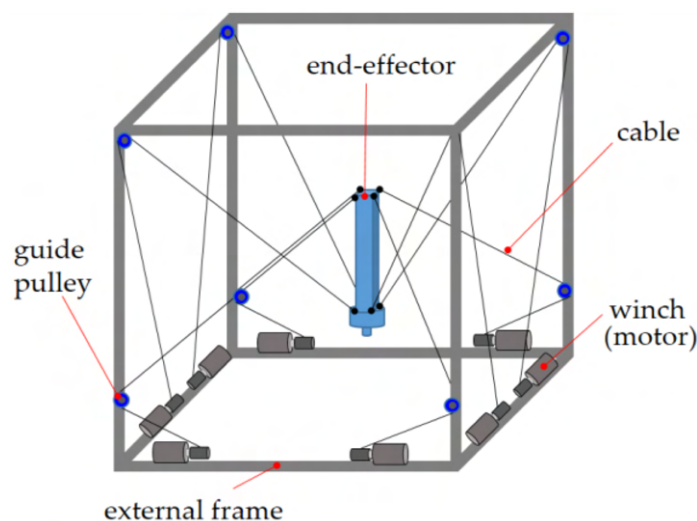


Figure 1.1: CDPR simple architecture

the positions where the cables are connected to the frame, creating a reconfigurable architecture) are changed by an actuation system called winch. Most robots' winches are fixed to the machine frame to simplify the electric connection with the power and control system. However, designs where the winches are located on the mobile platform were proposed, especially if the robot must be deployable.

Many cable robots use sensors to indirectly measure the effective length of the cables: through encoders on the drum or with a linear measurement system on a pulley tackle. The direct determination of the cable length is difficult to achieve practically. Alternatively, the position and orientation of the mobile platform are directly measured. For a couple of applications, it is also necessary to determine the tension in the cables. This is mainly done by force sensors connected to one end of the cable or to some pulleys in between. When using a winch with a drum, one can also measure the cable force with a torque sensor in the drive-train.

The mobile platform may broadly vary in its size. On the one hand, the platform may weigh some grams and dimensions of a couple of millimetres. Contrary, there are examples of massive platforms with a size of some dozens of meters and a weight of more than 800 tons. For cable robots, the most important properties of the platform are the relative location of the distal anchor points with respect to the reference point of the platform, the centre of gravity, the mass, and the inertia tensor.

The machine frame is the mechanical structure that carries the winches or the proximal anchor points. The machine frame is a closed framework structure made from steel or aluminium bars in many laboratory and industrial setups. Especially for larger robots, the winches might as well be attached to decentralized structures such as towers or buildings. Using winches or cables on multiple flying or swimming structures such as helicopters, balloons, ships, off-shore platforms, and submarines was proposed. Integrated cable robots use whatever is appropriate from the surrounding machinery or building as a supporting structure.

The cables can be made of different materials. The most widely used cable materials are steel and synthetic fibres such as high-modulus polyethylene fibre, aramid (kevlar), or polyester. However, other materials, such as hemp, can also be employed. Lately, smart cables with integrated electric wires have been proposed and used in prototypes to supply the mobile platform with electric energy or fieldbus signals.

1.1 Classification

The main classification of cable robots is done by defining the number of cables and the number of controllable degrees of freedom of the EE. This kinematic criterion was first introduced by Ming [1]. If the robot has m cables and n degrees of freedom, it is possible to define:

- $m < n \leq 6$: the robot is under-constrained and, in general, cannot withstand arbitrarily applied wrenches. Taking into account gravity or other applied forces and torques, one or more poses in which the robot is in stable or unstable equilibrium may exist. Still, some degrees of freedom cannot be controlled through cables in general. The number and direction of the controllable degrees of freedom vary throughout the workspace. This class of robots is called incompletely restrained positioning mechanism;

- $n = m$: the robot is kinematically fully-constrained, but the force equilibrium depends on the applied forces such as gravity. There is a limited range of forces and torques the robot can withstand depending on the magnitude and direction of the applied force;
- $n + 1 = m$: the robot can be fully-constrained through the cables in certain poses. Different types of motion patterns are possible. The forces that the robot can withstand depend on the minimum and maximum forces in the cables that can be generated by the robot. Robots of this class are referred to as completely restrained positioning mechanisms;
- $n + 1 < m$: the robot is over-constrained, and forces have to be distributed between the cables. These robots are called redundantly restrained positioning mechanisms. As pointed out by Merlet [2], these robots are not kinematically redundant since they have only one solution to the inverse kinematics problem. The redundancy relates to the number of kinematic constraints and, thus, also to their actuation since there are more kinematic constraints than degrees of freedom. Therefore, the static forces of the robot are generally undefined.

This kinematic classification is directly associated with the EE motion in the robot's workspace. The motion pattern of the platform is a pose-dependent property, and it can change throughout the workspace. A well-known defect in the motion pattern is a singular configuration where the robot loses or gains degrees of freedom. The term motion pattern is quite general. Therefore, it is possible to restrict the following discussion to motion patterns that can be expressed by superposition of the three purely translational displacements and three purely rotational displacements, where their directions are arbitrarily identified with translation along and rotation about the axes of a Euclidian coordinate system.

Verhoeven [3] created an exhaustive list of possible motion patterns for fully parallel cable robots (Fig. 1.2) and proved that this list is complete. However, the underlying assumptions are strict since it is assumed that each cable is independently actuated. Mainly it was shown that no designs without translational degrees of freedom exist and that it is not possible to create Schönflies-motion generators based on fully parallel cable robots. Beyond the assumption of Verhoeven, it is possible to add cables without actuation to the robot. This can be done by appropriate control schemes or connecting two or more cables to one actuator. A simple way of achieving this effect is by coiling two or more cables onto the same drum or connecting them to the same linear drive. The motion can also be constrained with mechanical elements such as prismatic joints.

Once the first kinematic categorization is clear, it is essential to understand better the properties of the over-constrained CDPR that are typically adopted in many application cases [4]. These robots have a number of actuated cables higher than the EE degrees of freedom so that the wires can pull each other in order to withstand applied wrenches in arbitrary directions. However, constraint redundancy makes the inverse static equilibrium underdetermined (assuming that bodies are rigid). Namely, infinite cable tensions exist that statically maintain the EE in a prescribed configuration. Thus, the workspace computation for over-constrained robots mainly determines if a suitable force distribution, or tension distribution, exists for a given EE pose. Determining a force distribution that is optimal according to the application requirements

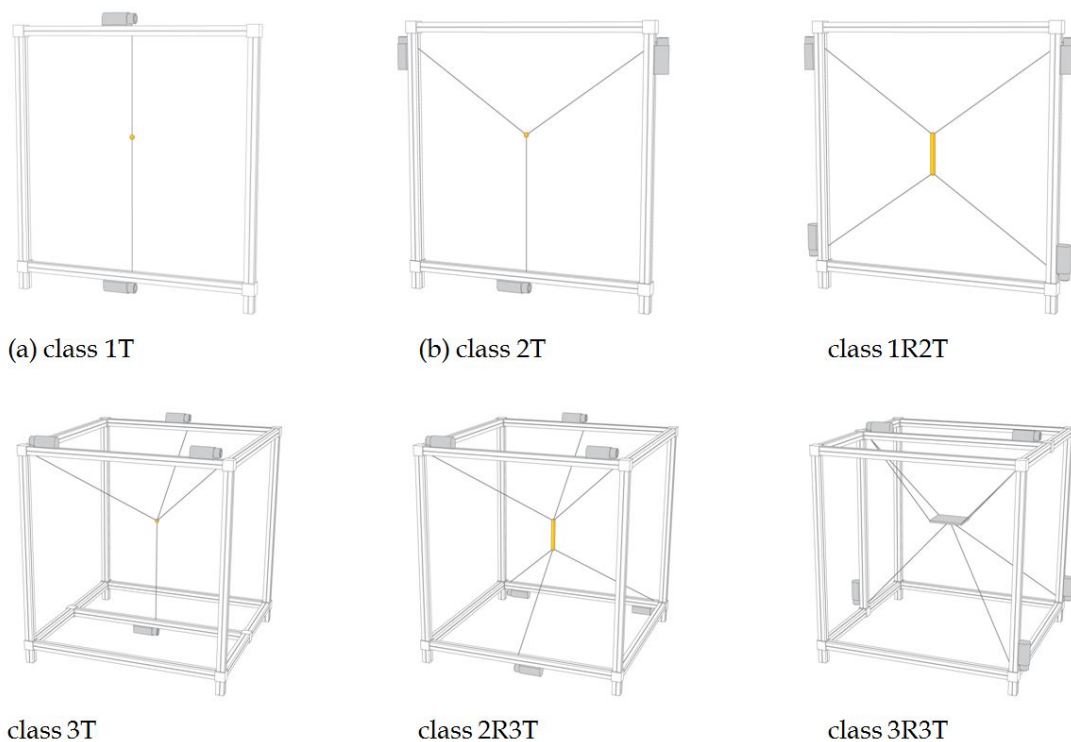


Figure 1.2: All possible motion patterns, where R is the rotational and T is the translational EE degree of freedom

and continuous along a prescribed trajectory can be crucial. This problem is very well-known in literature: many authors treated the problem by minimizing the norm of the cable-tension array [5]. Thus, several strategies for real-time applications were also proposed based on a geometric interpretation of the problem equations [6–8]. Others approaches were proposed: (i) gradient-based optimization [9], (ii) linear programming [10], (iii) Dykstra method [11], (iv) barycentric approach and improved implementations [12, 13].

1.2 Fields of Applications

Cable robots have been proposed to be used in a very wide range of applications. As with many other robotic systems, the development of new ideas for applications is mostly driven by replacing a manual or mechanized process with a robotic solution that allows for fully automatic operation. As proved in many industrial applications, robot systems are well suited to reduce labour costs in production, increase the quality of process execution, or shorten the cycle time. Thus, cable robots may open new fields of application where industrial robots cannot be applied due to restrictions with respect to the size of the workspace, the payload, or the required cycle time.

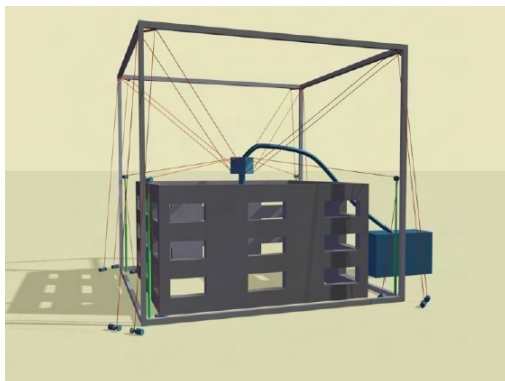
However, cable robots present some other advantages; since thin cables can withstand hundreds of kilograms, the use of multiple cables allows the robot to employ lighter structures and smaller motors. Compared with traditional parallel robots, CDPRs have much smaller inertia, a higher payload-to-weight ratio, and simple mechanical construction. In addition, due to the extensive range of cables, CDPRs can be applied in challenging tasks that require movement within a very large reachable work-

space and with the possibility to reconfigure the robot easily. For these reasons, CDPRs can be adopted in several applications where high payloads and wide workspaces are required, including manufacturing, logistics, and construction, to name a few.

1.2.1 Production Engineering

In the sector of production engineering and manufacturing, robots succeeded in efficiently automating industrial processes, especially for handling, welding, painting, and assembly. Therefore, numerous research projects on cable robots were dedicated to investigating production tasks. Bosscher proposed to use cable robots for contour-crafting [14] where a mobile frame was designed to move between construction sites. Bosscher describes a cable robot with up to twelve cables where a group of eight lower cables are mounted on vertical guideways (Fig. 1.3a). By continuously changing the configuration, interferences between the lower cables and the currently built structure are avoided. A handling and assembly system for large-scale products, like collectors for concentrated solar power plants (Fig. 1.3b), was studied by Pott [15]. The required workspace for the assembly of the parabolic reflector panels of some ten meters with payloads of some hundred kilograms is clearly out of reach for industrial robots but can be realized with cable robots, allowing for significantly reduced energy consumption.

Moreover, a number of production tasks require the positioning of specific equipment around a large workpiece or product, such as ships, aeroplanes, blades of wind-mills, as well as steel structures such as motors, generators, and gearboxes. Typical tasks to perform are painting, welding, grinding, or blast cleaning. Especially noncontact processes [16] seem very adequate for cable robots since taking measurements for inspection, maintenance, or quality control is easy to realize.



(a) Cable robot for contour-crafting



(b) Cable robot for solar panels installation

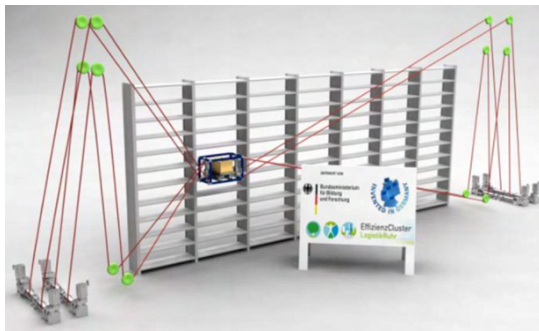
Figure 1.3: CDPR architecture for production engineering

1.2.2 Handling and Logistics

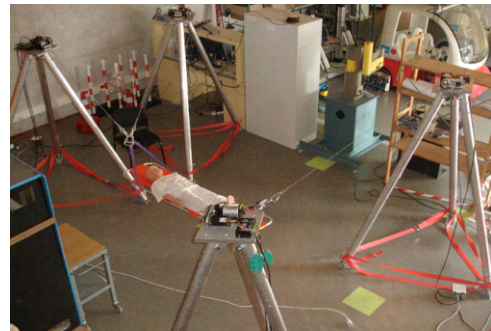
Handling and logistics are promising fields of application for cable robots. Two of the main advantages of cable robots can be fully exploited: cost-efficient robot designs for a very large workspace and very high dynamics allow for high throughput in handling, sorting, and palletizing. Already in the 1990s, the idea of building ultra-high speed pick-and-place manipulators by means of a cable-driven robot was addressed with the FALCON robot by Kawamura [17]. Then in 2012, the CABLAR system was developed

by Bruckmann [18, 19] as a storage-retrieval machine (Fig. 1.4a). The authors demonstrated the efficiency of selecting counterweights and springs for realizing the inner tension of a cable robot used as a storage and retrieval system. This included simplified modelling of the energy and power demands as well as a careful design of the selected trajectories suitable to represent the application-specific motions. Massive improvements of power and energy demand around 20–50% using counterweights are possible and are validated in endurance tests using a demonstrator.

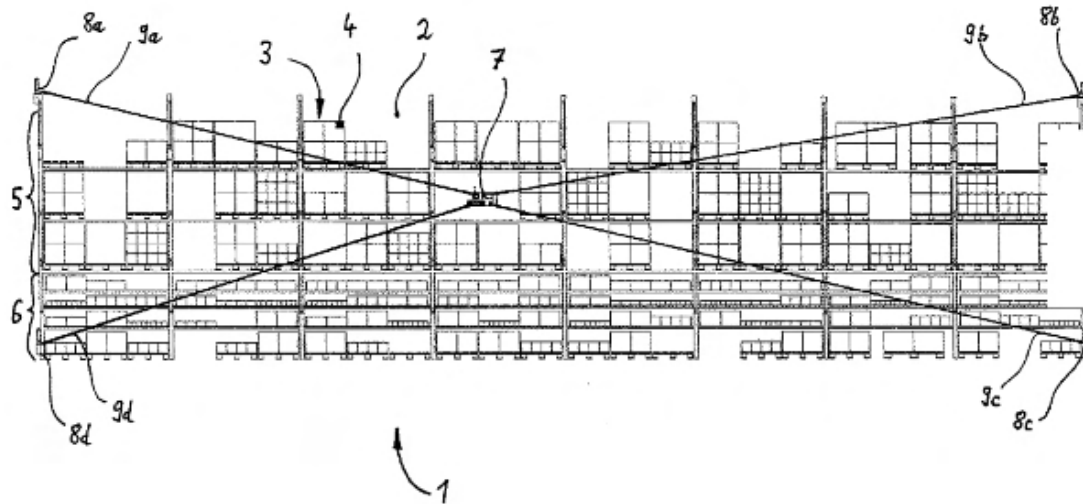
Later, Merlet [20] proposed a portable crane for heavy load handling and rescue where some kind of aerostat was employed to fix pulleys in mid-air (Fig. 1.4b). This system can be set up rather quickly but may have some limitations in regard to lifting capacity and stability on uneven surfaces, especially for rescuing people after a natural catastrophe. Due to their lightweight structure, cable robots were proposed to be used as sensor platforms in different scenarios. The patent proposed by Bauer [21] exploits the huge workspace to move optical and radio sensors through shelf storage systems in order to inspect and locate the stored goods (Fig. 1.4c).



(a) CABLAR storage-retrieval machine



(b) Cable robot for rescue



(c) Device for inspection inside a storage system

Figure 1.4: CDRP architecture for handling and logistics

1.2.3 Robotics in Construction

The construction industry is one of the most important economic sectors across the world [22]. Despite its enormous economic importance, the construction industry

is beset with inefficiencies: productivity has been increasing steadily in the last five decades. Robotic and automated systems have the potential to revolutionize and provide many advantages to this labour-intensive sector [23–25], reducing labour costs while improving productivity and quality (see Appendix A). Moreover, robotic systems can reduce injuries and free workers from conducting dangerous tasks.

A specific sector of the construction industry that could be revolutionized by robotics, and in particular by CDPRs, is represented by large-scale façade activities. Different works can be performed on a building façade: cleaning, painting, maintenance inspection, module installation and other less common tasks. All of these activities share some technical problems that robotics has to take into account and that are often present in façade operations:

- external workspace subjected to unpredictable weather events such as wind effect [26]. The robotic architecture must guarantee a certain safety factor and a robust mechanical stiffness to support the external efforts [27].
- human-hazardous environment that is very difficult to be reached. The robotic system must guarantee a straightforward and safe machine installation that does not endanger human beings [28]. If the robot is built above the public footway in front of the building, it must comply with restrictive standards according to DIN 5692: Entertainment technology & Flying systems [29].
- multifarious features describe a single specific façade: such as balconies, windows, rail guides, drainpipes and others. Robotic architecture must be aware of these features, and a robust sensing system is often adopted [30, 31].
- several façade sizes and geometries: from a planar 2-floor façade to a curve high-rise building [23]. The robotic architecture must guarantee a certain level of flexibility regarding workspace reconfigurability and accuracy.

Although these different sets of problems, robotics could introduce various advantages, of whom:

- reducing the number of on-the-job injuries related to the dangerous on-site façade environment, such as falls from height;
- increasing the productivity of the working task by adding an autonomous-fast system;
- improving the quality of the service by reducing human errors;
- decreasing the costs associated with working salaries and the rental of scaffolding equipment, which often represents a high investment and is often related to thefts during building-renovation activities;
- speeding up the activities, reducing the total working time on the façade, and decreasing the residents' annoyance.

1.2.3.1 Cleaning Task

Modern buildings are becoming larger and high-rise as scientific technology develops, and this trend will continue. High-rise buildings that beautify urban landscapes are expected to incur a significant amount of cost in the aspect of construction as well as maintenance. The current maintenance work on the exterior walls is mainly done with conventional rope and gondolas, which is the cause of frequent safety accidents and falling productivity. As for the exterior wall cleaning of ordinary high-rise buildings, conventional ropes are mainly used [32]. The worker cleans as he comes down while suspended by a rope fixed on the rooftop of a building. The cleaning work is primarily conducted in a team of two persons. When the worker reaches the bottom of a building as a certain area of work has progressed, he moves back to the initial position on top of the building to proceed with the work. The facility supplies the cleaning water, and the workers clean it with cleaning tools. The cleaning tools used are the vacuum compressor for holding the body on the exterior walls, the sponge tool that cleans while supplying the detergent, and the rubber squeezer that wipes the moisture. Adjunctively, plastic pieces or blades of knives are used to remove the foreign substance that has adhered to the wall.

Although many robotic solutions to implement this manual process have been suggested by researchers, there is no single popular solution commercially available yet. Seo et al. [33] investigated façade-cleaning robots and analyzed their climbing mechanisms, cleaning methods, and application issues. They introduced two criteria to determine the performance of façade-cleaning robots: the obstacle-overcoming capability and the cleaning performance. For attachment mechanisms, four categories were defined: vacuum suction, vortex suction and magnetic adhesion, wire or rope (Fig. 1.5), and bio-inspired types, which represent a potential future possibility not yet developed in commerce.

One example of a gondola robot was presented in [34]. In this article, a window-cleaning robot passively overcame obstacles by applying a series of elastic actuators and tristar wheels (Fig. 1.5a). The robot adhered to the façade mounted on a gondola and contacted the façade by the force generated from the parallel manipulator that can extend and contract with respect to the distance that changes under the surface condition between the gondola and façade. Another multifunctional façade and exterior finishing robot based on the design of a traditional gondola was introduced by Pan et al. [35]. The additional frame below the gondola (Fig. 1.5b) hosted the robot end-effector, and the space between the frame structure constituted the robot's work-

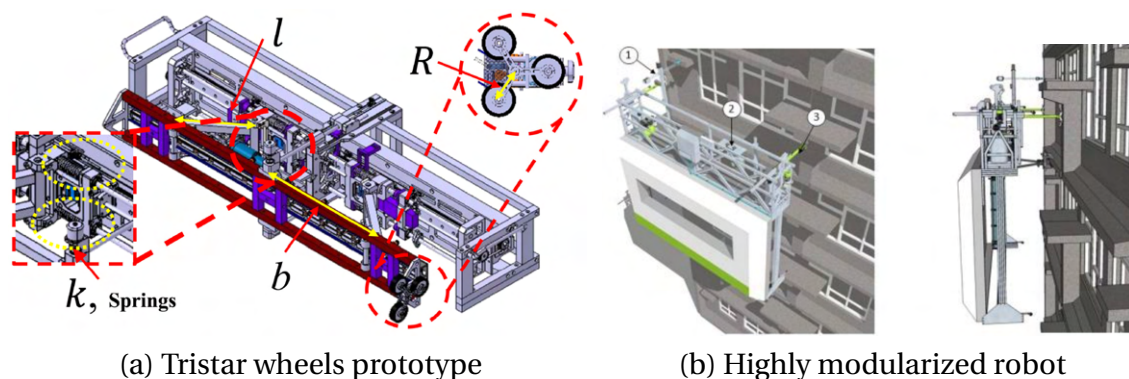


Figure 1.5: Examples of gondola robot for cleaning task

ing trajectory. Two electric motors near the hoisting devices on top of the robot were used to actuate the up-and-down movement. The robot system was highly modularized, meaning that the shape and size of the robot can be easily changed by the design of the target buildings. The system consisted of three subsystems: a detection system, a stabilization system, and a final positioning system.

On the other hand, one application of the rope mechanism was the Sypron robot [36]. The author proposed a new system that consisted of two robots working for the cleaning process: a lifting robot and a cleaning robot. However, single-wire winch-type robots cannot move in the horizontal direction without relocation of the wire winch; moreover, they are unstable under external forces that act like a pendulum. To this regard, Chae et al. [37] designed and developed a novel wall-cleaning robot Edelstro-M2 (Fig. 1.6a). The two main contributions of the study were: (i) the parallel rope control using the dual rope climbing mechanism, allowing high mobility with free movement in both the horizontal and vertical directions on the wall and increasing the resistance to external forces compared to the single wire type; (ii) installation of additional infrastructures was unnecessary.

Ultimately, CDPRs have been tested to fulfil cleaning tasks on an external façade (Fig. 1.6b). In [38], interference was defined as a limit to the workspace. However, even after interference has occurred between cables or with the surface, the mechanism might still be able to function. It can be concluded that a CDPR is suitable for interaction with a large surface. Within the workspace, this surface can have any shape. A method has been developed in which linear cable theory is used to analyze cable interference and wrench feasibility for an over-actuated CDPR while considering the effects of cable mass. This method can be used to design CDPRs for surface interaction, which was done for a facade cleaning application. In addition, Shao et al. [39] presented a four-cable CDPR optimization model. They studied different cable arrangements to optimize the workspace ratio and the cable force: the most feasible option was the horizontal-cross mode. Then, a prototype was developed with winch modules, a cleaning module, and a control system.

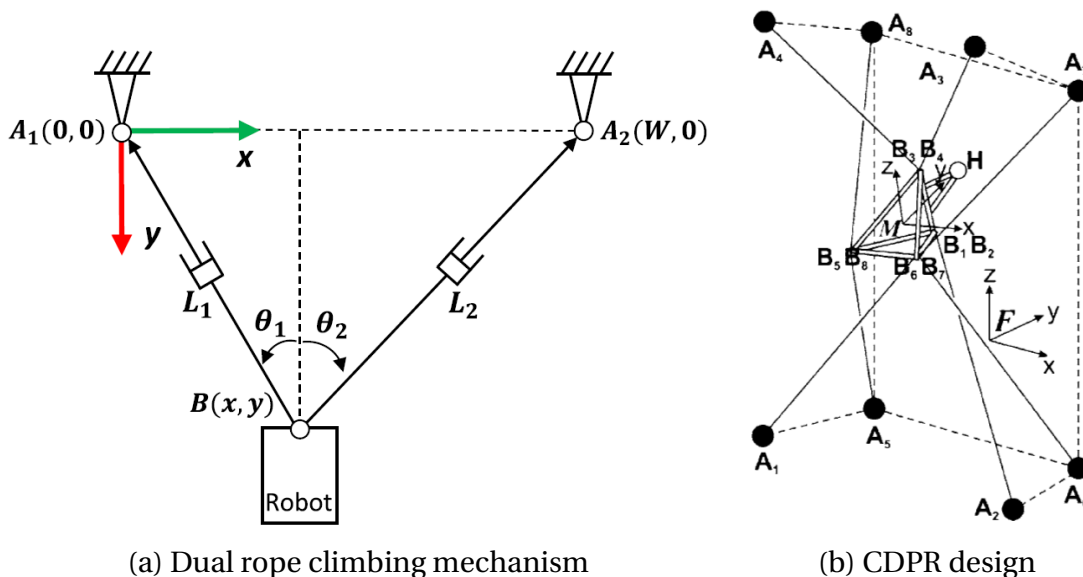


Figure 1.6: Applications of cables

In conclusion, the main technical requirements for the cleaning task can be summarized as follows: (i) except for gravity, there is little concentrated external force and torque in the process; (ii) high dynamic motion is not required; (iii) the workspace coverage rate is the most crucial index; (iv) considering the distributed wind disturbance during cleaning, the robot needs to have good stiffness; (v) obstacle-overcoming capability is necessary.

1.2.3.2 Painting Task

A different on-site activity performed on a building façade is painting. This task is similar to the cleaning one and shares many technical requirements. In detail, the principal difference between these two processes is the end-effector. It is widespread to have anthropomorphic harm designed to paint. In [40], the authors developed an automatic spraying robot with a compact structure, lightweight, ample joint torque and good adaptability. Good spray-proof performance was carefully designed according to the spraying environment to adapt to the confined spraying space. The robot arm adopted the hollow-skew wrist with three degrees of freedom, which had sufficient flexibility to accommodate spraying for complex surfaces. The same robotic arm is equipped in a two-axis cartesian robot to obtain a different architecture [41].

A particular application of robotic painting is adopted in marking robots [42]. When installing equipment at construction sites, it is necessary to draw many lines on the site's walls as marks that indicate installation positions of equipment, for example, positions of anchor bolts, by using surveying instruments such as automatic levels, transits, and tape measures.

Lau et al. patented a CDPR to maintain a building façade [43]. The robot system included a platform cooperating with a least four pairs of cables for positioning the platform at a distance from a building façade (Fig. 1.7). At least one robot arm was situated on the platform and manipulated a building façade maintenance tool. An actuator drove the cables to move the platform to arbitrary positions along the building façade. A controller cooperated with the actuator to instruct the actuator to drive the wires and to control the movement of the robot arm, such that driving the actuator and

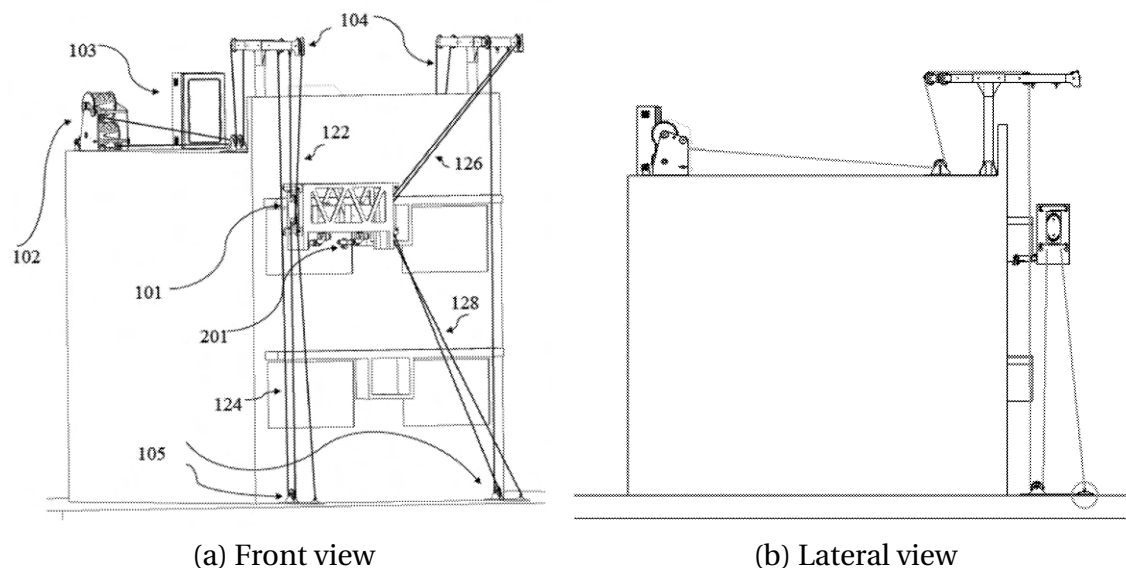


Figure 1.7: CDPR architecture for painting and cleaning

movement of the robot arm are coordinated by the controller; any position deviations in the platform were compensated for by positioning or motion of the robot arm. This robot was capable of painting and cleaning.

1.2.3.3 Maintenance Inspection Task

Building façades perform various functions such as ventilation, daylight management, interior providing convenience for users, energy saving and information display [44]. For these reasons, the interest in wall inspection has been increasing in recent years, and there have been studies exploring automatic methods to replace human workers to conduct the inspection work, such as developing inspection robots [45].

The first robot inspection category is represented by the Unmanned Aircraft System (UAS), known as drones (Fig. 1.8a). With mounted thermal cameras, UAS can collect thermal information from different angles and altitudes. Moreover, UAS not only captures images horizontally, obliquely, and vertically from different angles around a building but can also fly at a lower altitude and through two buildings to capture fine details, reducing time and labour. To explore factors affecting the performance of 3D thermal mapping for energy audits using infrared thermography mounted on UAS, Hou et al. [46] proposed a method for testing different combinations of flying configurations and comparing the results derived from those different combinations. In [47], the authors developed a low-cost and accessible methodology for identifying cracks on walls using off-the-shelf consumer drones, free and open-source photogrammetry software, and deep learning libraries.

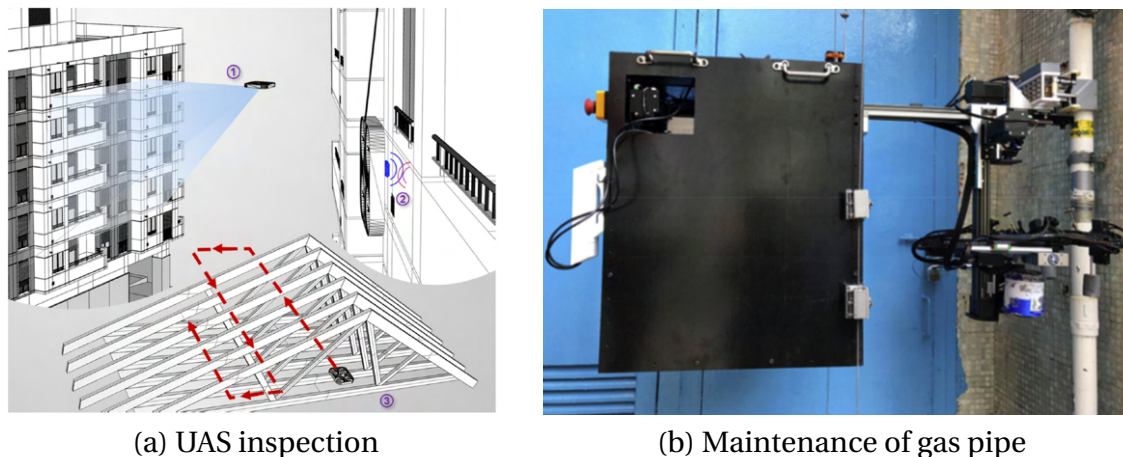


Figure 1.8: Different robotic architecture for maintenance task

A different UAS application is represented by thermal exchange detection through the building envelope, which is one of the primary sources of energy loss. Therefore, rapidly detecting and locating areas of significant heat loss and air leakage on the building envelope remains a crucial challenge for improving the energy efficiency of buildings [48]. The authors presented a quadcopter equipped with an RGBD camera, thermal sensor, and ground penetrating radar sensor to automatically survey a building envelope in less time, especially over hazardous and inaccessible areas.

The benefits of using UAS for building inspection are numerous. Autonomous navigation enables a high level of automation, and the flight ability allows the UAS to reach points on structures or roofs which are otherwise difficult or dangerous to access. Nev-

ertheless, the current autonomous features of UASs are pretty limited. For instance, there are inevitable mismatches between the planned flight paths and real paths followed by the drone due to localization errors caused by built-in GPS. Under most regulations, drones are not allowed to fly without an operator. They need to stay within the operator's visual line of sight.

Wall-climbing robots represent the second robot inspection category [49]. Moon et al. [50] proposed a vertical climbing mechanism that can move along the built-in guide rail installed at the edge of a building. Instead, Koh et al. [51] presented a fully operational robotic prototype for the preventive maintenance of high-rise exterior gas pipes (Fig. 1.8b). The core contribution of this research was the development of a comprehensive teleoperated robotic system equipped with a laser-guided gripper module for stabilizing its relative pose concerning the gas riser. Multi-configurable work tools, which were equipped with feedback control, can compensate for varying contact conditions. The robot removed rust through the polishing process and coated the pipe with an anti-rust compound through the painting process.

Finally, Schröder developed a CDPR for vertical green maintenance [52]. The moving platform of cable-driven robots can be fully constrained with a minimum of 7 cables. Still, estimations for setting up a fully constrained robot in a flat working space lead to high cable tension when forces orthogonal to the façade occur. Thus, high-power winches need to be installed. To avoid this problem, reducing the number of cables leads to increasing uncontrolled degrees of freedom. An incompletely restrained positioning mechanism with four transmission elements driven by two brushless DC motors was set up for this task: the winch motors can control the height and the horizontal motion parallel to the façade (Fig. 1.9).



Figure 1.9: Mobile platform for green maintenance

1.2.3.4 Modules Installation Task

The need for ameliorating the insulating properties of existing buildings is growing. The European Parliament promoted an energy-saving guideline to achieve high energy efficiency and to ensure that the long-term renovation strategies deliver the necessary progress towards the transformation of existing buildings into nearly zero-energy buildings, in particular by an increase in deep renovations [53]. The constructional implementation of these energy-oriented refurbishment processes mostly includes an optimization of the façade's external insulation, often executed as External Thermal Insulation Composite Systems in order to reduce internal thermal loss. For this purpose,

in [54], the authors introduced the concept of a mono-material thermal insulation system based on an easily reusable as well as highly insulating mineral material.

On the other hand, a different constructional implementation includes new insulating layers added to the existing building [55]. There are already experiences with the installation of prefab façade components on existing façades, but their installation is primarily based on manual tools and techniques. To introduce robotic systems, the main issues to resolve are:

- the component uploading. There must be a way to place the component that has to be installed. In the case of building renovation, the material supply cannot be done from the interior, but from the exterior, from the foot of the building. For an automated supply of components from the bottom of the building, it would be needed a hoist that could upload components;
- the accuracy of the positioning of the platform. An automated component fixation needs to be positioned with accuracy. Constant calibration and adjustment of the device are needed to perform accurately;
- the risk prevention. Working on the heights must be a secure task;
- the storage. The material arrives at the working place in big quantities and, most of the time, cannot be used directly on the façade; it must be stored for a while.

Iturralde et al. studied the existing auxiliary bodies and structures for reaching any part of the building [56]. They identified five principal architectures: the scaffolding robot, the robotic crane, the hanging robot, the climbing robot and the bridge crane robot. The existing support systems must be adapted and modified to provide proper kinematic performance. The authors classified the overmentioned architectures by the installation time, the task performances and the building type. For this purpose, they underlined some requirements that the future automated supporting system device should accomplish.

- Stability: the device must provide enough stability for operating with different end-effectors, actuators and sensory devices.
- Security: any automated device must be secure, especially working in a building envelope. On the one hand, it must be secure to avoid any collapse and failure of the system in the buildings' nearby space. The system has to work without interfering or creating any injury to the workers or any other people.
- Rapid installation: the supporting system must be installed rapidly; otherwise, it wouldn't be competitive compared to traditional systems.
- Affordability: the overall costs of the use and performance of the system must be cheaper than the traditional methods.
- Modularity and adaptability towards building typology: the system must be adaptable to most buildings, or at least, it should be usable within the same building type. This enables a wider market coverage; therefore, the system can be more profitable and efficient.

- Modularity and adaptability towards building material: the system should be adaptable to different façade materials. If the future support system is directed towards installing just one type of material, the spreading of the device might be reduced to some extent. A wide range of products that can be installed could enable better penetration into the market.

To better understand the manufacturing and installation process of prefab façade components, a study on the installation of the timber-based module was conducted in [57]. Furthermore, the authors proposed a novel approach that automated the modules' customization, manufacturing and installation processes. The solution integrated systems such as accurate coordinate acquisition, parametric design, digital elements manufacturing, and robotic assembly and installation of the modules [58].

Apart from the insulation modules, there are also other examples of façade modular installations, such as the curtain wall installation for high-rise buildings. High-rise building facades commonly incorporate curtain wall modules (CWMs), but the conventional method for on-site installation is unsafe and inefficient. During installation, CWMs are lifted by crane, hoist, or telescopic handler to the attachment location and then fixed to brackets preinstalled on the building. The conventional installation method requires considerable manual handling to guide the large, heavy, suspended wall modules into position. This presents a risk of collision, which can cause human injury or damage to the CWM. Johns et al. [59] critically reviewed state of the art in CWM installation methods and discussed the potential incorporation of related mechanical and informational technologies.

The installation of façade modules may be efficiently performed using a mobile platform able to move in front of the building. CDPRs can efficiently perform such tasks since all the degrees of freedom of their mobile platform can be controlled across a large workspace while handling heavy loads [60]. Hussein et al. [61] formulated a CDPR configuration optimization problem with the maximum cable tension as the objective function to be minimized. Indeed, maximum cable tension is a crucial parameter since the various mechanical components of the CDPR must withstand this maximum value safely, and their characteristics strongly depend on it. The authors computed the smallest maximum cable tension vectors allowing, by construction, wrench-feasibility constraints to be satisfied. The problem of determining such maximum tension vectors was formulated as a minimization problem with linear inequality constraints. The set of optimal solutions was shown to be a convex polytope; thus, it contained infinitely many solutions. Hence, there existed various smallest maximum tension vectors allowing a required wrench set to be generated with feasible cable tensions, and the calculations of two different smallest maximum tension vectors were presented.

This research led to the development of the Hephaestus project [62–64]. The work performed through the Hephaestus project featured for the first time a CDPR designed, built and deployed specifically for the construction sector, with the primary purpose of installing CWMs and comprising two main tasks: brackets installation and CWM placement. The advantages of CDPRs in Hephaestus were their large workspace, high payloads and modularity that facilitated transportation (Fig. 1.10).

The conceptual framework consisted of three sub-systems: a cable-driven parallel robot for rough positioning, a set of robotic tools named modular end effector on top of the CDPR for fine positioning, and a control system executing the commands and synchronizing the tasks. Firstly, the eight-cable CDPR was designed by adopting three

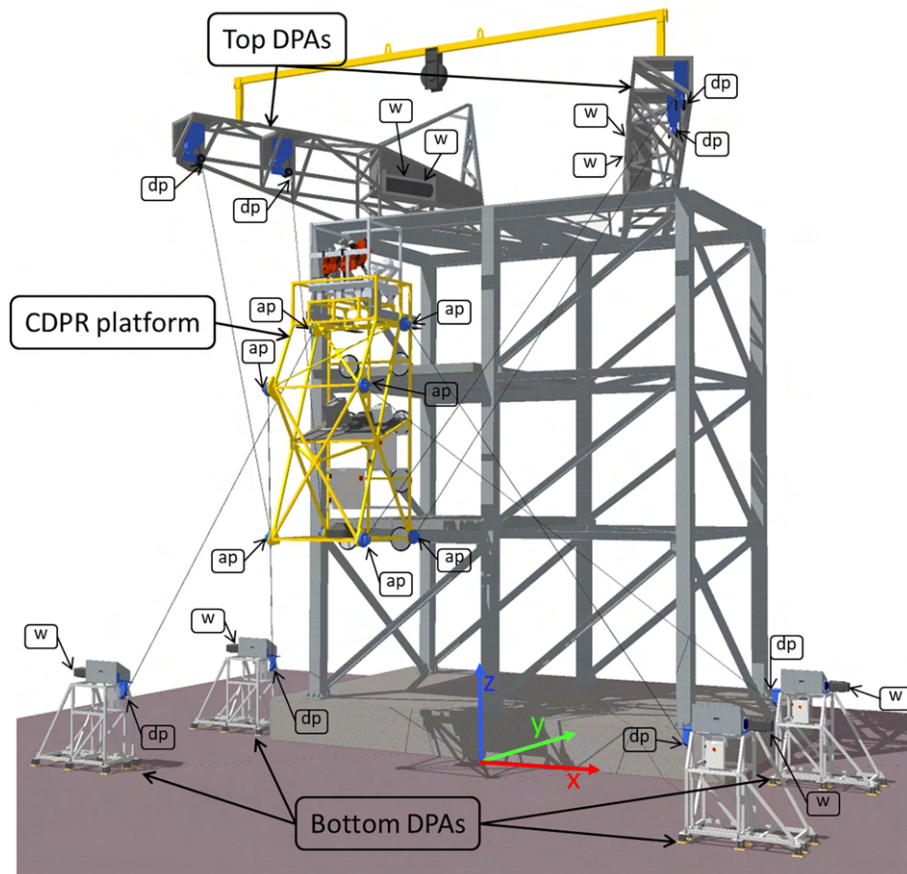


Figure 1.10: Hephaestus CDPR

criteria:

- workspace (based on the CDPR needed to access pick-and-place points for the CWM);
- wrench capability (based on the CDPR needed to be able to carry the designated loads);
- wind resistance (based on the CDPR needed to withstand horizontal forces).

Therefore, the stable configurations of the CDPR were investigated, and the study result was a set of stability polygons, which are the loci in the XY platform coordinates for the centre of mass at which the platform will be stable within the designated workspace. Each polygon was computed for a different value of the load applied on the platform while considering a wind force of up to 500 N from any horizontal direction. Then, analysis and definition of the trajectories to perform the different tasks for assembling CWMs were performed. The typical trajectory of the CDPR was the CWM installation trajectory. It consisted of picking and placing each of the ten panels. The trajectory lay mainly within the workspace, but the upper mounting positions were at the border of the workspace. Finally, the modular end-effector was designed, and the control system was developed. The experiences and results in real scenarios defined a path for future marketization of the Hephaestus robot.

Chapter 2

Design Peculiarities for CDPRs

Once the significant fields of CDPR application have been depicted, it is possible to identify the main peculiarities that the proposed prototype should acquire. This thesis aims to design a CDPR that can be implemented on-site, simulating, for example, the façade operations like painting or insulating an external building wall. The robot should satisfy all the application's requirements: high power density, the ability to be easily reconfigured and deployability. To this end, the first part of the next chapter will present the state-of-the-art of reconfigurable CDPRs. Then, the applications that require high deployability will be described in the second section.

2.1 Reconfigurable CDPRs

A CDPR configuration refers to the positions of the cable exit points, the positions of the cable anchor points on the moving platform, and the cable layout between these two sets of points. In most classical applications, the CDPR has a fixed configuration determined during its design. While fixed-configuration CDPRs are relevant in many cases, some more demanding applications require reconfiguration capabilities. For example:

- to avoid cable collision inside the workspace [65]. Perrault et al. [66] studied the geometric analysis of interferences between two cables and between a cable and an EE edge. Their work provides an exhaustive symbolical analysis of this phenomenon. The results lead to an exact description of the interference regions inside a constant-orientation workspace of any given CDPR. Moreover, Aref et al. [67] studied the cable-to-cable, cable-to-body and cable-to-work piece collisions of a six-degrees-of-freedom cable-driven redundant manipulator. The study was based on designing a full-force feasible mechanism for the entire workspace, and then the workspace boundaries were determined by a collision-free algorithm. The authors demonstrated that this approach is practical for real-time applications since its analysis takes less computational time. Youssef et al. [68] avoided interference between cables while maintaining the trajectory of the mobile platform. An algorithm was created in order to detect a near collision between any two cables and determine which cable is in a higher position; hence, it moves up the corresponding attachment point to increase the shortest distance between the two cables until it reaches a safe threshold value.
- to avoid cable collision with human [69]. The authors investigated the collision

avoidance among cables and human limbs (such as a moving obstacle in a dynamic workspace) in CDPR using Karush-Kuhn-Tucker (KKT) method. This idea applies by moving the linear displacement of attachment points on the rails to increase the shortest distance between cables and human limbs to a safe distance. This distance is computed by the KKT method as a collision detection algorithm. So, this algorithm can detect obstacles as quickly as possible. After distance detection, the algorithm moves reels or attachment points on the rails while keeping the desired trajectory of the EE unchanged.

- to avoid cable slackness [70]. Bettega et al. introduced a method to reconfigure the exit point continuously while the EE is moving. The authors referred to the three-cable translational-reconfigurable CDPR with a single reconfigurable exit point and under the assumption that the robot displaces a known load quasi-statically. This strategy still has some considerable limitations and lacks generality, but it represents a first attempt to exploit continuous reconfigurability through an analytical and efficient strategy.
- to reduce the number of winches. In this way, the installation and maintenance costs are reduced, and a limited number of winches can be used when reconfigurations are allowed.
- to increase the robot's flexibility and obtain better performances under certain constraints [71–74]. Nguyen et al. focused on using gradient-based optimization tools to solve the CDPR reconfiguration systematically. The CDPR reconfiguration is divided into two sub-optimization problems. The first problem consists of finding the bounds on the reconfiguration parameters in which all the nonlinear constraints, including wrench feasibility and geometric constraints, are satisfied. The CDPR reconfiguration is transformed into a classical box-constrained problem that can be solved with standard optimization tools. Two reconfiguration strategies are considered: offline reconfiguration and online reconfiguration. Two criteria are introduced to quantify the robot's performance in terms of power consumption: the sum of cable tensions and minimal energy consumption of the CDPR.
- to overcome the effects of cable failure recovering the originally expected trajectory, and complete the trajectory tracking task [75].

Exit point reconfigurations can be performed in a continuous [76] or discrete manner [77]. The first one (Fig. 2.1) consists of cable exit points mounted on mobile bases, e.g. a mobile crane [78, 79], a trolley on a rail [80–84] or a flying platform [85–88]. Such a reconfigurable CDPR has a continuous set of possible configurations. In particular, in [87], the main contribution of this approach lies in the combination of results deriving from the static analysis of cable-driven manipulators with the application of a cost-based motion-planning algorithm to solve manipulation queries. Instead, in [86], a new type of flying parallel robot was studied. The robot is composed of two quadrotors linked by a rigid articulated passive chain that can be assimilated to a flying parallel robot. The study of the dynamic model showed decoupling properties. Those properties have been exploited to design a controller dedicated to this new flying robot.

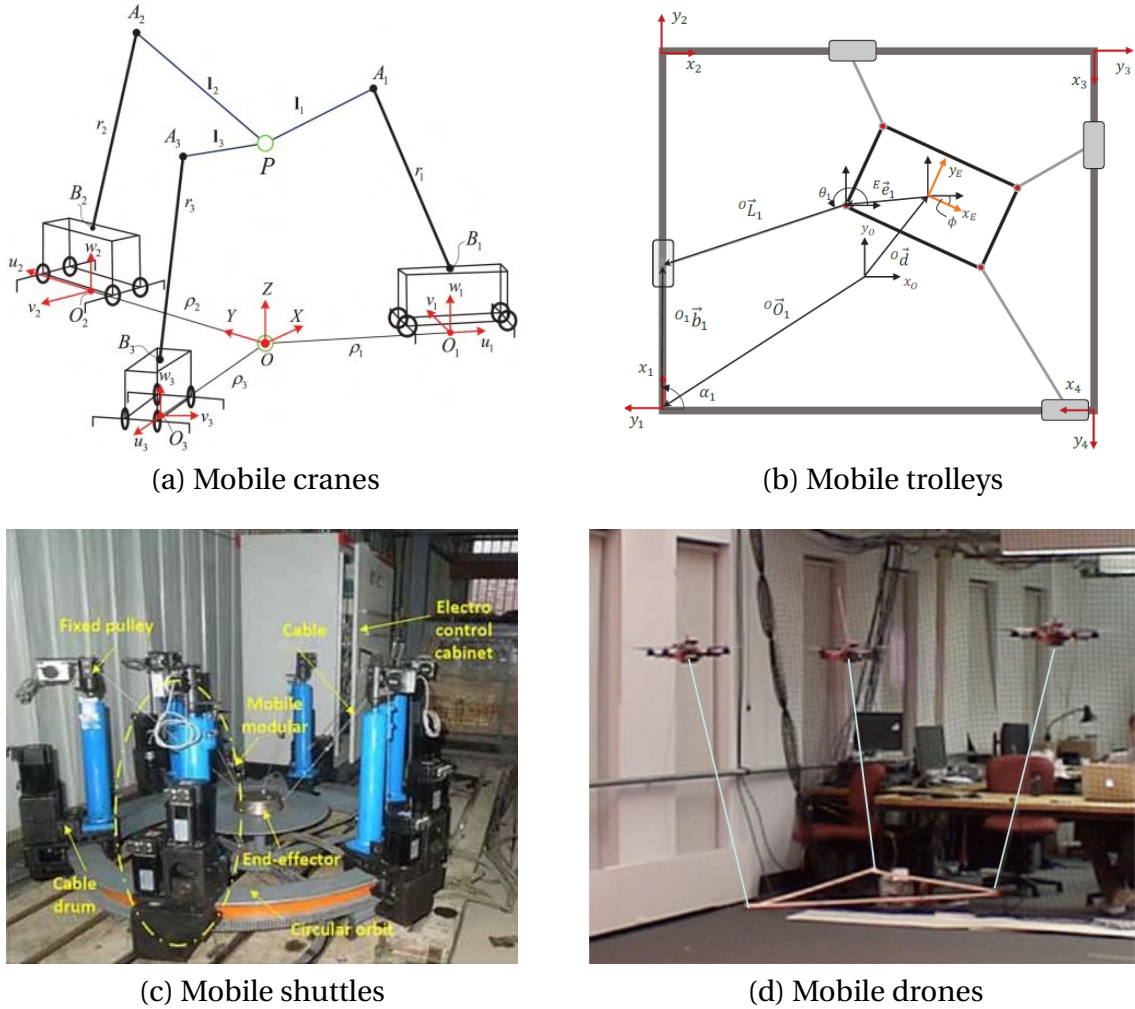


Figure 2.1: Different reconfigurable CDPRs performing continuous reconfiguration

On the contrary, the set of possible reconfigurations is discrete when the cable exit points can be positioned at a large but finite number of locations, such as those of a grid of possible exit point positions. From a technical point of view, modifying a cable exit point amounts to moving or changing the last pulley, which directs the cable toward the moving platform. The National Institute of Standards and Technologies (NIST) has already performed preliminary studies on reconfigurable CDPRs as part of the NIST RoboCrane project [89]. Izard et al. [90] also studied a family of reconfigurable CDPRs, named ReelAx, to investigate the potentialities of CDPRs in industrial contexts. However, no reconfiguration strategy has been proposed by the authors. More detailed studies have been performed by Rosati et al. [91], which focused on planar reconfigurable CDPRs. They suggested using movable exit points to maximize a local performance index across the CDPR workspace. In 2012, Zhou et al. [92] suggested increasing the number of the robot's degrees of freedom by mounting the winches on mobile bases (Fig. 2.2a). In [93], Zhou used an alternative concept for CDPRs. A set of cables with constant lengths are connected to linear motors. The cables are either attached to the platform or pull the platform using idler pulleys (Fig. 2.2b). A planar case study has been investigated to show the concept's advantages in both cases.

Finally, Gagliardini et al. [94] considered discrete reconfigurations because the use of continuous reconfigurations for industrial applications over large structures can be

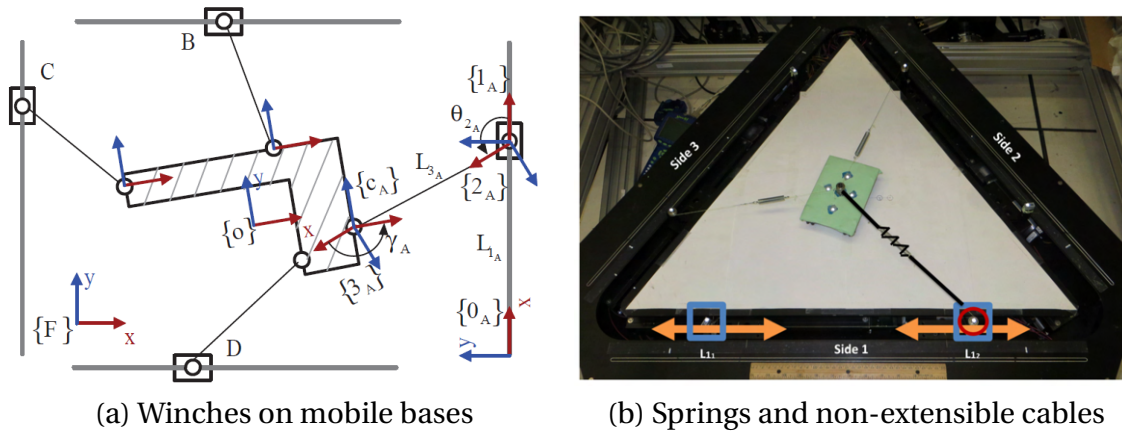


Figure 2.2: Zhou's alternative design for planar CDPRs

prohibitive since several additional motorized degrees of freedom must be used to reconfigure the cable exit points continuously. In the context of a cluttered environment which precludes the use of a fixed-configuration CDPR, the authors introduce means to select and optimize the sequence of discrete reconfigurations permitting the mobile platform of a reconfigurable CDPR to follow a prescribed path. Quasi-static working conditions are considered. The prescribed path is discretized into a finite set of points. The cable exit points of the CDPRs under study can be positioned at the points of a user-defined grid of possible locations (Fig. 2.3). The user also defines a set of constraint functions that ensure the robot's proper functioning. The prescribed path is deemed successfully followed if all these constraints are satisfied at all points of the discretized path.

The optimization problem was solved by first generating a so-called feasibility map. For each possible CDPR configuration, this map stores the feasibility of the points of the prescribed path. A point is feasible if the corresponding platform pose satisfies all constraint functions; it is unfeasible otherwise. From this map, feasibility transitions are then defined. These transitions represent the reconfigurations that can be per-

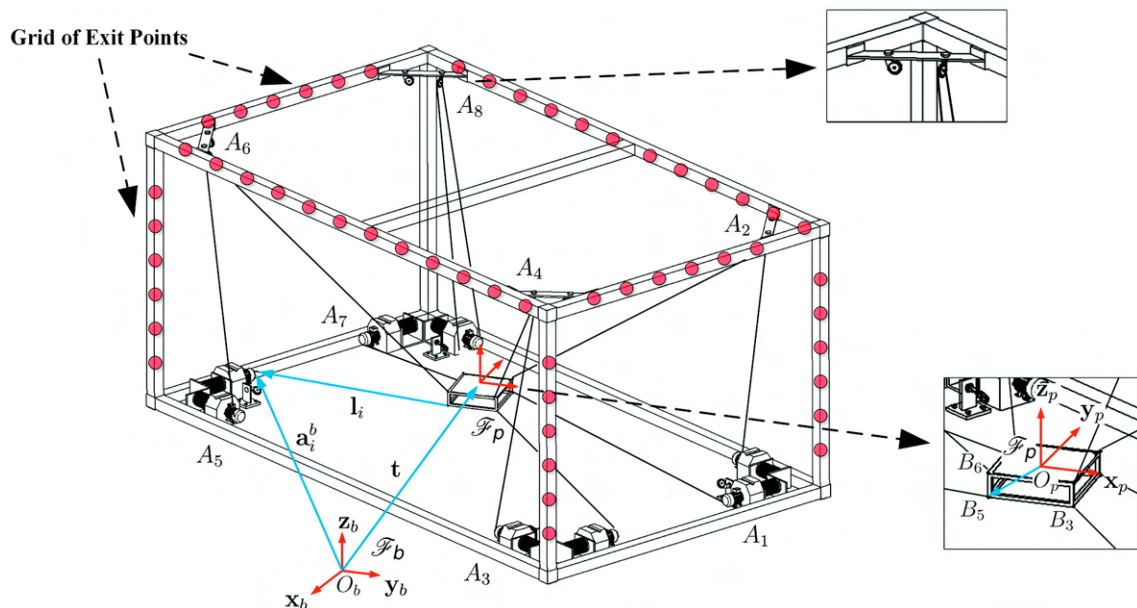


Figure 2.3: Discrete reconfigurable CDPR

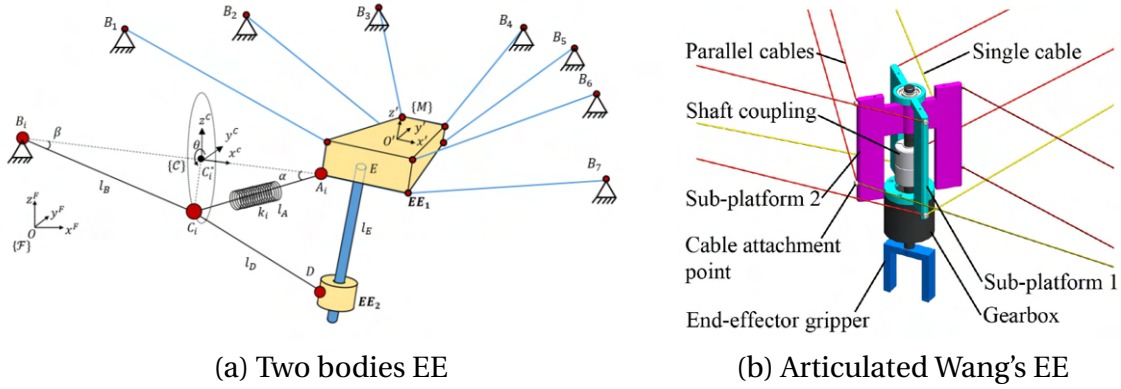


Figure 2.4: Reconfigurable mobile platform to allow motions

formed along the prescribed path. The feasibility map is next analyzed to find dominant configurations and then to determine minimum sets of configurations that allow the CDPR platform to follow the whole prescribed path while satisfying all constraint functions, resulting in a reduced feasibility map. This analysis aims at reducing the number of configurations to be considered in the next step. This next step uses the feasibility transitions to build a graph whose nodes represent the feasible CDPR reconfigurations along the prescribed path and whose arcs are weighted using a user-defined cost function, a relevant example being the number of cable exit point changes required for a given reconfiguration. Finally, the graph is searched using Dijkstra's algorithm, which eventually determines the optimal reconfiguration strategy, i.e., the sequence of feasible reconfigurations that permit to follow the whole prescribed path while optimizing a cost function.

To conclude, reconfigurability could be implemented by modifying the EE structure directly. In [95], the authors proposed the analysis of a cable-driven robot with a reconfigurable platform with one of its cables acting in two bodies of the EE at the same time. This is the compliant actuator that acts on two different bodies of the same end effector by considering its position and modifying its tension (Fig. 2.4a). Meanwhile, Wang et al. [96] introduced a novel cable arrangement using cable parallelograms for CDPRs to generate Schönflies motions. In this regard, a novel articulated moving platform is designed to enhance the rotational capability of CDPRs about the vertical axis. The proposed articulated moving platform has a simple structure, and no cable loop is required to drive the moving platform (Fig. 2.4b). The proposed robot retains an internal degree of freedom for the moving platform reconfiguration, which is formulated as an optimization problem to improve the robot's performance.

2.2 Deployable CDPRs

If the state of the art concerning reconfigurable CDPRs is well-defined and articulated, especially from a scientific point of view, as presented in the previous section, it is not the same for deployable cable-driven robots. In particular, only a few scientific papers dealt with this specific topic; instead, many patents were drafted.

From a scientific point of view, Chesser et al. [97] propose the following set of key requirements that a deployable motion system should have, focusing their attention towards an additive manufacturing process [14] and prototyping a new system called

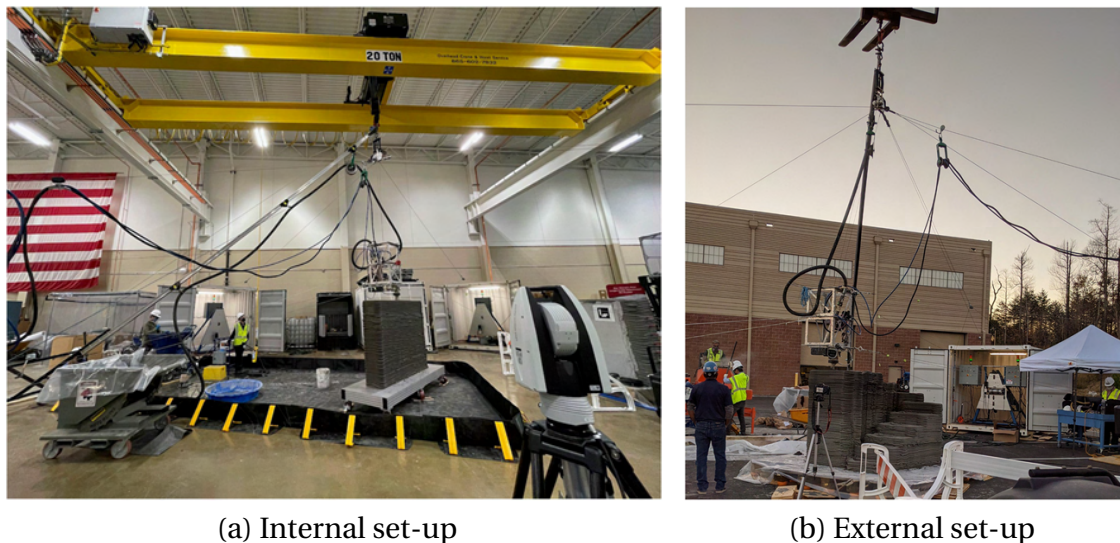


Figure 2.5: SkyBAAM system test: internal and external experiments

SkyBAAM (Sky Big Area Additive Manufacturing, Fig. 2.5):

- The cable winches should be concentrated into several base stations. This minimizes the number of pieces of equipment that need to be set up and calibrated in the field. Furthermore, using a large frame or series of towers to hold the winches should be avoided since this would add significant effort to the setup.
- The system should only have translational degrees of freedom and no rotational ones if the task's requirements allow this choice. Material extrusion systems typically operate in planar layers with no change in the orientation of the nozzle required. Yet, many existing CDPRs used for additive manufacturing found in the literature have six degrees of freedom. Since three translational degrees of freedom are all that is necessary, the additional ones would only add to the complexity of the machine, making it harder to deploy effectively.
- The system should only have a single overhead cable winch. Many fully constrained CDPRs have several elevated cable winches. However, to make the system easily deployable, it is desirable to have all the cable winches on the ground except for the one that keeps the system suspended. This single point could be suspended by a conventional crane or a simple lifting device to minimize special equipment needed for deployment.

Experimental data from a prototype SkyBAAM system show that the system can achieve sufficient accuracy for large-scale additive manufacturing using laser position feedback. This is further supported by demonstrating the system's ability to print large structures.

Moreover, Khalilpour et al. [98–103] proposed new control methods suitable for deployable robots. In deployable CDPRs, the kinematic parameters are not accurately measured, and as a result, the characteristics of the robot model are perturbed. This, in turn, introduces many challenges regarding controller design and meeting the required performance. In addition, employing precise position sensors such as laser tracker systems for measuring the end-effector position is too expensive or not techni-

cally feasible [104]. Therefore, the only option for achieving the EE position is to utilize forward kinematics equations and cable length measurements.

Concerning a different architectural design, Jordan et al. [105] introduced the actuation module of the CDPR directly in the mobile platform design (Fig. 2.6). While many deployments have relied on spatially distributed fixed sensors, this method has proven to have shortcomings based on the dynamic nature of phenomena and the requirements for in-field adaptation of sensors. Actuated sensor system research has been shown to advance sensing system performance substantially. Then, Borgstrom et al. [106] improved the system, which was constrained to a plane motion (2D navigation), limiting the number of robotic and sampling applications. The proposed novel system, NIMS3D, enables: (i) 3D navigation, (ii) high positioning accuracy, (iii) rapid deployment in non-ideal environments, even by a single user, (iv) indoor and outdoor operation with no change in performance characteristics, (v) low fabrication cost due to the use of commercially available parts.

Other relevant research studies about different deployable CDPR applications were presented [107,108]. Bosscher et al. [109,110] introduced a new robotic search and rescue system concept. This system can significantly increase the range of mobile robots and provide overhead views of the disaster site, allowing rescue workers to reach survivors as quickly as possible while minimizing the danger posed to rescue workers. Also, in this study, a deployment sequence is described, a rapid calibration algorithm is presented, and the manipulator's workspace is investigated.

Once the scientific literature is reviewed, it is possible to highlight the most relevant patents about reconfigurable and deployable CDPR (Fig. 2.7). The NIST RoboCrane [111–113] was one of the first modular cable-driven parallel mechanisms. The modularity of the invention provided not only work-volume reconfigurability but also enormous reconfigurability of the suspended platform. On-board winches (Fig. 2.7a) and control simplified the machine's architecture, improving high standards in terms of deployability. The adaptability of the invention to existing superstructures allowed a cost-effective alternative to robotic, tedious and repetitive tasks. Attaching the invention to existing walls and superstructures allowed minimal pre-process set-up and allowed



Figure 2.6: NIMS RD system developed for permanent installation

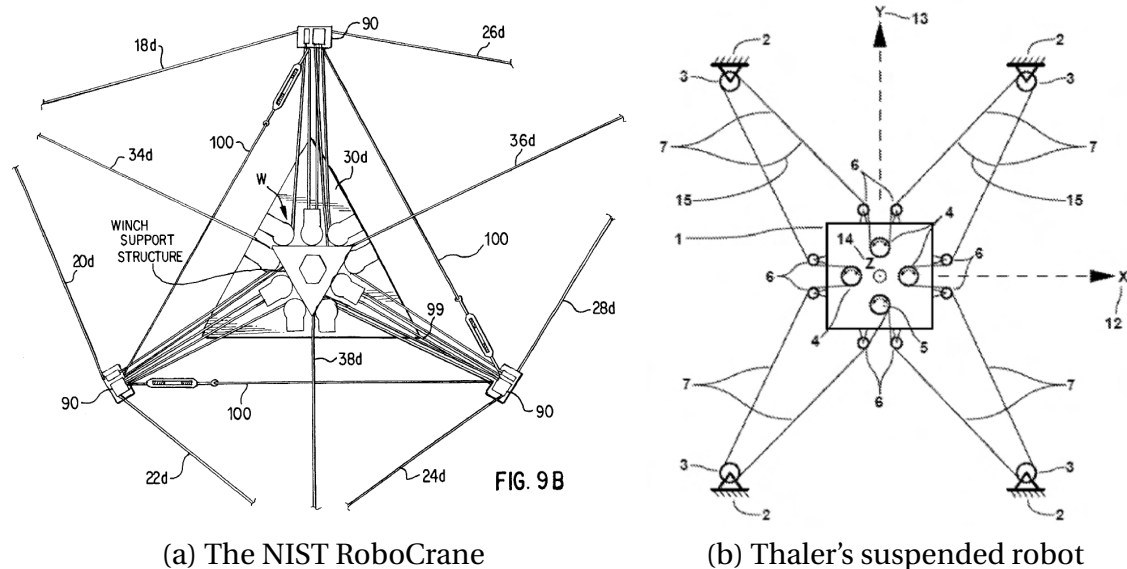


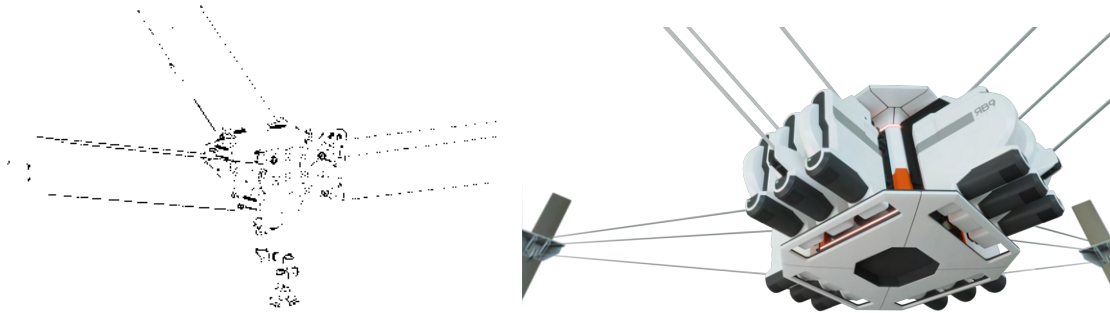
Figure 2.7: Preliminary concept of deployable EE

the EE to move to new locations with minimal set-up time. No additional fixturing to floors or lower-level structures, such as the classical Stewart platform, is necessary.

The same approach was then improved by Thaler et al. [114], presenting a suspended cable robot with the winches directly installed into the mobile platform (Fig. 2.7b). The present invention offered a technical solution to moving a platform in space, which was more compact, lightweight, and simple, and that provided a more rapid preparation and arrangement of the entire system on the location of use. The solution differed from previous ones by introducing an endless cable that creates a close loop between the mobile platform and the main structure. The author suggested many applications of this suspended mobile platform, for example, embedding an aerial camera [115].

Recently, Vachon [116] has discovered that stability in a suspension cable robot can be improved by using at least three groups of three cables arranged in a parallelogram manner (Fig. 2.8). The ability to remain stable when subjected to forces acting on the robot platform or EE is significantly increased. Moreover, this stability can be improved by locating cable actuation and cable uptake within the robotic platform, as the weight of these components enhances the stability. Further advantages of locating cable actuation and cable uptake within the automated platform are simplifying installation and centralising components at the robotic platform. The design of the patented system includes: (i) a platform member; (ii) at least three cable groups, each one of the cable groups being arranged on one side of the platform member and having at least three cable connection supports spaced apart to form vertices of a vertically-arranged polygon to provide parallelogram support for the platform member about three axes, wherein in use each cable group can extend between the platform member and a wall or ceiling anchor to provide the platform with gravity stabilized resistance to motion from forces and torques acting on the platform suspended from the cable groups within a predetermined limit; (iii) a drive associated with each of the cable groups operable to control a length of the cable groups between the platform member and the anchor, wherein the drive controls a common length for each cable within each one of the at least three cable groups.

In conclusion, the deployable architecture of CDPR has been implemented in many different applications. To cite a few more of them, in [117], the robot is responsible for cleaning and inspecting containers and tanks in commercial ships. In [118], the authors investigated a possible application of a deployable robot for industrial plant maintenance. Finally, in [119], a brick-layer machine is developed by exploiting a re-configurable CDPR architecture.



(a) Patent sketch

(b) Commercial rendering

Figure 2.8: RBOT9 prototype

Chapter 3

Conceptual Design

The objective of this chapter is to identify a conceptual design for the CDPR. The final result is the derivative of complex and not trivial mechatronic design iterations, searching between different types of possible solutions concerning the robot's kinematics, actuation units and sensors. During this process, the definition of the design constraints is a relevant topic, due to the large combination of solutions that could be implemented. To this point, the state of the art, depicted in the previous chapters, gains importance as it is considered a starting point for the next study. The CDPR applications previously described can be recapped in terms of the main technical features. In particular, the construction sector represents a potential customer industry for planar, overconstrained CDPRs that do not suffer from the typical disadvantages of cable robots. Instead, they can offer:

- modularity and environment adaptability of the robotic architecture: CDPR can be easily installed in- loco thanks to its high modularity, and it can be efficiently reconfigured to ensure high flexibility concerning its workspace and load capability;
- high payload-to-weight ratio: with small motors and thin cables the CDPR can withstand high payloads with relatively small machine inertia, especially in the construction field this feature represents an important advantage;
- stability: due to the overconstrained design the robot can withstand the plane reactions and other external disturbances that arise from outside the work plane, such as wind reaction forces for example;
- reliable motion pattern: the planar overconstrained architecture awards high performances for the EE planar translation, with the possibility to slightly control the mobile platform orientation;
- rapid installation: thanks to deployable and reconfigurable features presented in the second chapter, CDPR with a completely actuated EE can be installed in less time.

This chapter is structured as follows: first of all, a brief introduction to the different types of servo-winchs usually adopted in the field of cable robots is presented. Then, the task that the robot should perform is described in terms of physical constraints and a possible machine frame is developed. Therefore, three different solutions are presented. In conclusion, the final conceptual design is shown, selecting the solution

with a morphological matrix that analyzes all the relevant aspects of the proposed designs, focusing on the advantages and disadvantages that each of them could have.

3.1 Actuation Unit for CDRP

Different cable-driven applications usually have highly different requirements: even though the principal mean of transmission is a cable, its actuation unit and guidance system are engineered according to other principles. For industrial applications, guidance systems are usually a combination of fixed and swivelling pulleys, whose geometry and installation configuration are dictated by geometric and loading conditions of the operation (many research prototypes have even simpler guidance systems, such as eyelets where cables may slide through).

Conversely, the design of the actuation unit is driven by application requirements in terms of rated power, cable tension, and speed, but also by the requirements of the control system. The most common one is the ability to feedback control the EE pose. The estimation of the cable lengths provides EE pose information, thanks to well-established techniques in the solution to the forward kinematic problem and thanks to the fact that no sensors other than the ones embedded in the actuators for their low-level feedback control, such as a rotary encoder or a load cell, need to be added to the robot.

Concerning actuation, the most straightforward way to wind a cable is using a smooth drum connected to a motor. Unfortunately, it is not trivial to determine how the cable is wound over the drum (Fig. 3.1a), as the axial and radial winding distances are not a function of the motor angle. As an alternative, cables can be overlapped with a self-reversing screw allowing for a correlation between cable and motor displacement (Fig. 3.1b). Unfortunately, the transmission ratio τ is a function of the absolute motor angle, which may not be known at start-up time, and, furthermore, a varying radius implies varying tension-speed limits for a given motor-rated power. The possibly simpler and commercially available solution for a constant and known τ is to use a hoist and a linear actuator for its control. However, if long cables need to be used, the installation space, transmission ratio, and cable wear increase alongside the number of pulleys in the hoist.

The solution that implements constant transmission ratio τ is called servo-winch. This is possible thanks to two main aspects: (i) the cable exit point from the drum

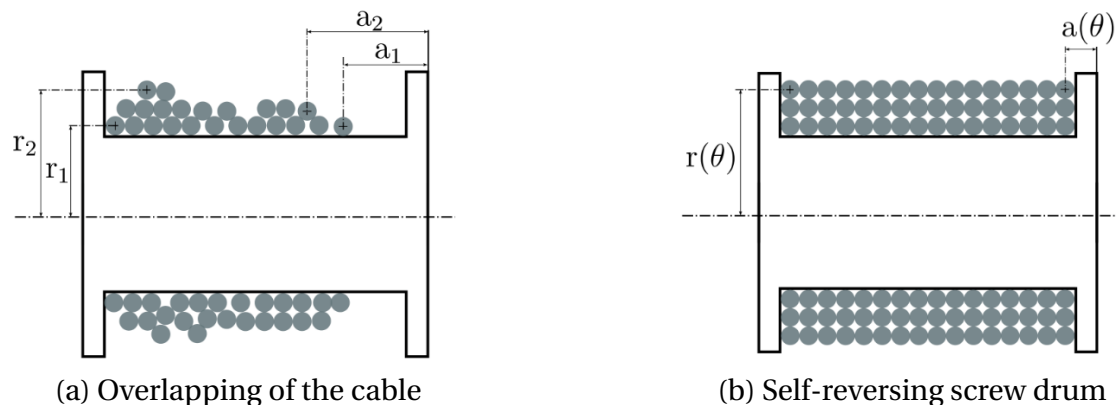


Figure 3.1: Smooth drum connected to a motor

has a known constant direction; (ii) the cable overlapping on the drum is avoided by grooving the drum, as a screw, to accommodate the cable and reducing cable wear too. There are several solutions in the literature to achieve such desired design requirements, which can be organized into different classes: the rototranslating winch, the spooling-helper winch and the spline winch [120].

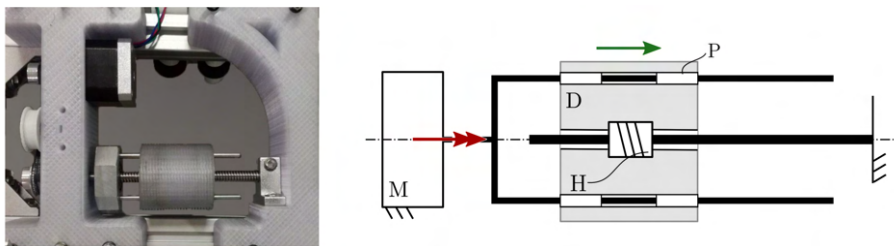
3.1.1 Rototranslating Winch

Two main solutions refer to this category of actuated servo-winch (Fig. 3.2): (i) the rototranslating-drum design and (ii) the translating-motor design.

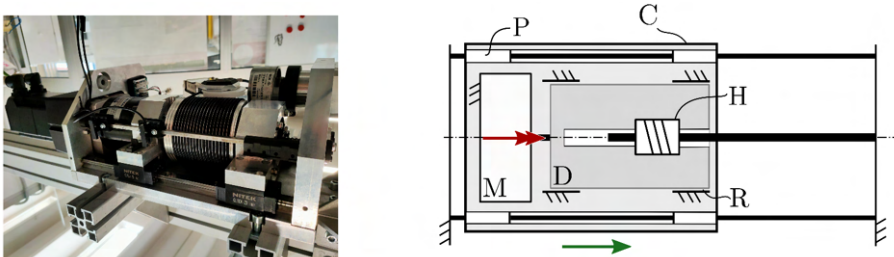
In the first solution (Fig. 3.2a), by rototranslating the drum, the cable exit point and its direction are fixed concerning the winch frame, while the cable is coiled and uncoiled. The rotational motion of the motor is converted into the rotational and translational motion of the drum by a screw-nut system, that simulates a helicoidal pair. The screw shaft is fixed to the winch frame, and the drum slides on passive prismatic joints along two rods parallel to the drum axis. The motor, which is fixed, can be coupled to the drum using a transmission such as a synchronous belt. By simply considering that the drum rotates and translates, and for each motor turn, a complete helix is wound or unwound, the transmission ratio τ can be evaluated as a function of the screw transmission ratio τ_s , with h as the helix pitch, and the radius of the drum r_d as:

$$\tau = \sqrt{\tau_s^2 + r_d^2} \quad [\text{m/rad}], \quad \text{where} \quad \tau_s = \frac{h}{2\pi} \quad [\text{m/rad}] \quad (3.1)$$

The second solution instead, consists of translating the entire motor-drum system on a linear guide (Fig. 3.2b). Concerning the previous case, the motor and the drum are directly connected and mounted on a carriage. The motor is fixed concerning the carriage, whereas the drum can rotate supported by two bearings. The rotational motion of the drum is transformed into the translation of the carriage along two prismatic pairs thanks to a helical pair. As for the previous design, the latter is usually realized using a screw-nut system, where the nut is fixed to the drum. The two solutions have the



(a) The rototranslating-drum design



(b) The translating-motor design

Figure 3.2: Rototranslating servo-winch architectures

same kinematic behaviour, and the transmission ratio of the translating-motor design is calculated with the same Eq. 3.1.

Compared to the previous solution, the translating-motor design has a different shape factor: the major size is represented by the axial length of the motor plus the winch, instead the rototranslating-drum design has a shape factor which is nearly one (axial and radial lengths are similar thanks to the belt transmission).

3.1.2 Spooling-helper Winch

This solution implements an auxiliary cable guiding device equipped with a pulley, called a spooling helper (Fig. 3.3). Similar to the concept of the self-reversing screw, but only using a traditional screw-nut system, the spooling helper continuously follows the variable cable exit point on the rotating drum by translating parallel to the drum axis to ensure that the cable direction connecting the drum and the spooling helper is constant. The rotation of the motor-drum system is transmitted to the spooling helper using a synchronous belt. Thanks to a helical pair, the spooling helper slides onto two fixed rods, that simulate prismatic joints. The translational displacement of the spooling helper is equal to the axial displacement of the cable exit point, thanks to the constant pitch of the drum grooving helix and the screw helix that guides the spooling helper.

In this solution, the transmission ratio differs from the rototranslating one (Eq. 3.1) because of the translational displacement of the spooling helper device. In this way, the drum dynamics is simplified because the spooling-helper component is sliding and the drum is rotating, decoupling the two movements that are simultaneously present in the rototranslating winch architecture. The spooling-helper device works as a local buffer that gathers up the cable from the drum, depending on its relative position with respect to the winch frame. Therefore, the screw transmission ratio modifies the previous formulation, introducing an additional term in the equation:

$$\tau = \sqrt{\tau_s^2 + r_d^2} - \tau_s \quad [\text{m/rad}] \quad (3.2)$$

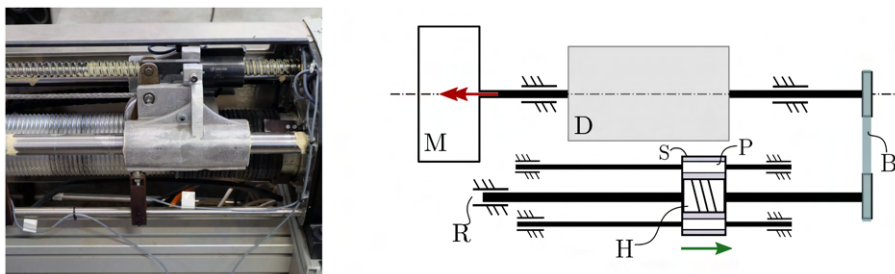


Figure 3.3: Spooling-helper servo-winch architecture

3.1.3 Spline Winch

This design concept (Fig. 3.4) aims to merge the benefits of the rototranslational-drum design with the ones of the translating-motor system. The motor is fixed to the winch frame, while the drum can:

- rotate since a spline shaft is rigidly attached to the motor axis, and a spline nut is attached to the drum. The spline shaft-nut pair is effectively a prismatic joint, designed to transmit torque while allowing axial translation;
- translate since a screw shaft is rigidly attached to the winch frame, and a screw nut is attached to the drum. This is the classical helical pair used in all winch designs.

The drum is supported via two plates: a revolute joint and two prismatic joints are embedded into each plate, so that the drum can freely rotate with respect to the plates, and the drum-plates assembly can translate with respect to the winch frame. The motor is coupled to the ball spline shaft through a bellow coupling (torsionally stiff but flexural compliant). Instead of a regular spline shaft, a ball spline shaft is chosen due to its zero-backlash and low friction properties; this component is widespread and cost-effective due to its frequent use in machining equipment tool-change systems. A ball screw shaft is also attached to the winch frame, on the opposite side concerning the ball spline shaft. The ball spline and ball screw nuts are rigidly attached to two drum covers, which are free to rotate with respect to the floating plates thanks to radial bearings, and are rigidly attached to a tube drum. The choice of decomposing the drum in two covers allows for critical weight reduction and saves machining waste.

Since the drum rototranslates, the overall transmission ratio τ of the spline winch is the same as the rototranslating-drum one (Eq. 3.1).

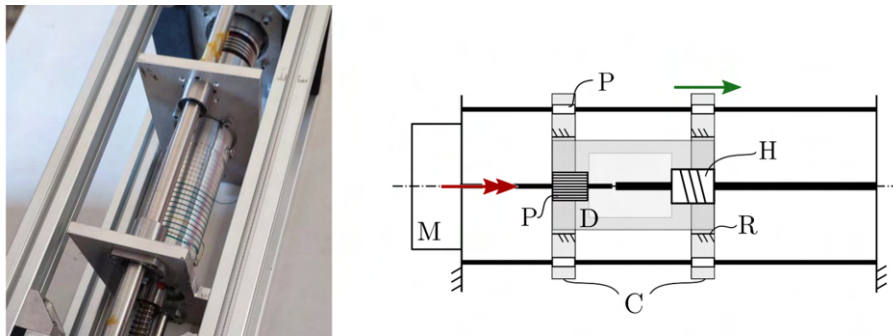


Figure 3.4: Ball-spline servo-winch architecture

3.2 Task Requirements

As presented in the earlier section, the design of the actuation unit is driven by application requirements in terms of rated power, cable tension, and speed. To this end, it is important to define the task requirements that the proposed robot should satisfy.

The robot EE should be able to move in a vertical plane, without changing its orientation concerning the machine frame, and perform a painting task (see Section 1.2.3.2). In [121], the authors analyzed the painting task performed by an anthropomorphic robot: they estimated the reaction force applied by the air and painting jet against a surface, as a perpendicular force of approximately 50 N. This parameter was set to be the maximum orthogonal force with respect to the vertical EE plane of motion. In addition, the maximum allowed cable tension is set to 600 N and the cable velocity is expected to be between 0.2 and 1 m/s, according to a quasi-static painting motion. Both these two design parameters are set according to the state of the art and past

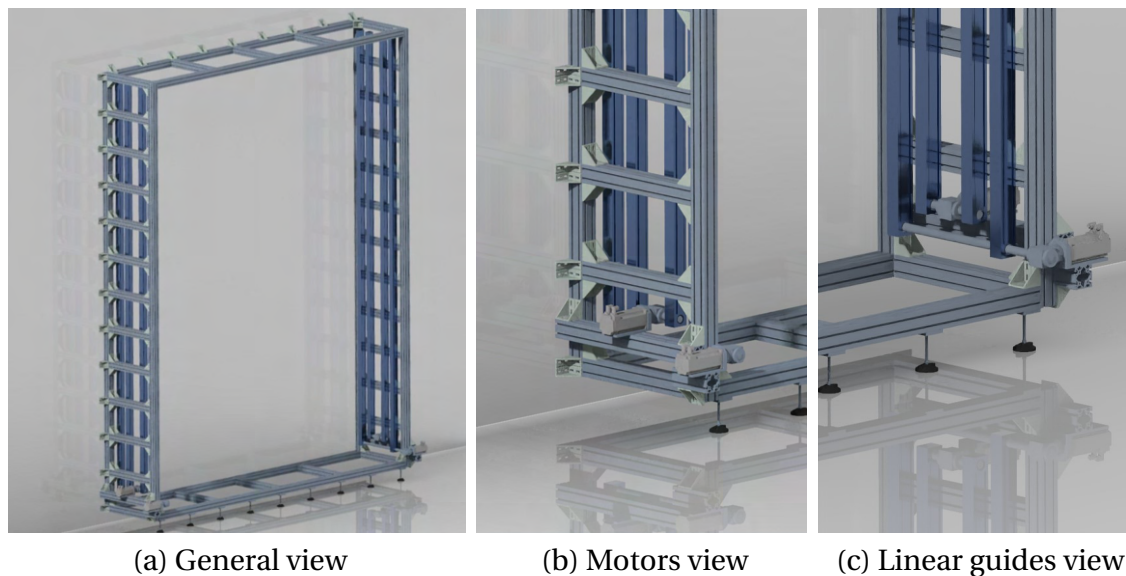


Figure 3.5: The extruded aluminium frame

analyses performed on CDPR. In this preliminary study, all the high-dynamic effects are neglected.

As a consequence, the selected CDPR design is planar and overconstrained. Theoretically, the motion of the EE is a pure planar translation in the vertical plane, parallel to the painted wall. On the other hand, the external disturbances and applied loads could generate different types of motion for the robot EE. Therefore, it is necessary to implement an overconstrained architecture that allows, with 8 cables, a spatial workspace, providing for internal forces and torques able to stabilize the mobile platform. For this reason, the robot's workspace is no longer restricted to a vertical plane but, instead, it becomes a spatial solid, which has a negligible third dimension compared to the other two that define the vertical plane of motion. The author continues to use the planar attribution, even though this feature is not theoretically correct but ensures a control fringe of external disturbances.

Concerning the reconfigurable feature of the prototype (see Section 2.1), the frame represents an essential component of the robot. It is designed with extruded aluminium profiles (fig. 3.5), that guarantee high modularity, lightness with load resistance and a low cost of fabrication. The frame is firstly designed as a 4m x 0.8m x 5m parallelepipedon (Fig. 3.5a), but these lengths will be optimized in the next chapter once the final design is chosen. Moreover, the frame must ensure some relevant design aspects:

- the possibility to move discretely or continuously the anchor point of the cables that are fixed to the frame. So, four couples of linear motion guides are installed on the lateral walls of the frame (represented in blue in Fig. 3.5c). Each couple is actuated by a single electric motor (Fig.3.5b). These are essential to ensure continuous reconfigurability but represent potential high-cost components. To this end, the discrete reconfiguration will be adopted in a second phase of the design procedure to decrease the robot costs;
- the distance between the EE, which is the automatic spray gun, and the painted wall must be limited: the frame is directly installed on the wall. The structure

is closed and it is sustained by mechanical feet linked to the horizontal floor, to ensure better stability.

- the installation of safety components, such as the horizontal aluminium profiles (Fig. 3.5b), that both (i) prevent a possible human operator collision with the linear motion guides and (ii) represent a support structure for the latter, while the robot is performing the task.

The robot requirements demand specific types of cable guidance systems and sensors. In particular, in many of the aforementioned CDPR applications, the cable guidance system is made up of (i) fixed guiding pulleys, that only change the cable direction to satisfy the design constraints, usually embedded with a load cell for the cable tension measurement; (ii) swivelling pulley, usually embedded with an incremental rotary encoder that ensures important angular displacement data for the robot control; (iii) eyelet connecting points, which are less common in the latest applications due to the high cable wear rate that they produce. As an example, a translating-motor winch is shown in Fig. 3.6, with all the different types of pulleys and sensors.

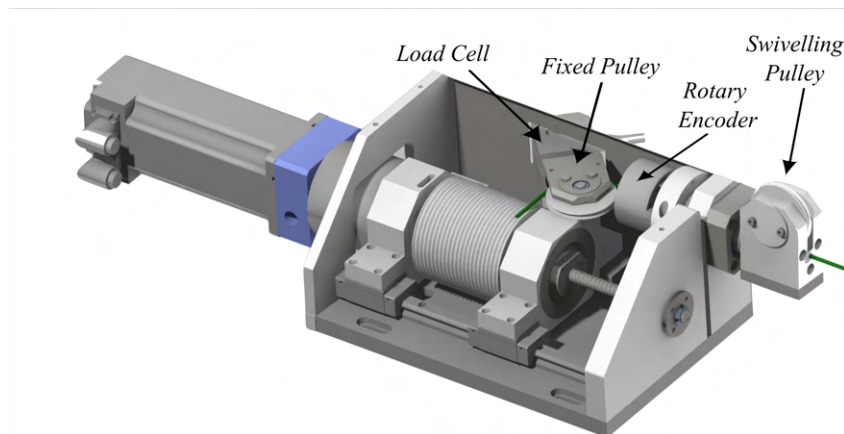


Figure 3.6: Example of guiding system and sensors

3.3 Design solutions

In this section, three different solutions will be presented by analyzing their principal characteristics. All the proposed solutions are the result of different design iterations: the main actuation units, guiding systems and sensors are the same as the one presented in the previous section, but one solution could differ from another only by changing their arrangement and combination between the frame and the mobile platform EE.

3.3.1 Frame Traslating Motor

As the title suggests, this solution implements the translating-motor servo-winchs directly installed into the linear motion guides of the machine frame (Fig. 3.7a). To obtain a planar architecture the eight cables are routed in a special network (Fig. 3.7b): four different parallelograms are identified, with a particular cable-crossing configuration [16]. Each parallelogram is actuated by a translating-motor winch. In this regard,

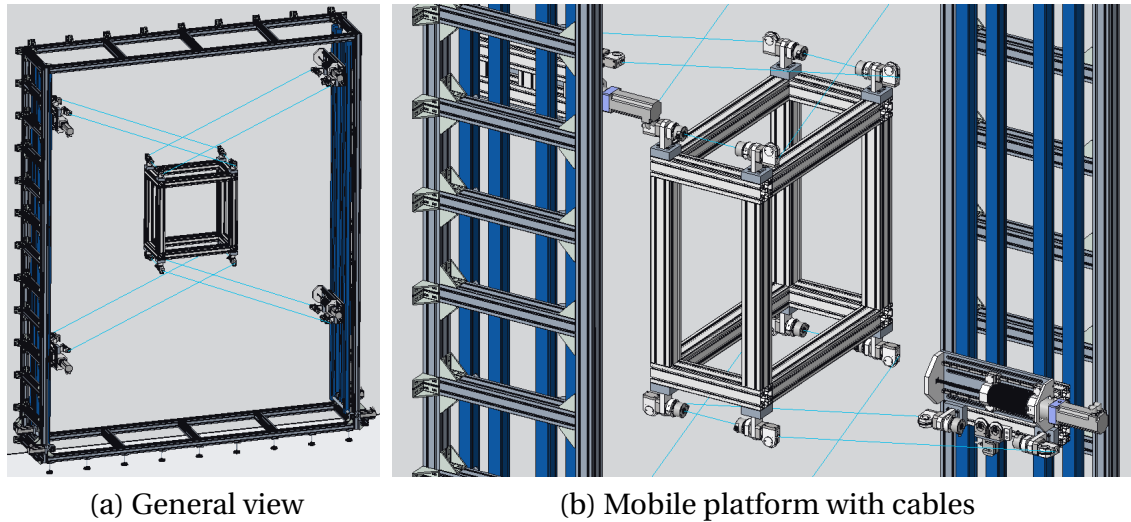


Figure 3.7: Frame translating motor solution

the winch's drum is designed with two grooving helixes, because the two different cables of a single parallelogram are routed into the same servo-winch. So, the motors are installed directly on the linear guides, able to translate in the vertical direction. The cable exits from the actuation unit and it is routed through two swivelling pulleys installed on the EE edge. These pulleys are equipped with two incremental rotary encoders. Then, the cable returns to the actuation unit and it is routed into the servo-winch.

Concerning the servo-winch drive unit, the two cables require a different drum design: it has two grooving helixes and for this reason, it has a very high axial size. If L is the total length of the cable, routed in a single parallelogram, h is the drum pitch, r is the drum radius, and n_w the number of cable winding, the axial length of the drum l_d is calculated as:

$$l_d = hn_w \quad [\text{m}], \quad \text{where} \quad n_w = \frac{L}{2\pi r} \quad (3.3)$$

Due to the kinematics of the translating-motor design, this axial length l is multiplied by a factor of 2 because the drum must wind up all the total length L of the cable, plus the translational drum length that is required to correctly route the two cables, which

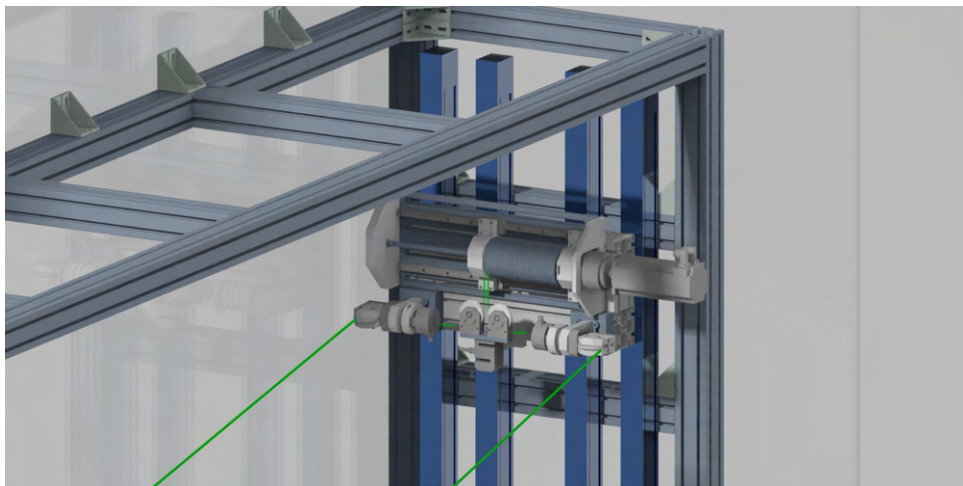


Figure 3.8: Two-grooving drum servo-winch

is namely equal to L .

From a mechanical point of view, the servo-winch is structured as follows (Fig. 3.8): the rototranslation of the drum is provided by the screw-nut coupling and the two guides that simulate a prismatic joint. The drum has two threads for the different segments of the cable. The cable exit points are close. Immediately after the drum, the cables are routed through two fixed pulleys, connected to a single load cell. In this way, it is possible to measure a mean cable tension. Then, the cables are directed through the mobile platform by two swivelling pulleys, embedded with rotary encoders.

3.3.2 EE Spooling-helper Motor

This second solution differs from the previous one because of the actuation units directly installed into the mobile platform. This feature is relevant for deployable architecture (see 2.2) due to the centralised power station: all the motors and sensors are settled into the EE. As a consequence, the frame is less complex and only four pairs of swivelling pulleys are attached to it. They represented the frame anchor points which are always movable in the vertical direction, to add a reconfigurable feature to the prototype.

The solution is represented in Fig. 3.9a. As in the first design, the planar architecture is made up of eight cables arranged in four parallelograms. The cables are crossed, passing from the bottom of the frame to the top of the mobile platform and vice-versa. The solution is slightly different because the cables remain in the right and left spaces, with respect to the EE (Fig. 3.9b), instead of in the previous solution (Fig. 3.7b) they remain in the upper and lower volume of the workspace. These cable interference considerations will be better discussed in the next chapter, once the conceptual design is chosen.

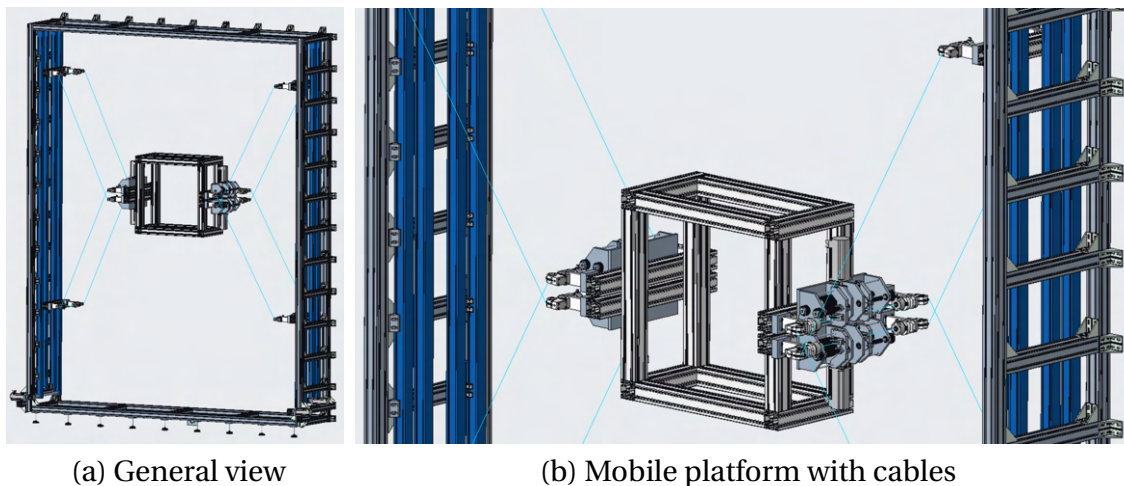


Figure 3.9: EE Spooling-helper motor solution

The servo-winch unit has a complex structure (Fig. 3.10). As in the first solution, one electric motor is responsible for two cables, having one motor for each parallelogram. Therefore, the motor is connected to two different drums thanks to a right-angle gearbox. Each drum has a spooling-helper device: a moving pulley, embedded with a load cell, is responsible for the correct orientation of the cable direction. The spooling-helper pulley is synchronised with the drum because the driving shafts are connected

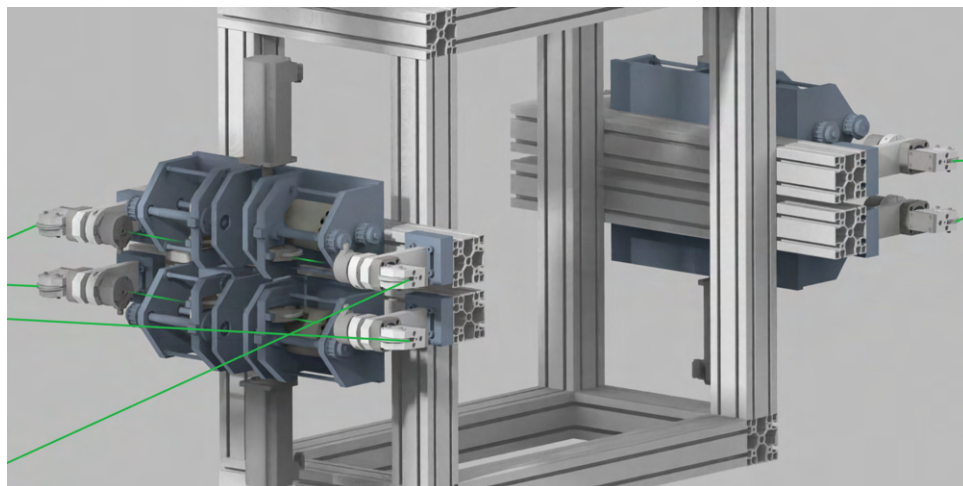
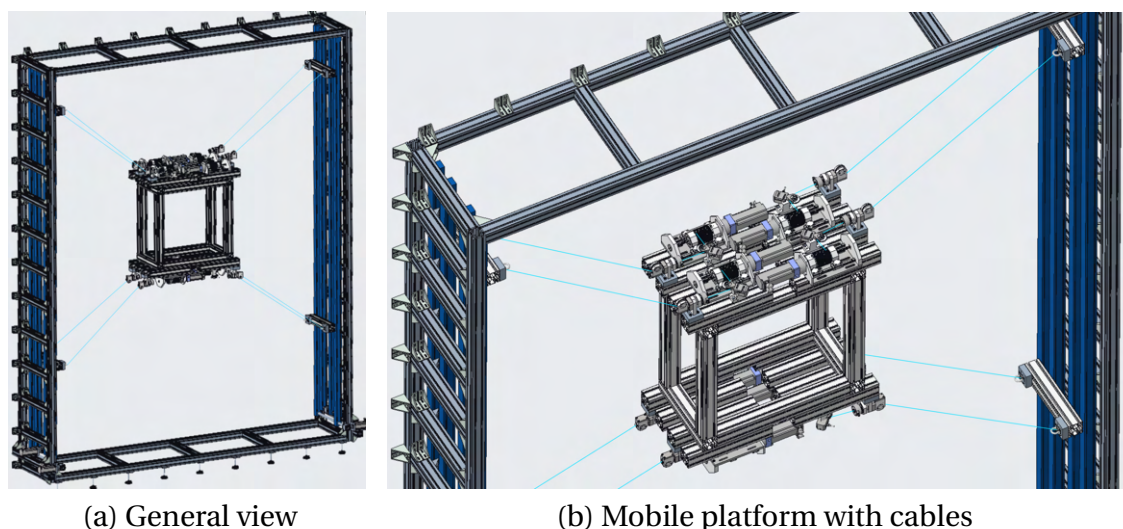


Figure 3.10: Spooling-helper winch

through a belt transmission. Finally, the cables pass through two swivelling pulleys with their encoders and are routed to the frame linear guides.

3.3.3 Eight EE Motors

The third solution has a different kinematics architecture (Fig. 3.11a). The cables are now uncoupled and the parallelograms are not present. Each cable is driven by a single servo-winch. So, the number of electric motors has doubled from four to eight. The actuation units are all installed into the mobile platform (Fig. 3.11b) and the frame anchor point is represented by a simple eyelet, installed in pairs into the frame linear guides. By introducing the uncoupling of the cables, the design flexibility increases. On the other hand, there are eight different drive axes for the control and sensor systems.



(a) General view

(b) Mobile platform with cables

Figure 3.11: Eight EE motors solution

The servo-winch is designed according to the aforementioned characteristics (see 3.1). In Fig. 3.12, the basic translating-motor winch is selected. In this way, it is easy to implement the load cell with a fixed pulley, and a rotary encoder with a swivelling pulley. The geometric shape of the overall actuation system is not optimized and the

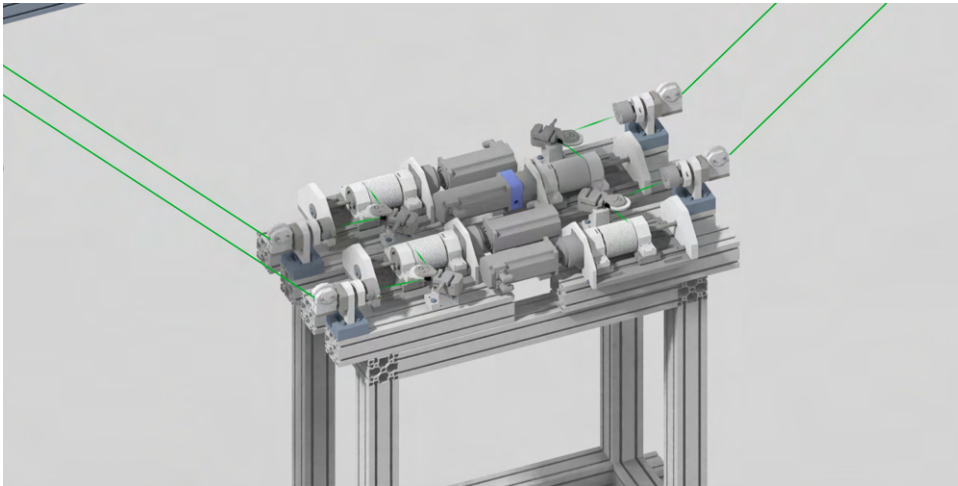


Figure 3.12: Four motors in the EE

arrangement inside the EE is just schematically represented in the rendering picture. In this solution, the servo-winch architecture could be freely chosen since no specific geometrical boundaries are set. In the next section, a specific design will be studied by analyzing the winch dynamics.

3.4 Morphological Decision Matrix

Once the three major solutions are presented, the factors that influence the decision process must be defined and for each solution, a potential score is estimated, based on the principal design characteristics. The design factors are:

- Overall complexity: this feature should be estimated by counting the number of different components (such as sensors, guiding elements, actuation elements, and frame anchor points), the mechanical design complexity in terms of customized components and winch design, and finally the number of actuated axes;
- Centralised factor: it should be calculated by analyzing the deployable and reconfigurable aspects as presented in the second chapter. For example, a solution has a higher centralised factor if its actuation and sensing units are all installed in a close environment, compared to a solution with all the units spread around the architecture;
- Load and dynamic capability: this feature is estimated by analyzing the servo-winch and its installation configuration inside the robot. Different winches have various dynamical behaviours, especially in different installation situations;
- Design flexibility: it should account for the solution's ability to adapt to different tasks in terms of velocity, force and torque applied to the EE. If a solution had high modularity or independent actuation, sensing or guiding system, it would score a high mark in this feature;
- Cost: this feature is connected to the production and maintenance costs of the mechanical components. One solution with high costs scores a lower value.

| Design factor | Solution 1 | Solution 2 | Solution 3 |
|----------------------------|------------|------------|------------|
| Overall complexity | 3 | 2 | 3 |
| Centralised factor | 1 | 5 | 4 |
| Load & dynamics capability | 2 | 4 | 2 |
| Design flexibility | 2 | 1 | 4 |
| Cost | 3 | 1 | 3 |

Table 3.1: Morphological decision matrix

Each solution can score a value between 1 to 5, where: 1 is very low; 2 is low; 3 is medium; 4 is high; 5 is very high. Obviously, these grades refer to a specific design factor: for example, if a solution has a factor cost equal to 1, it means that it has high costs and is not an optimum solution in terms of prices. All the solutions' scores are depicted in the morphological decision matrix (Table 3.1).

The first solution is the frame translating motor design (see 3.3.1). Its overall complexity is medium (3) because it has only four electric motors and the number of components is relatively small. The centralised factor is very low (0) due to its motor installation inside the frame guides. Load and dynamics capability and design flexibility are low (2) because the rototranslating winch does not have high dynamics capacity, especially if the motors are installed into the frame and do not ensure high flexibility. Concerning the cost factor this solution has a medium score (3), all the mechanical components are standard and do not require a high cost of fabrication.

The second solution is the EE spooling-helper motor design (see 3.3.2). Its overall complexity is low (2), despite having only four electric motors, there are a large number of high-complexity mechanical components. The centralised factor is very high (5) due to its actuation and sensing system installation inside the EE. Load and dynamics capability are high (4) because the spooling-helper winch has optimal performances. Concerning the design flexibility, this solution has a very low score (1), due to its mechanical complexity it is not flexible at all. Finally, the cost factor is low (2) because of the high cost of fabrication: many components are customized.

To conclude, the third solution is the eight EE motors design (see 3.3.3). Its overall complexity is medium (3) because it has eight electric motors but a small number of standard components. The centralised factor is high (4) but not like solution 2 because there is a larger number of motors and sensors installed into the EE. Load and dynamics capability is low (2) because the rototranslating winch does not have high dynamics capacity. The design flexibility is very high (5), due to its modularity and uncoupling of the eight different cables. Concerning the cost factor this solution has a medium score (3).

As it is shown in the morphological decision matrix, there is not an absolute optimal solution. In fact, the best is a combination of solution 2 and solution 3. From the mechanical point of view, the solution 2 spooling-helper winch has a better score in terms of load and dynamics capability than the rototranslating winch adopted in solution 3. On the other hand, the decoupling of the cables is optimum in terms of design flexibility and modularity. Moreover, the standard spooling-helper winch design has a lower complexity and the costs are limited compared to the particular application of solution 2, with customized components. Both of the solutions share the installation of the drive unit directly into the EE mobile platform.

In conclusion, the ultimate conceptual design for the eight-cable, planar, overconstrained, robot is derived. The shown design iteration procedure highlights the main features reported in the next lines. Before summarizing them, the author clarifies a particular aspect linked to the prototype development. During the cost evaluation of each solution, the cost factor has become more and more relevant. To this end, the actuation linear guides that were presented in the frame description (see 3.2), are now an oversized cost that can be easily deleted by adopting a discrete reconfiguration approach. The fixed anchor point can be modified off-line, by simply moving the eyelet anchor point from one aluminium extruded profile to another, considering that the frame lateral wall is made up of many little horizontal profiles, as in the Fig. 3.5a. So, the final conceptual design can be summarized as follows:

- 8 frame anchor points, of which the upper 4 can be moved in the vertical direction changing the extruded aluminium profile as their frame reference. The frame anchor point is a simple eyelet;
- 8 mobile platform anchor points, with 8 motors directly installed into the platform. Each cable is independent: the final design is an eight-cable, planar, overconstrained robot;
- the servo-winch is designed according to the spooling-helper architecture, maximizing the load and dynamics capability with a restricted geometrical shape;
- the guiding pulleys and sensors are directly installed into the mobile platform, guaranteeing the deployable feature with a high centralised factor;

Chapter 4

Optimisation Algorithms for Mechanical Design

The state of the art for deployable and reconfigurable CDPR is now clear. For the first type, the configuration requirements can be rehashed by highlighting the centralisation of the electric servo-winch and sensing system directly into the mobile platform. On the other hand, concerning the reconfiguration capability of the robot, there are two distinct approaches: discrete and continuous reconfiguration. The first one is selected in the presented prototype due to the cost constraint.

The principal performance indexes for this CDPR architecture are estimated based on the feasible workspace. In particular, the wrench feasibility analysis is very common for CDPR, and the related workspace volume is a key index for this application. Inside the workspace computation, the cable interference check is a relevant aspect. Moreover, for overconstrained CDPR, it is necessary to adopt a strict interference check algorithm to avoid unfeasible points inside the workspace.

Once the performance indexes are defined, the implementation of optimisation algorithms helps to find the theoretically global optimum mechanical design for a specific cost function. In this thesis, the local optimum algorithm and genetic algorithm are applied to solve a multivariable problem, minimizing the worthless workspace volume, calculated as the difference between the maximum installation volume and the actual workspace. The genetic algorithms implement a stochastic approach to solve the minimizing problem, instead, the local optimum algorithms apply a gradient-based method to converge to a solution, starting from a particular point. The combination of both guarantees a widespread group of possible solutions to be analyzed.

This chapter aims at finding the mechanical design of the robotic prototype, by starting from the results derived in the previous chapters. The eight-cable, planar, overconstrained architecture has been chosen, but the cable configuration and the specific location of the sixteen anchor points have not been selected yet. The result of the optimisation algorithms is the final mechanical design, answering these specific requirements. In the first section of the fourth chapter, a general overview of optimisation problems is set, emphasising the two main categories of the adopted algorithm: local optimum gradient-based approach and genetic algorithm. Then, it is necessary to define a cost function to be evaluated and minimized, according to the performance indexes. The cost function is the worthless workspace volume, written with respect to sixteen anchor-point variables. Therefore, the wrench feasible workspace computation is presented and a novel cable interference check is introduced. Finally, the results

of the optimisation process are derived and the final workspace is computed.

4.1 Optimisation Algorithms

A typical engineering design optimisation process is shown in Fig. 4.1. The role of the designer is to provide a problem specification that details the parameters, constants, objectives, and constraints that are to be achieved. The designer is responsible for crafting the problem and quantifying the merits of potential designs. The designer also typically supplies a baseline design or initial design point to the optimisation algorithm. An optimisation algorithm is used to incrementally improve the design until it can no longer be improved or until the budgeted time or cost has been reached. The designer is responsible for analyzing the result of the optimisation process to ensure its suitability for the final application. Misspecifications in the problem, poor baseline designs, and improperly implemented or unsuitable optimisation algorithms can all lead to suboptimal or dangerous designs.

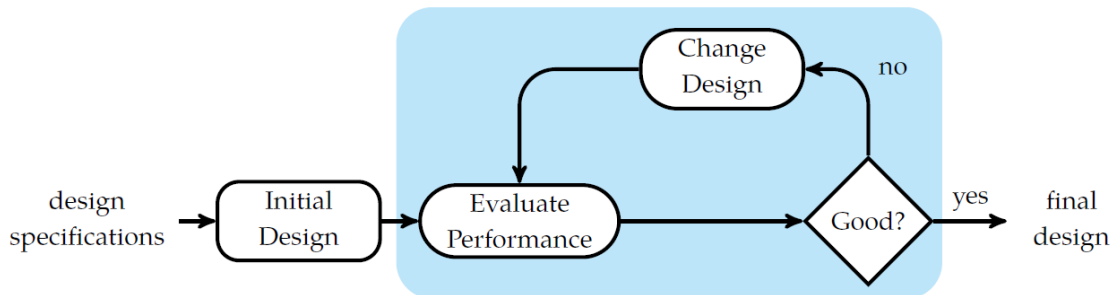


Figure 4.1: Engineering design optimisation process

There are several advantages of an optimisation approach to engineering design. First of all, the optimisation process provides a systematic, logical design procedure. If properly followed, optimisation algorithms can help reduce the chance of human error in design. Sometimes intuition in engineering design can be misleading; it can be much better to optimise with respect to data. Optimisation can speed the process of design, especially when a procedure can be written once and then be reapplied to other problems. Traditional engineering techniques are often visualized and reasoned about by humans in two or three dimensions. Modern optimisation techniques, however, can be applied to problems with millions of variables and constraints. Also in this project, the number of design variables is high: there are sixteen anchor points and for each of them the three cartesian dimensions must be defined. The theoretical number of optimisation variables is 45.

There are also challenges associated with using optimisation for design. We are generally limited in our computational resources and time, and so our algorithms have to be selective in how they explore the design space. Fundamentally, the optimisation algorithms are limited by the designer's ability to specify the problem. In some cases, the optimisation algorithm may exploit modelling errors or provide a solution that does not adequately solve the intended problem. When an algorithm results in an apparently optimal design that is counterintuitive, it can be difficult to interpret. Another limitation is that many optimisation algorithms are not guaranteed to produce optimal designs.

4.1.1 Basic Optimisation Problem

The basic optimisation problem is:

$$\min_{\mathbf{x}} f(\mathbf{x}); \quad \text{where } \mathbf{x} \in \mathcal{X} \quad (4.1)$$

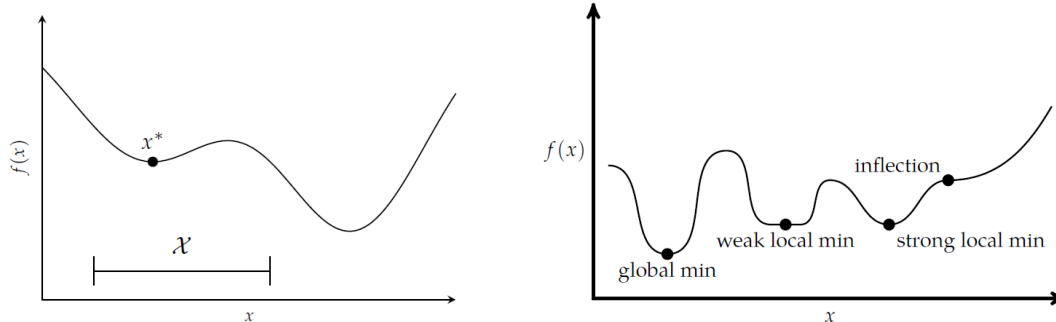
Here, \mathbf{x} is a design point and f is the so-called cost function to be minimized. A design point can be represented as a vector of values corresponding to different design variables. An n -dimensional design point is written as:

$$[x_1, x_2, \dots, x_i, \dots, x_n] \quad (4.2)$$

Any value of \mathbf{x} from among all points in the feasible set \mathcal{X} that minimizes the objective function is called a solution or minimizer. Fig 4.2a shows an example of a one-dimensional optimisation problem. This formulation is general, meaning that any optimisation problem can be rewritten according to Eq. 4.1. If the maximum of the function must be found instead, the problem can be reformulated by minimizing $-f(\mathbf{x})$ without losing in generalities. The new form is the same problem in that it has the same set of solutions.

Many problems have constraints. Each constraint limits the set of possible solutions, and together the constraints define the feasible set \mathcal{X} . Feasible design points do not violate any constraints. Constraints are typically written as inequalities or equalities. If constraints involve strict inequalities, then the feasible set does not include the constraint boundary. A potential issue with not including the boundary could occur if the optimal solution lies on it. In this configuration, an infinite number of values exists near the boundary solution. To avoid such issues, it is often best to include the constraint boundary in the feasible set.

Another important aspect of the optimisation method is the analysis of critical points. Fig. 4.2b shows a monodimensional function with several labelled critical points, where the derivative is zero. When minimizing the function, we wish to find a global minimizer, a value of x for which $f(x)$ is minimized. A function may have at most one global minimum, but it may have multiple local minimizers. Unfortunately, it is generally difficult to prove that a given candidate point is at a global minimum. Often, the best to do is to check whether it is at a local minimum. A point x^* is at a local minimum (or is a local minimizer) if there exists a $\delta > 0$ such that $f(x^*) \leq f(x)$



(a) Mono-dimensional problem

(b) Critical points

Figure 4.2: Basic optimisation problem

for all x with $\|x - x^*\| < \delta$. In the multidimensional context, this definition generalizes to there being a $\delta > 0$ such that $f(\mathbf{x}^*) \leq f(\mathbf{x})$ whenever $\|\mathbf{x} - \mathbf{x}^*\| < \delta$.

Fig. 4.2b shows two types of local minima: strong local minima and weak local minima. A strong local minimizer, also known as a strict local minimizer, is a point that uniquely minimizes f within a neighbourhood. In other words, \mathbf{x}^* is a strict local minimizer if there exists a $\delta > 0$ such that $f(\mathbf{x}^*) \leq f(\mathbf{x})$ whenever $\mathbf{x}^* \neq \mathbf{x}$ and $\|\mathbf{x} - \mathbf{x}^*\| < \delta$. A weak local minimizer is a local minimizer that is not a strong local minimizer. The derivative is zero at all local and global minima of continuous, unbounded objective functions. While having a zero derivative is a necessary condition for a local minimum, it is not a sufficient condition. Fig. 4.2b also has an inflexion point where the derivative is zero but the points are never minima. An inflexion point is where the sign of the second derivative of f changes, which corresponds to a local minimum or maximum of f' .

Many numerical optimisation methods seek local minima. Local minima are locally optimal, but we do not generally know whether a local minimum is a global minimum. The conditions for local minima assume that the objective function is differentiable. In a multidimensional context, the following conditions are necessary for \mathbf{x} to be at a local minimum of f :

1. $\nabla f(\mathbf{x}) = \mathbf{0}$, the first-order necessary condition (FONC);
2. $\nabla^2 f(\mathbf{x})$ is positive semidefinite, the second-order necessary condition (SONC).

The FONC tells us that the function is not changing at \mathbf{x} . Fig. 4.3 shows examples of multivariate functions where the FONC is satisfied. The SONC tells us that \mathbf{x} is in a bowl. The FONC and SONC can be obtained from a simple analysis. In order for \mathbf{x}^* to be at a local minimum, it must be smaller than those values around it:

$$f(\mathbf{x}^*) \leq f(\mathbf{x}^* + h\mathbf{y}) \Leftrightarrow f(\mathbf{x}^* + h\mathbf{y}) - f(\mathbf{x}^*) \geq 0 \quad (4.3)$$

If we wrote the second-order approximation for $f(\mathbf{x}^*)$, we get:

$$f(\mathbf{x}^* + h\mathbf{y}) = f(\mathbf{x}^*) + h\nabla f(\mathbf{x}^*)^\top \mathbf{y} + \frac{1}{2}h^2\mathbf{y}^\top \nabla^2 f(\mathbf{x}^*)\mathbf{y} + O(h^3) \quad (4.4)$$

We know that at a minimum, the first derivative must be zero, and we neglect the higher-order terms. Rearranging the terms and having in mind the Eq. 4.3, we get:

$$f(\mathbf{x}^* + h\mathbf{y}) \simeq f(\mathbf{x}^*) + \frac{1}{2}h^2\mathbf{y}^\top \nabla^2 f(\mathbf{x}^*)\mathbf{y} \Leftrightarrow \frac{1}{2}h^2\mathbf{y}^\top \nabla^2 f(\mathbf{x}^*)\mathbf{y} \geq 0 \quad (4.5)$$

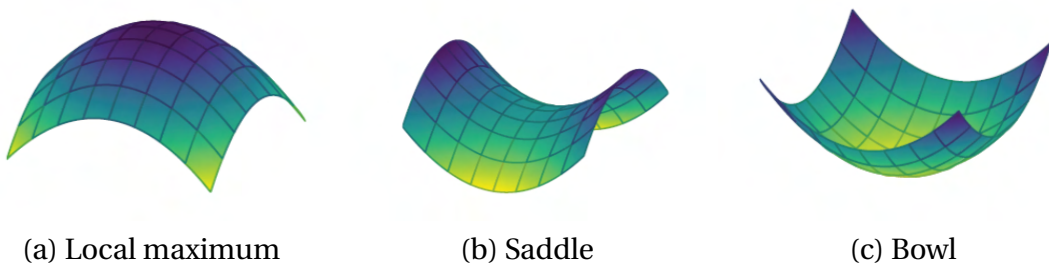


Figure 4.3: Example of first-order necessary condition satisfied

This is the definition of a positive semidefinite matrix, and we recover the SONC. Looking at Fig. 4.3, it is possible to distinguish three different situations: in the local maximum the gradient at the centre is zero, but the Hessian is negative definite (Fig. 4.3a); in the saddle, the gradient at the centre is zero, but it is not a local minimum (Fig. 4.3b); in the bowl, the gradient at the centre is zero and the Hessian is positive definite (Fig. 4.3c). It is a local minimum.

4.1.2 Local Optimum Algorithm

As presented in the previous section, optimisation is concerned with finding the design point that minimizes (or maximizes) an objective function. Knowing how the value of a function changes as its input is varied is useful because it tells the direction to improve on previous points. The change in the value of the function is measured by the gradient in multiple dimensions. There are different types of algorithms that use local models to incrementally improve a design point until some convergence criterion is met. These algorithms are called *local optimum* algorithm and they use first- and second-order models built from gradient or Hessian information. One example of this type of algorithm is the *fmincon* MATLAB[®] function, which will be adopted in the mechanical design optimisation procedure.

A common approach to local optimisation is to incrementally improve a design point \mathbf{x} by taking a step that minimizes the objective value based on a local model. The local model may be obtained, for example, from a first- or second-order Taylor approximation. Optimisation algorithms that follow this general approach are referred to as descent direction methods. They start with a design point \mathbf{x}_0 and then generate a sequence of points, sometimes called iterates, to converge to a local minimum. The choice of \mathbf{x}_0 can affect the success of the algorithm in finding a minimum. Domain knowledge is often used to choose a reasonable value. When that is not available, there are specific techniques that can search over the design space.

The iterative descent direction procedure involves the following steps:

1. Check whether \mathbf{x}_k satisfies the termination conditions. If it does, terminate; otherwise, proceed to the next step.
2. Determine the descent direction \mathbf{d}_k using local information such as the gradient or Hessian.
3. Determine the step size or learning rate α_k . Some algorithms attempt to optimize the step size so that the step maximally decreases f .
4. Compute the next design point according to:

$$\mathbf{x}_{k+1} \leftarrow \mathbf{x}_k + \alpha_k \mathbf{d}_k \quad (4.6)$$

Concerning the first-order method, an intuitive choice for descent direction \mathbf{d} is the direction of the steepest descent. Following the direction of the steepest descent is guaranteed to lead to improvement, provided that the objective function is smooth, the step size is sufficiently small, and we are not already at a point where the gradient is zero, called a stationary point. The direction of the steepest descent is the direction opposite the gradient ∇f , hence the name gradient descent. It is defined as:

$$\mathbf{g}_k = \nabla f(\mathbf{x}_k) \quad (4.7)$$

where \mathbf{x}_k is the design point at the descent iteration k .

In gradient descent, the direction of the steepest descent is typically normalized:

$$\mathbf{d}_k = -\frac{\mathbf{g}_k}{\|\mathbf{g}_k\|} \quad (4.8)$$

Jagged search paths result if the chosen step size leads to the maximal decrease in f . In fact, the next direction will always be orthogonal to the current direction, as it is demonstrated in the following lines. If the step size is optimised at each step, we have:

$$\alpha_k = \operatorname{argmin}_{\alpha} f(\mathbf{x}_k + \alpha \mathbf{d}_k) \quad (4.9)$$

The above optimisation implies that the directional derivative equals zero. In this regard, we have:

$$\nabla_{\mathbf{d}} f = \nabla f(\mathbf{x}_k + \alpha \mathbf{d}_k)^{\top} \mathbf{d}_k = 0 \quad (4.10)$$

Where:

$$\mathbf{d}_{k+1} = -\frac{\nabla f(\mathbf{x}_k + \alpha \mathbf{d}_k)}{\|\nabla f(\mathbf{x}_k + \alpha \mathbf{d}_k)\|} \quad (4.11)$$

Hence:

$$\mathbf{d}_{k+1}^{\top} \mathbf{d}_k = 0 \quad (4.12)$$

which means that \mathbf{d}_{k+1} and \mathbf{d}_k are orthogonal (Fig. 4.4).

Gradient descent can perform poorly in narrow valleys. For this reason, a lot of different first-order approaches can be performed: another example is the conjugate gradient that borrows inspiration from the optimising quadratic functions. Regarding the second-order method instead, the Hessian for multivariate optimisation is implemented. Knowing the function value and gradient for a design point can help determine the direction to travel, but this first-order information does not directly help determine how far to step to reach a local minimum. Second-order information, on the other hand, makes a quadratic approximation of the objective function and approximates the right step size to reach a local minimum. For this reason, incorporating second-order information in descent methods often speeds up convergence.

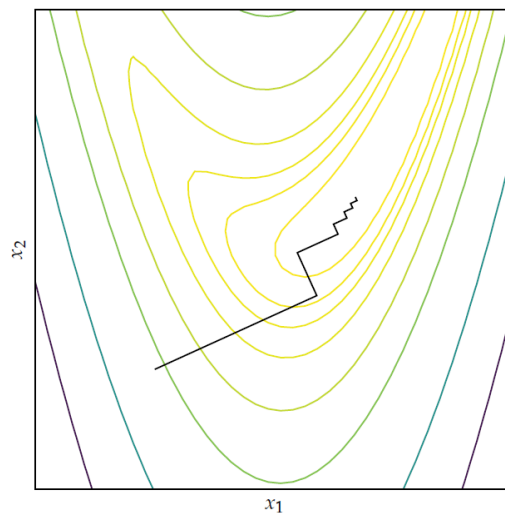


Figure 4.4: Example of zig-zagging gradient descent for a two-dimensional problem

4.1.3 Genetic Algorithm

If the previous methods are strongly related to finding a local optimum point, the genetic algorithm is suited for searching for a global one instead. The genetic algorithm is part of population methods, based on stochastic approach. These methods use randomization strategically to help explore the design space for an optimum. Randomness can help escape local optima and increase the chances of finding a global optimum, especially if the problem has a large number of variables.

Population methods involve optimisation using a collection of design points, called individuals. Having a large number of individuals distributed throughout the design space can help the algorithm avoid becoming stuck in a local minimum. Information at different points in the design space can be shared between individuals to globally optimise the objective function.

Population methods begin with an initial population, just as descent methods require an initial design point. The initial population should be spread over the design space to increase the chances that the samples are close to the best regions. It is often possible to constrain the design variables to a region of interest consisting of a hyperrectangle defined by lower and upper bounds \mathbf{a} and \mathbf{b} . Initial populations can be sampled from a uniform distribution (in Fig. 4.5 the boundaries are set by $\mathbf{a} = [-2; -2]$, $\mathbf{b} = [2; 2]$). Another common approach is to use a multivariate normal distribution centred over a region of interest. Uniform and normal distributions limit the covered design space to a concentrated region. The Cauchy distribution has an unbounded variance and can cover a much broader space (Fig. 4.5). On the other hand, genetic algorithms start with a random initial population.

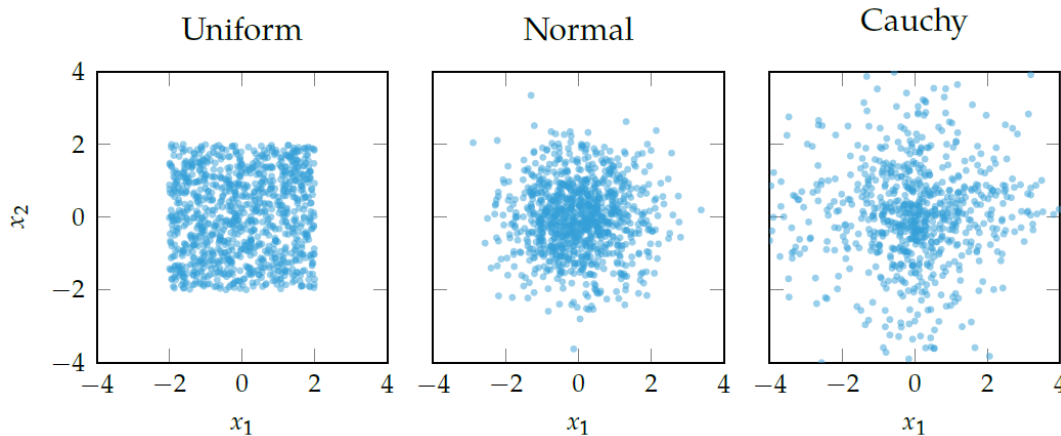


Figure 4.5: Initial population distribution

Genetic algorithm borrows inspiration from biological evolution, where fitter individuals are more likely to pass on their genes to the next generation. An individual's fitness for reproduction is inversely related to the value of the objective function at that point. The design point associated with an individual is represented as a chromosome. At each generation, the chromosomes of the fitter individuals are passed on to the next generation after undergoing the genetic operations of crossover and mutation.

There are several ways to represent chromosomes. The simplest is the binary string chromosome, a representation that is similar to the way DNA is encoded. Binary strings are often used due to the ease of expressing crossover and mutation. Unfortunately, the process of decoding a binary string and producing a design point is not always straight-

forward. Sometimes the binary string might not represent a valid point in the design space. It is often more natural to represent a chromosome using a list of real values. Such real-valued chromosomes are vectors in \mathbb{R}^n that directly correspond to points in the design space.

Selection is the process of choosing chromosomes to use as parents for the next generation. For a population with m chromosomes, a selection method will produce a list of m parental pairs for the m children of the next generation. The selected pairs may contain duplicates. There are several approaches for biasing the selection toward the fittest:

- In truncation selection, we sample parents from among the best k chromosomes in the population.
- In tournament selection, each parent is the fittest out of k randomly chosen chromosomes of the population.
- In roulette wheel selection, also known as fitness proportionate selection, each parent is chosen with a probability proportional to its performance relative to the population.

Since we are interested in minimizing an objective function f , the fitness of the i -th individual x_i is inversely related to $y_i = f(x_i)$. There are different ways to transform a collection y_1, \dots, y_m into fitnesses. A simple approach is to assign the fitness of individual i according to $\max[y_1, \dots, y_m] - y_i$.

Furthermore, crossover combines the chromosomes of parents to form children. As with selection, there are several crossover schemes:

- In single-point crossover (Fig.4.6), the first portion of parent A's chromosome forms the first portion of the child chromosome, and the latter portion of parent B's chromosome forms the latter part of the child chromosome. The crossover point where the transition occurs is determined uniformly at random.

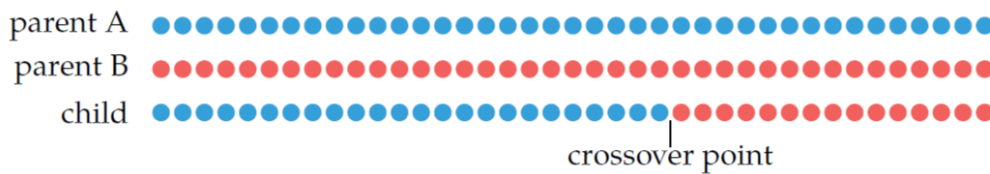


Figure 4.6

- In two-point crossover (Fig. 4.7), we use two random crossover points.

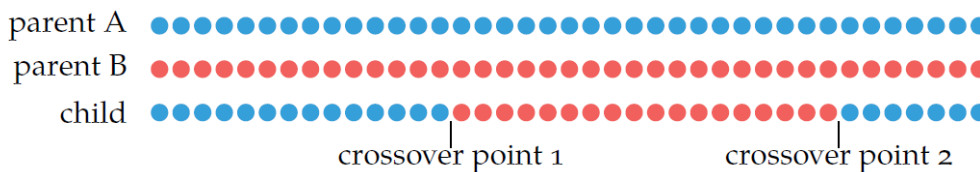


Figure 4.7

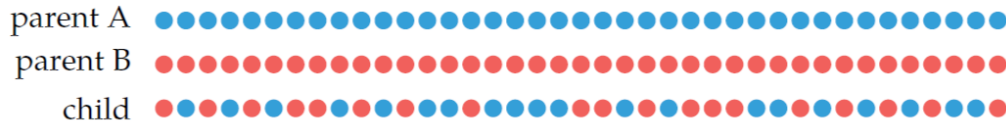


Figure 4.8

- In uniform crossover (Fig. 4.8), each bit has a fifty per cent chance of coming from either one of the two parents. This scheme is equivalent to each point having a fifty per cent chance of being a crossover point.

Note that the previous crossover methods also work for real-valued chromosomes. We can, however, define an additional crossover routine that interpolates between real values.

If new chromosomes were produced only through crossover, many traits that were not present in the initial random population could never occur, and the most-fit genes could saturate the population. Mutation allows new traits to spontaneously appear, allowing the genetic algorithm to explore more of the state space. Child chromosomes undergo mutation after crossover. Each bit in a binary-valued chromosome typically has a small probability of being flipped. For a chromosome with m bits, this mutation rate is typically set to $1/m$, yielding an average of one mutation per child chromosome. Mutation for real-valued chromosomes can be implemented using bitwise flips, but it is more common to add zero-mean Gaussian noise.

To conclude, a genetic algorithm with truncation selection, single-point crossover, and Gaussian mutation with $\sigma = 0.1$, is applied to a typical optimisation test function called Michalewicz function. The visual result, extrapolating four important generations, is presented in Fig. 4.9. This example clearly explains how a genetic algorithm could find a global minimum, in yellow in the figure, even though local minima are present. Instead, a local minimum optimisation algorithm would not be able to find the global one if its starting point is not well-defined. To this end, in the next sections, a hybrid optimisation procedure will be depicted: (i) firstly, a genetic algorithm is run, using *ga* MATLAB[®] function, to find a design point possibly near to the global minimum solution; (ii) secondly, the *fmincon* function is implemented, starting from the *ga*'s result, to better converge to this solution.

4.2 Cost Function Definition

Once the optimisation techniques are illustrated, it is necessary to correctly define the function f , usually called the cost function, to be optimised. In this regard, the most

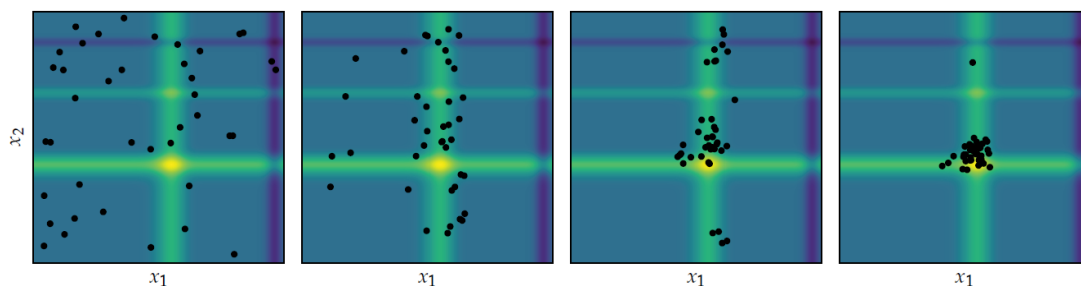


Figure 4.9: Genetic algorithm application

common performance indexes for CDPR are calculated for the workspace analysis. In this thesis, the cost function to be minimized is defined as the weighted sum of the worthless workspace volume and a barycenter factor that accounts for the workspace symmetry with respect to the frame. The weighted coefficients have been selected according to experimental evidence because during the optimisation simulations, different combinations of factors were tested and the 80%-20% weighting criteria produced the best design result. Therefore, the cost function to be minimized is defined as:

$$f(\mathbf{x}) = \frac{4}{5}V_w(\mathbf{x}) + \frac{1}{5}\lambda(\mathbf{x}) \quad (4.13)$$

Where the worthless volume $V_w(\mathbf{x})$ is expressed as function of the percentage workspace $V_{ws}(\mathbf{x})$:

$$V_w(\mathbf{x}) = 100 - V_{ws}(\mathbf{x}) \quad [\%] \quad (4.14)$$

And the barycenter factor $\lambda(\mathbf{x})$ is represented as a percentage factor, normalising the distance between the workspace and the frame centres $\mathbf{p}_{ws}(\mathbf{x})$, with respect to a maximum distance set to 1m:

$$\lambda(\mathbf{x}) = \frac{\|\mathbf{p}_{ws}(\mathbf{x})\|}{1} \cdot 100 \quad [\%] \quad (4.15)$$

The two coefficients V_w and λ are both expressed as percentage values in order to obtain a coherent formulation for the cost function.

The cost function $f(\mathbf{x})$ is evaluated by the cable anchor points: eight frame points and eight mobile platform points. For each anchor point, there are three variables associated with the three dimensions x_i, y_i, z_i of the i -th anchor point. So, the variable design vector is structured as follows:

$$\mathbf{x} = [x_1, y_1, z_1, \dots, x_i, y_i, z_i, \dots, x_{m-1}, y_{m-1}, z_{m-1}] \quad (4.16)$$

where m is the number of cables, set to 8 in this thesis. One frame anchor point is fixed to have a reference origin point in the simulation, and for this reason, the total number of elements inside the variable \mathbf{x} is equal to 45.

Therefore, the volume of the workspace $V_{ws}(\mathbf{x})$ and the position vector of its barycentre $\mathbf{p}_{ws}(\mathbf{x})$ represent the cost function parameters to be evaluated. In the next section, a wrench-feasible algorithm is presented to compute the total workspace of the CDPR. In this algorithm, a cable interference check for the overconstrained architecture is defined.

4.2.1 Workspace Computation

The presented wrench-feasible workspace algorithm is based on the Gouttefarde et al. study [8], where a particular case in which the number of cables m is equal to the number of EE degrees of freedom $n + 2$, as in the thesis design where $m = 8$ and $n = 6$.

The cable tension vector $\mathbf{t} \in \mathbb{R}^m$, is said feasible if it satisfies:

$$\mathbf{0} \leq \mathbf{t}_{min} \leq \mathbf{t} \leq \mathbf{t}_{max} \quad (4.17)$$

The tensions have to be non-negative since the cables cannot push on the mobile platform. The maximum values \mathbf{t}_{max} are generally set by the breaking loads of mechanical parts or by the maximum actuator torques, while positive values in \mathbf{t}_{min} should avoid

where each inequality defines a half-plane bounded by a line corresponding to values of μ for which one cable tension is equal to the boundaries \mathbf{t}_{min} or \mathbf{t}_{max} . The intersection of the $2m$ half-planes identifies the feasible polygon \mathcal{A} (Fig. 4.10).

The polygon edges can be followed to reach a feasible point (if it exists) and then to compute all the feasible polygon vertices in order. The knowledge of the vertices (in a clockwise or counterclockwise order) completely determines the polygon geometry and thus allows a direct determination of various tension distributions. The algorithm can start at any intersection point (feasible or not) between two lines bounding half-planes defined by inequalities of Eq. 4.21. Moreover, the vertices are determined in a clockwise or counterclockwise order which allows a direct determination of various cable tension distributions, by different methods such as the 2-norm optimal distribution, the 1-norm optimal distribution, the centroid, and the weighted barycentre [8].

To this end, the workspace computation is done by discrete points. The pose of the EE is tested inside the workspace limits, set by the maximum installation size of the frame. So, testing for each of the three dimensions x, y, z the EE pose, if the tested point is feasible, in terms of the aforementioned wrench feasibility, it is saved. In this manner, all the workspace is searched and the percentage volume $V_{ws}(\mathbf{x})$ is estimated as the feasible points out of the total tested points. On the other hand, due to the discrete formulation of the workspace, calculated as a set of points, the barycentre $\mathbf{p}_{ws}(\mathbf{x})$ is estimated as the mean of all the feasible points.

4.2.2 Cable Interference

Another important condition that must be implemented in the feasible workspace computation, is the cable interference check. Especially for overconstrained robots, where the high number of cables arranged in different directions could create an obstacle for the mobile platform movement, the interference check gains particular importance. As presented in the second chapter (see 2.1), this thematic represents a classical and well-known problem for CDPR [66]. In this thesis, the classical interference check is extended to consider other two special conditions.

First of all, the cable segments are theoretically represented by straight lines (Fig. 4.11). The interference between the cable lines is calculated by checking the shortest distance between them and searching for all the possible combinations of cables. The frame anchor points are D_i and D_j , defined by their position vectors \mathbf{d}_i and \mathbf{d}_j with respect to the absolute frame $Oxyz$, the cable unit vectors are \mathbf{u}_i and \mathbf{u}_j , so the coordinates of two generic points \mathbf{p}_i and \mathbf{p}_j along the corresponding lines are given by:

$$\mathbf{p}_i = \mathbf{d}_i + k_i \mathbf{u}_i \quad \mathbf{p}_j = \mathbf{d}_j + k_j \mathbf{u}_j \quad (4.22)$$

Where k_i and k_j are two scalar values that span the points along the lines. The direction versor of the common normal line is calculated with the cross-product $\mathbf{n} = \mathbf{u}_i \times \mathbf{u}_j$. If the two cable lines are parallel, their versors cross-product is null and they do not produce interference. Instead, by projecting the two points D_i and D_j along this normal versor \mathbf{n} , the scalar distance d_{ij} is:

$$d_{ij} = \frac{|\mathbf{n} \cdot (\mathbf{p}_i - \mathbf{p}_j)|}{\|\mathbf{n}\|} = \frac{|\mathbf{n} \cdot (\mathbf{d}_i - \mathbf{d}_j)|}{\|\mathbf{n}\|} \quad (4.23)$$

Since the normal versor \mathbf{n} is orthogonal to both the cable versors \mathbf{u}_i and \mathbf{u}_j . If the scalar distance d_{ij} is smaller than a minimum distance, set to 8 mm because of the cable

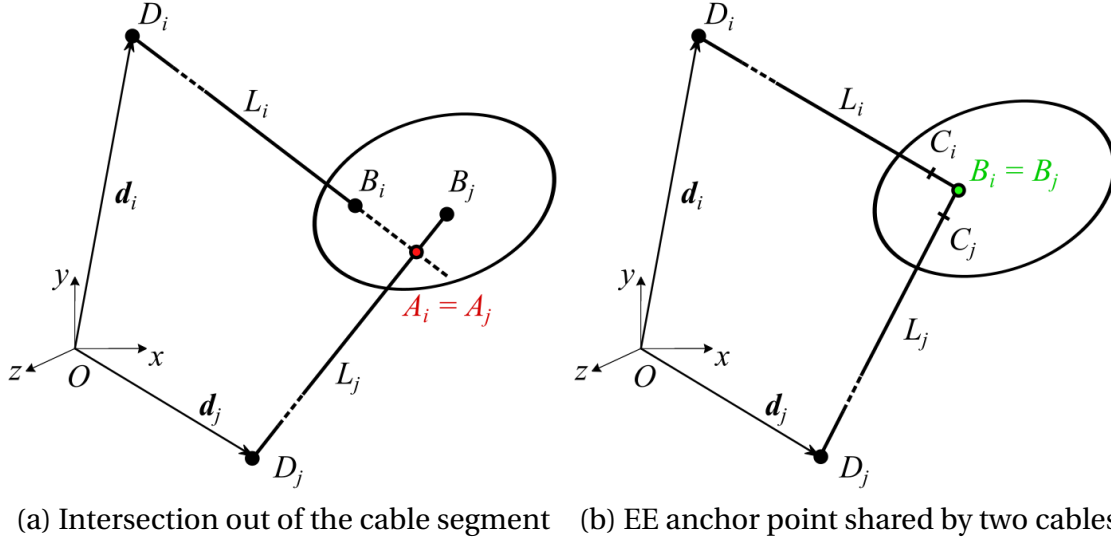


Figure 4.11: Two special cable interference conditions

diameter of 3 mm and a tolerance of 5 mm, the cables are producing interference and the tested pose point is not feasible, although it is a wrench-feasible point. This is the classical cable interference check for CDPRs.

Other two particular situations can occur even though the first interference check has a negative result. If the distance d_{ij} is smaller than the set minimum distance, the cable lines are close but do not always produce real interference. In fact, the shortest distance is calculated between the cable lines, but real cables represent finite segments instead. To this point, the shortest distance could occur at a point that is inside the cable line but outside the cable segment, which represents the real cable length (Fig. 4.11a). Moreover, in many CDPR designs, the cable EE anchor points are shared, and more than one cable has the same mobile platform anchor point (Fig. 4.11b). This configuration would produce a negative result in the classical interference check and should be avoided in this implementation. The intersection points between the cable lines and the shortest distance line have to be calculated, and a further check to see if these points are inside or outside the real cable segments has to be done. To find the location for A_i and A_j , which are the points on each cable line closest to the other cable line, the scalar values k_i and k_j are calculated as:

$$k_i = \frac{(\mathbf{u}_j \times \mathbf{n}) \cdot (\mathbf{d}_j - \mathbf{d}_i)}{\mathbf{n} \cdot \mathbf{n}} \quad k_j = \frac{(\mathbf{u}_i \times \mathbf{n}) \cdot (\mathbf{d}_j - \mathbf{d}_i)}{\mathbf{n} \cdot \mathbf{n}} \quad (4.24)$$

Substituting these values inside the Eq.4.22, the position vectors \mathbf{p}_{A_i} and \mathbf{p}_{A_j} of the points A_i and A_j are defined in the absolute frame. Therefore, to understand if these points lie inside the cable segments, the following constraints must be satisfied:

$$|\mathbf{p}_{A_i} - \mathbf{d}_i| \leq L_i - t \quad \wedge \quad |\mathbf{p}_{A_j} - \mathbf{d}_j| \leq L_j - t \quad (4.25)$$

Where the actual cable lengths L_i and L_j are modified by a tolerance $t = |B_i - C_i| = |B_j - C_j| = 10$ mm, to avoid the configuration of a single EE anchor point shared by two different cables. The points C_i and C_j represent the cables' endpoint (Fig. 4.11b). If these relations are satisfied the cables are interfering and the tested pose point is definitely not feasible. The MATLAB[®] implementation is presented in Appendix B.

4.3 Optimisation Results

In this final section, the previous optimisation procedure is finally tested and the results are analyzed. The cost function $f(\mathbf{x})$, presented in Eq. 4.13, is obtained in a discrete manner. The algorithm tests, for each possible pose, if the actual point is feasible in terms of wrench and cable interference feasibility. To this end, the cost function is discretized and its step resolution is directly influenced by the number of tested points inside the workspace.

Concerning the variable \mathbf{x} instead, defined in the Eq. 4.16, the anchor points coordinates are restricted to a subset of feasible values. In particular, having in mind that the frame centre is the inertial reference frame origin, the aforementioned subset for the frame anchor point is defined in meter [m], $\forall i = 1, \dots, 7$ as:

$$\begin{cases} -4 \leq x_i \leq 4 \\ -0.5 \leq y_i \leq 0.5 \\ -3 \leq z_i \leq 3 \end{cases} \quad (4.26)$$

The optimisation process is subdivided into two main parts: (i) first research with a genetic algorithm, implementing the *ga* MATLAB[®] function, and (ii) second research optimising the previous results by using the *fmincon* MATLAB[®] function. The results

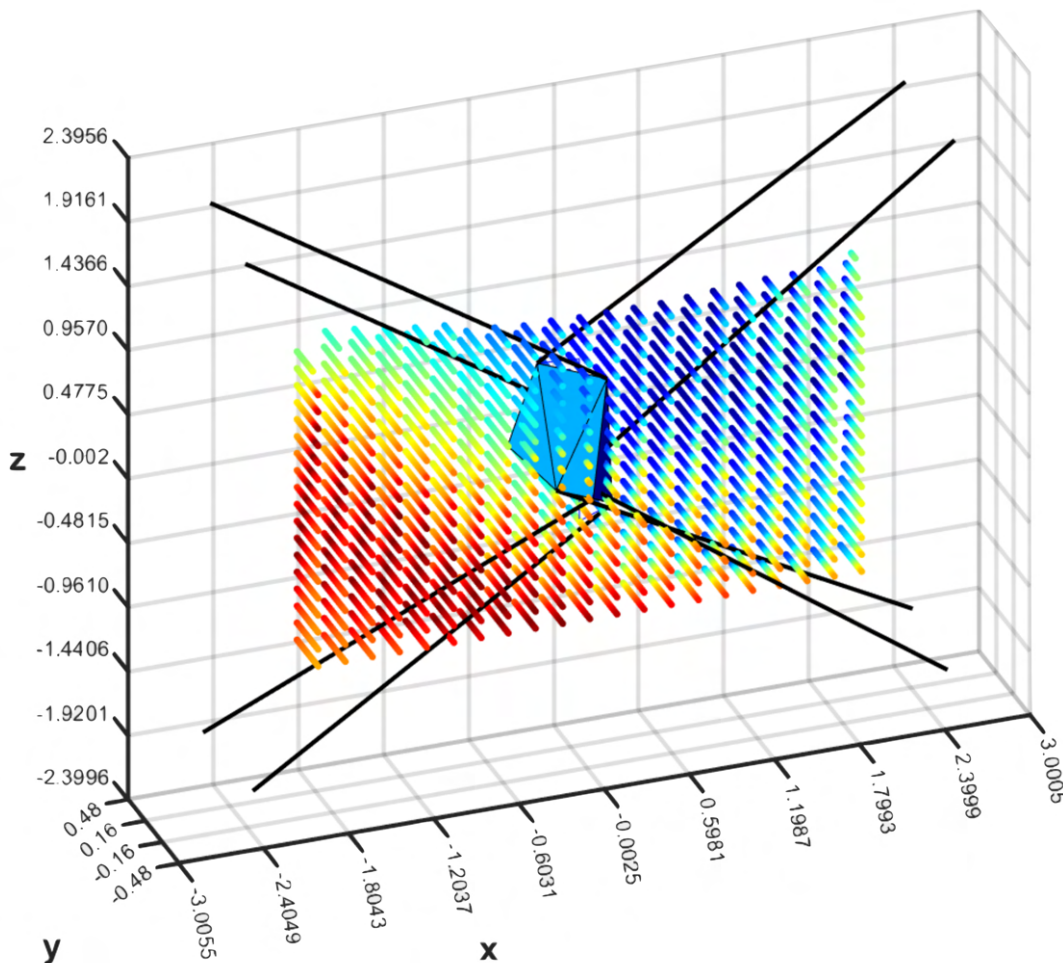


Figure 4.12: First *ga* design

coming from the genetic algorithm stand out because of their special peculiarities. Different simulations have been performed and the mechanical designs of the robot are shown in the next figures, noting that the x , y , z axes are expressed in meter [m]. More complete and detailed figures are presented in the Appendix C. In this section, the front, lateral and top view for each solution are shown, and technical data concerning the cable arrangement and mobile platform shape can be easily extrapolated. Moreover, the front and lateral views allow the reader to better understand the workspace size both in the vertical plane and in the y direction. The workspace feasible points are shown in colours, the cables are represented by black lines and the platform is the volume delimited by the EE cable anchor point, according to the *convhull* MATLAB[®] function.

The first design is shown in Fig. 4.12. It is a typical *ga* design because of the asymmetric and apparently random cable configuration. The stochastic approach of the genetic algorithm has the advantage of creating a mechanical design that human engineers could not directly consider by only using their expertise. The feasible workspace is symmetric and has a rectangular shape in the vertical plane. On the other hand, this solution is highly complex and can hardly be transformed into a real mobile platform due to the very particular cable arrangement. Another design derived from the genetic algorithm is presented in Fig. 4.13. In this configuration, the mobile platform takes up a larger volume and its design is strongly asymmetric, creating gravity torque contribu-

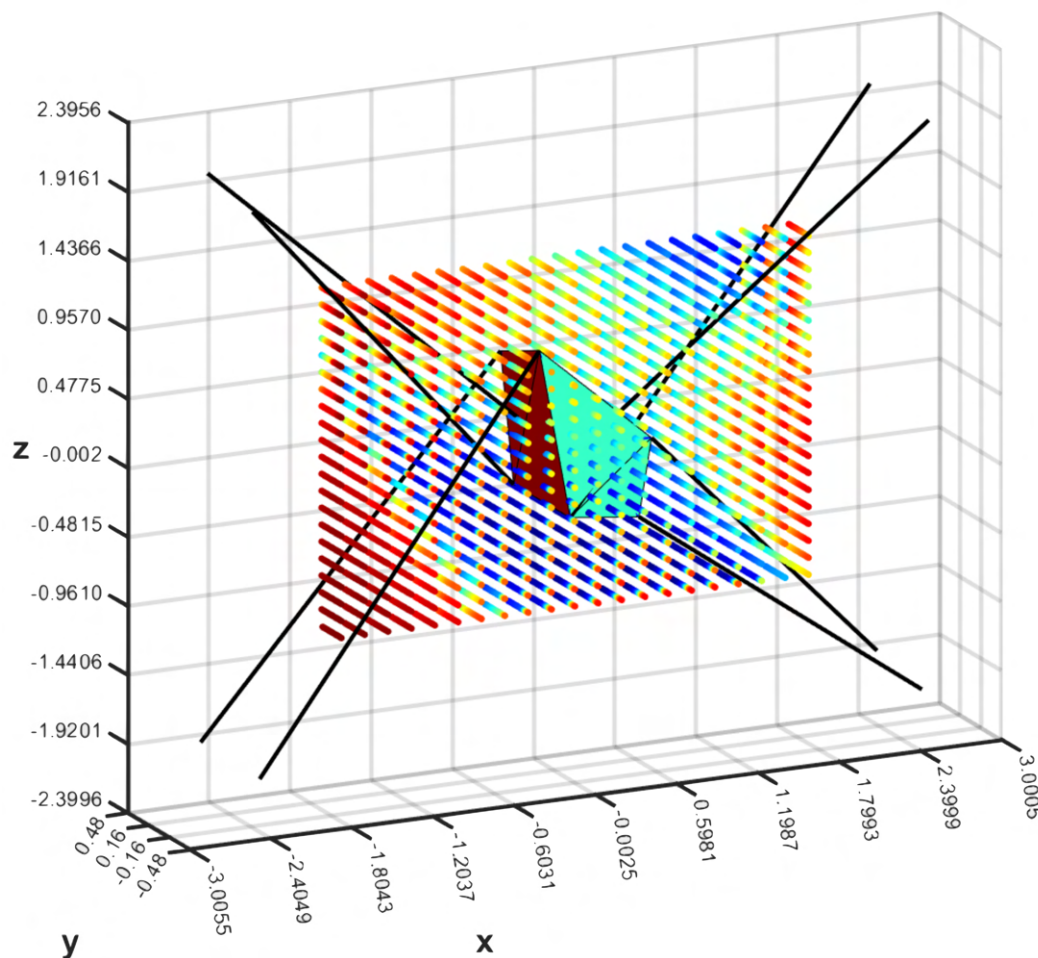
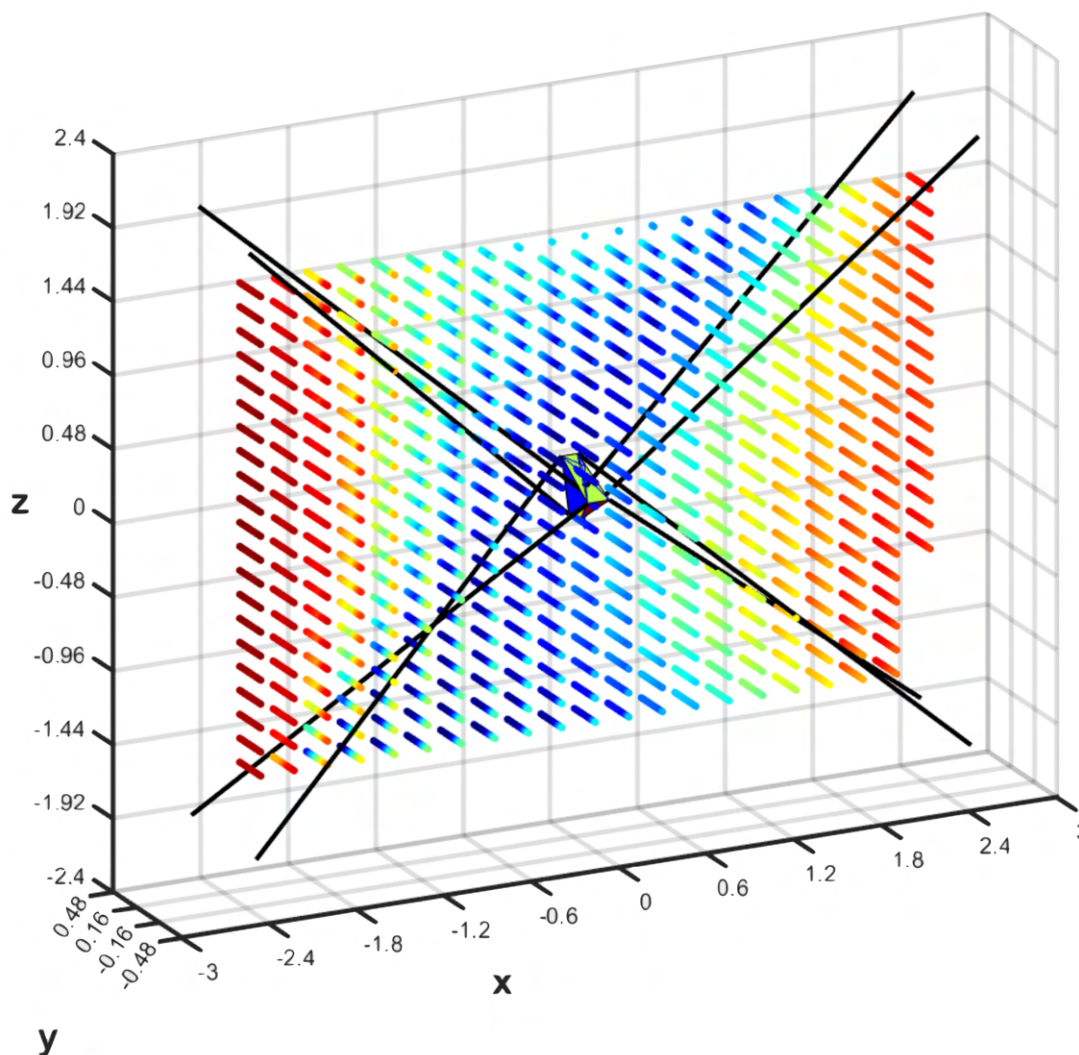


Figure 4.13: Second *ga* design

Figure 4.14: Third *ga* design

tions that must be compensated by the cables. The workspace seems to be a symmetric parallelepipedon, but its volume is reduced with respect to the previous case.

The third design is shown in Fig. 4.14. The volume of the feasible workspace is very high but there is a strange asymmetry with respect to the vertical plane $x = 0$. The mobile platform is represented by a compact structure, with small sizes and weights, representing a significant advantage for the deployable architecture. The frame installation points are slightly different with respect to the previous solutions, while the cable arrangement seems to have a clear pattern. This solution represents a good starting point for a second local optimisation procedure.

A fourth and final design is presented in Fig. 4.15. Even though a small asymmetry is present, the feasible workspace has a high volume, in particular, its upper part is high-saturated. With respect to previous solutions, this one has a smaller translational displacement in the y direction, as can be seen in the figure presented in Appendix C. On the other hand, the mobile platform has a peculiar symmetric shape, derived from the stochastic approach of the *ga* algorithm. Its volume is higher with respect to the previous case but its symmetry guarantees the correct barycenter position.

Therefore, this symmetric EE shape is an interesting feature that the algorithm found out. As for the third solution, there is a common design pattern: three cables

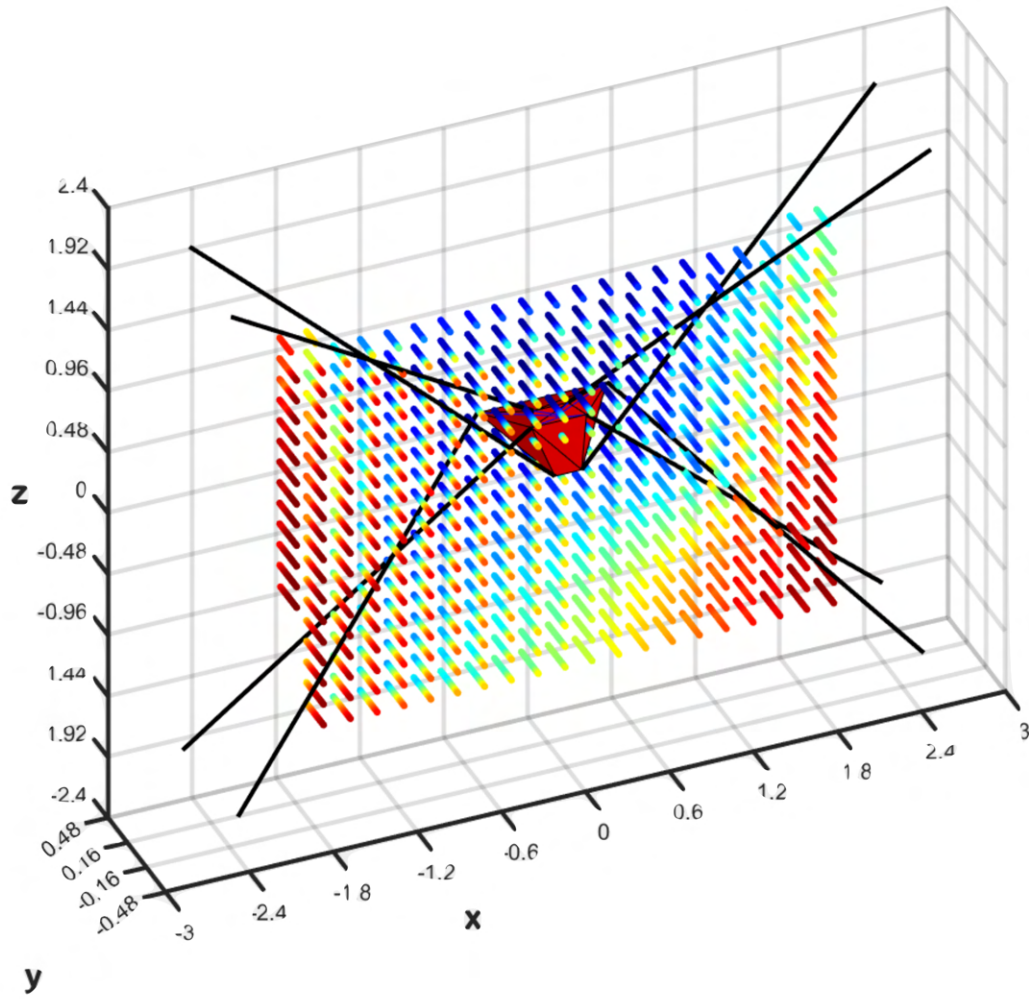
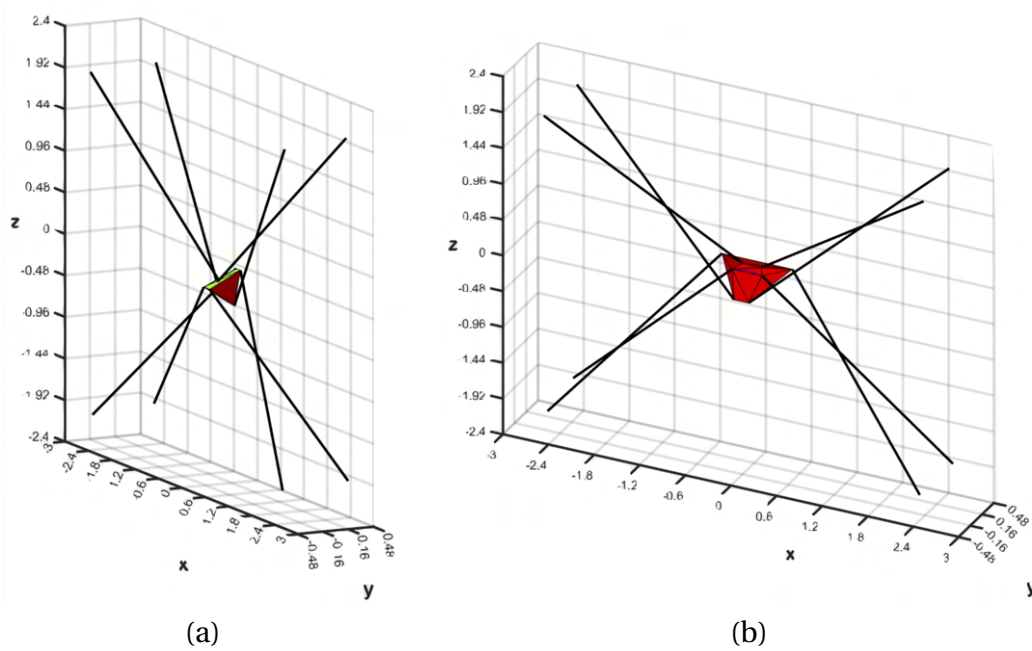
Figure 4.15: Fourth *ga* design

Figure 4.16: Two special EE cable configurations

grasp the mobile platform in the left and right planes, and the remaining two cables are in the upper plane of the EE. This is clear in the last design, but also in the previous one (Fig. 4.16).

To conclude, these four stochastic designs represent the starting point for a more accurate optimisation method, based on the local optimiser algorithm. To this end, also the EE anchor points are subjected to further limitations. In this way, the mobile platform should account for the space needed to install all the servo-winchs and their sensing and routine systems inside the EE. This approach accounts for both optimisation and mechatronic designs.

In particular, the over mentioned subset for the EE anchor point is defined in meter [m], $\forall i = 8, \dots, 15$ as:

$$\begin{cases} -0.8 \leq x_i \leq -0.25 \wedge 0.25 \leq x_i \leq 0.8; \\ -0.3 \leq y_i \leq 0.3 \\ -0.8 \leq z_i \leq -0.25 \wedge 0.25 \leq z_i \leq 0.8 \end{cases} \quad (4.27)$$

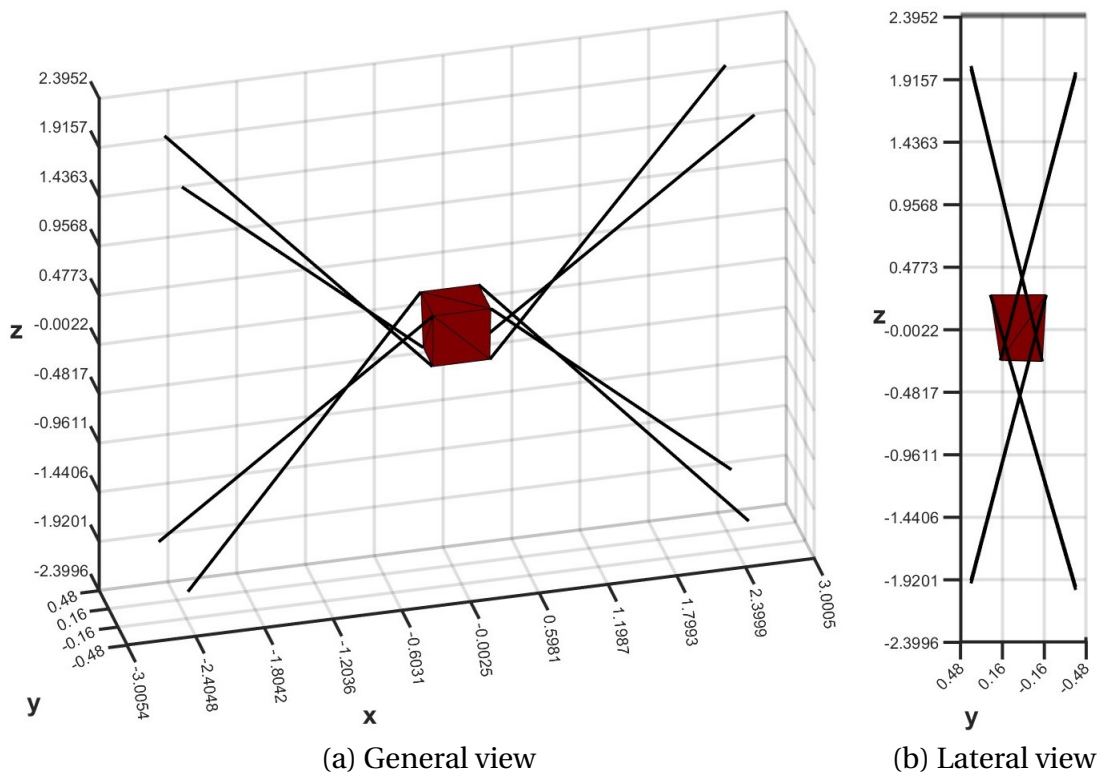


Figure 4.17: Optimised solution

Different simulation iterations have been performed and the final result is shown in Fig. 4.17. The cable arrangement is similar to the one produced by the last solutions of the *ga* algorithm, but in this case, the mobile platform and its anchor points are symmetrically spread among the space. The cable arrangement follows a specific path: upper and lower, left and right cables are crossed avoiding their interference by a geometrical offset. The volume of the mobile platform is compact, within the aforementioned boundaries set to the EE anchor points: 0.51m x 0.3m x 0.51m. This design allows the drive units implementation into the mobile platform.

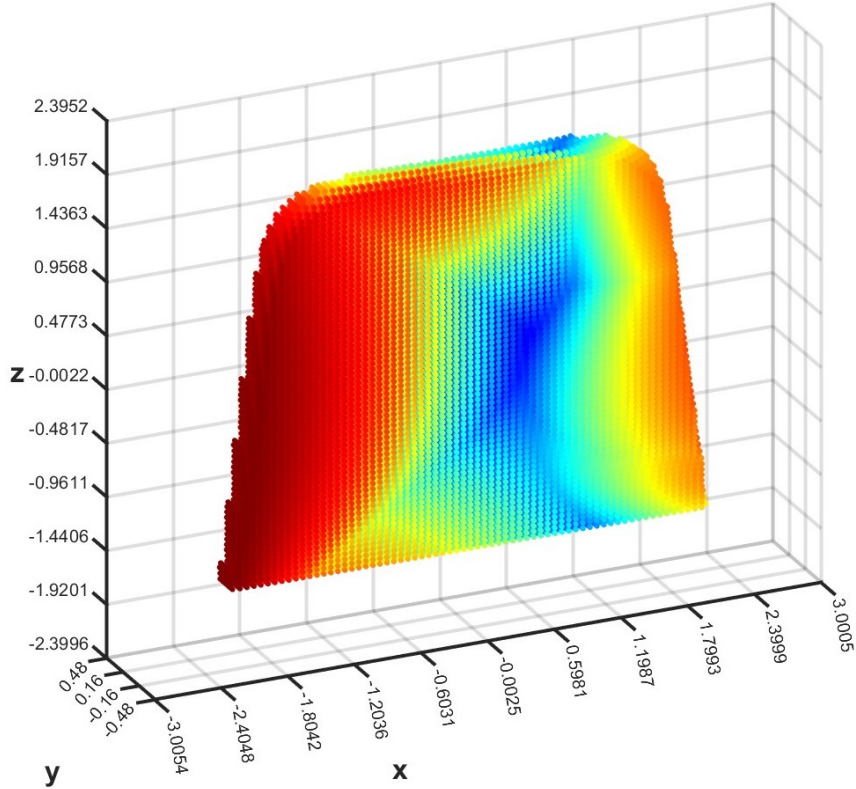


Figure 4.18: Final workspace

Concerning the final workspace (Fig. 4.18), its volume is about 3.5 m^3 and the mean vertical plane surface is about 12 m^2 . More detailed figures are presented in the Appendix C. The workspace geometry has a typical CDPR bell shape, in fact, the upper part of the volume requires high cable tension, instead the lower part is feasible because of the gravity effects. This simulation is run with an external force of 50 N, acting in the y direction, and a maximum cable tension of 600 N. The total frame size is $5 \text{ m} \times 0.8 \text{ m} \times 4 \text{ m}$, with an actual volume installation of 4.21 m^3 . The worthless volume rate V_w , presented in Eq. 4.14, is equal to 15.29 %. Considering the cable lengths, the maximum value raised from the simulation is about 5.92 m . This length is important for the winch drum design. A high value of maximum cable lengths requires a high diameter or axial length for the drum. All the relevant parameters of the simulation are resumed in Table 4.1.

| Parameter | Value |
|-----------------------------------|--|
| EE size | $0.51 \times 0.3 \times 0.51 \text{ [m}^3\text{]}$ |
| Frame size | $5 \times 0.8 \times 4 \text{ [m}^3\text{]}$ |
| Workspace vertical surface | $12 \text{ [m}^2\text{]}$ |
| Workspace volume | $3.5 \text{ [m}^3\text{]}$ |
| Maximum cable length | 5.92 [m] |
| Worthless volume percentage V_w | 15.29 [%] |

Table 4.1: Final design parameters

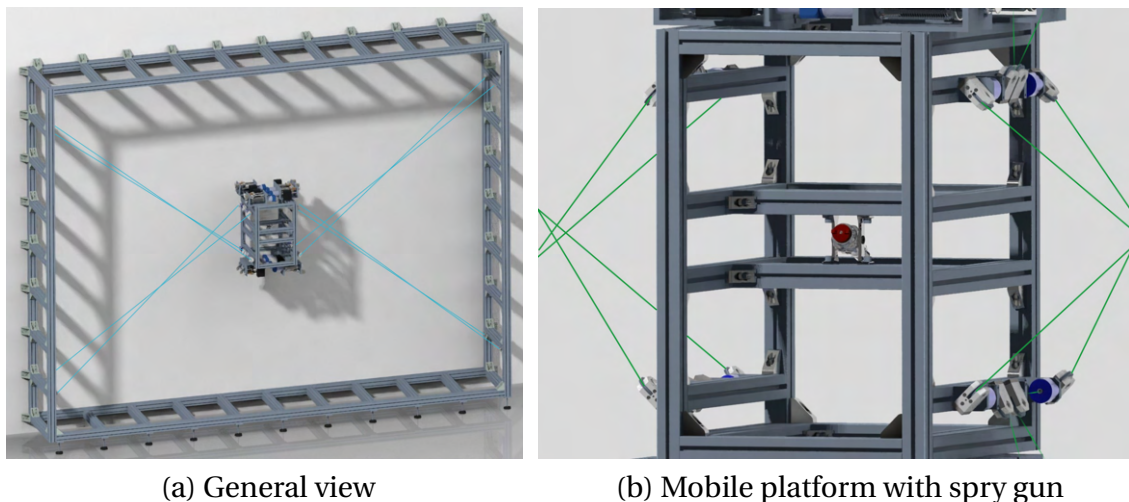
Chapter 5

Conclusions

Overconstrained cable-driven parallel robots represent an important class of parallel manipulators actuated by extendible cables. Their architecture allows the mobile platform to withstand important external loads, compared to classical CDPRs. In this thesis, an eight-cable, planar, overconstrained cable robot is designed for a painting task.

The construction sector represents a crucial industrial field where deployable and reconfigurable cable-driven robots could have large success, especially for large workspace planar manipulators. The presented architecture is not fully planar because of the three-dimensional nature of its workspace but can work in a vertical plane of about 12 m^3 and can withstand an out-of-the-plane reaction force of 50 N, thanks to the eight-cable architecture.

The demonstrated results are derived from a complex mechatronic design process, starting from the project constraints in terms of task requirements and architectural features, and ending with an optimisation process of the mechanical design. The major difficulties of the project were represented by the ample design constraints. A lot of different solutions for the actuation units and sensing systems were proposed and critically analysed during the design iterations. The morphological decision matrix helped to select the robot architecture and to understand where the actuation systems should have been installed. The deployable nature of this EE can guarantee high flexibility and modularity for the robot. In addition, the discrete reconfiguration could be easily im-



(a) General view

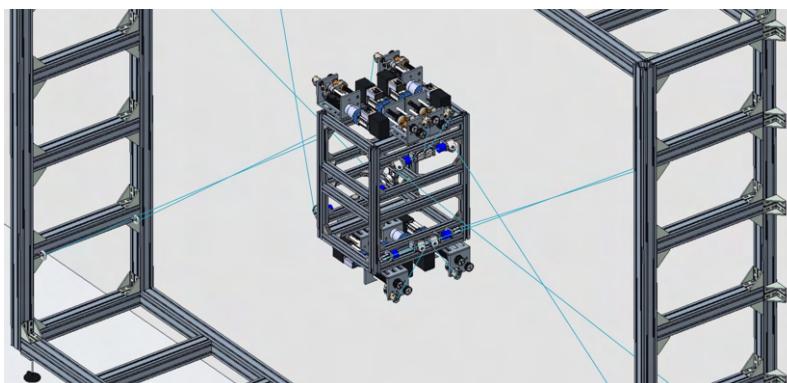
(b) Mobile platform with spray gun

Figure 5.1: Final design solution

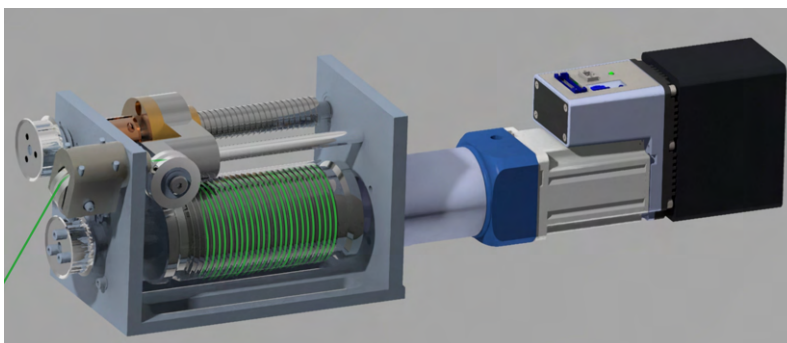
plemented offline, changing the feasible workspace by rearranging the frame anchor point both in the vertical z and horizontal x directions.

Concerning the cable arrangement and the CDPR specific architecture, the hybrid optimisation algorithm converged to an optimal solution. The stochastic nature of the genetic algorithm represents a powerful design tool if the cost function is correctly defined with respect to the design variables. The solutions derived from the *ga* algorithm are innovative in terms of cable arrangements and mobile platform geometry. On the other hand, the local optimiser was necessary to correctly derive the final solution. The cost function was defined by the wrench-feasible workspace, implemented with a novel cable interference check. These features lend a level of accuracy, and above all, reliability to the presented optimisation method. The final workspace has perfect symmetry with respect to the installation frame, and its volume is about 3.5 m^3 . For this reason, hybrid optimisation tools represent an innovative and functional approach to CDPR design and will be further studied in future applications.

Moreover, the mobile platform, that has been presented at the end of the optimisation procedure, must respect the construction boundaries set during the local optimisation. To this regard, in Appendix D, the mechanical transmission for the servo-winch has been depicted and the main parameters of the drum winch have been calculated. In particular, the drum radius R_d and the axial length L_d are the most relevant features. Furthermore, the integrated servo motor with its associated gearbox has been chosen, according to the weight and power constraints. The guidance and sensing system is made up of a load cell and a rotary encoder embedded in the last swivelling pulley which simulates the mobile platform anchor point for the cable. The mobile platform



(a) Mobile platform with cables



(b) Spooling-helper winch

Figure 5.2: Actuation installed into the EE mobile platform

frame is made up of extruded aluminium parts, exactly like the frame machine but with a small section.

To conclude, a rendering of the prototype is illustrated in Fig. 5.1. The machine accounts for:

- a wall frame of extruded aluminium with section $90 \times 90 \text{ mm}^2$, with external sizes of $5 \text{ m} \times 0.8 \text{ m} \times 4 \text{ m}$ (Fig. 5.1a), and horizontal lateral parts responsible for the offline reconfiguration of the robot. The frame anchor points are simple eyelets;
- eight flexible cables of diameter 3 mm (Fig.5.2a), maximum cable tension of 600 N and maximum length L_{max} of 6 m, according to the simulation performed in chapter 4;
- a mobile platform composed of eight spooling-helper servo-winchies (Fig. 5.2b) with external sensors and guiding pulleys directly installed into the EE frame, made up of extruded aluminium with section $40 \times 40 \text{ mm}^2$. Inside the mobile platform, a painting spray gun is installed (Fig. 5.1b).

Concerning possible outlooks, the prototype will be built in the IRMA Lab at the University of Bologna for further tests and experiments. Planar, overconstrained CD-PRs have been already tested in the laboratory but with not these important frame sizes. The construction sector demands large architecture and this prototype could represent a significant step forward in new technology development. Moreover, optimisation algorithms for CDPR design will be investigated because of their novelty and significant results.

Appendices

Appendix A

In-depth Analysis of Robotics in Construction

The construction industry is one of the most important economic sectors across the world [22]. Despite its enormous economic importance, the construction industry is beset with inefficiencies: productivity has been increasing steadily in the last five decades. Robotic and automated systems have the potential to revolutionize and provide many advantages to this labour-intensive sector [23–25], reducing labour costs while improving productivity and quality. Moreover, robotic systems can reduce injuries and free workers from conducting dangerous tasks.

To better understand how to implement these new technologies in the construction sector, it is possible to define the life cycle of a project [122]. It can be subdivided into different phases: (i) site investigation: the status of a construction site; (ii) design support: a more precise and actual design process; (iii) production: off-site processes; (iv) construction-installation: on-site processes; (v) quality check: completion of the construction and installation process to assess the quality and the correct execution of the process; (vi) maintenance-inspection: assess the status of a building until its life-end. In particular, robotic systems could have a significant impact in the (iii), (iv) and (vi) phases. Mainly if the task consists of a repetitive sequence of activities or if the end effector works with modular objects in a well-defined environment, such as in an automotive-production cell.

On the other hand, some factors limit the adoption of robotics in the construction industry [123]. In [25], the authors highlighted four major categories of limiting factors:

- *Contractor-side economic factors*: costs that construction companies must incur to adopt robotics. There are factors like: “high initial capital investment”, “no strong need to improve productivity”, and “lack of government incentives”. The high initial capital investments are justified when they reduce expensive manual labor and increase productivity. However, high capital investments represent a significant challenge in a sector where most companies are small subcontractors. Only a few big construction companies can assign resources to test new technologies. This is expected as construction is a low-profit and high-risk industry in which the adoption of new technologies is not feasible in practice and can affect the survivability of the companies.
- *Client-side economic factors*: costs that the client must incur to adopt robotics. The current practice that prioritizes “lowest price” as the most important measure to grant projects represents a significant limitation to innovation.

- *Technical and work-culture factors*: technical limitations of current technologies and work-culture-related factors. The first identified barrier is the high complexity of construction tasks that limits the effectiveness of robotic solutions. Moreover, efficient collaboration between humans and robots will be essential for successful adoption.
- *Weak business case*: unclear value that construction companies can obtain from adopting robotics. Depending on the specific application and technology, evaluating a cost-based investment analysis is possible, but there is not always hard evidence of positive return [124]. One of the limitations is the lack of flexibility and customization: every project and every client is different, and there is less certainty that the investments can be exploited in other future projects.

Robotic systems for construction were developed in the 1960s and 1970s, like in other industrial sectors. However, for all the abovementioned reasons, the adoption of robotics in the construction industry has been very slow [125]. Nevertheless, during the past ten years [126], other technological developments like the Industry 4.0 paradigm, Building Information Modelling (*BIM*), sensing technologies, additive manufacturing processes and artificial intelligence have driven the adoption of robotics in the construction industry as well.

More specifically, the BIM approach can generate and manage digital representations of the physical and functional entities' characteristics, creating a database where all digital information is elaborated. Especially in the building sector, where a multitude of different and parallel activities are continuously overlapping during working time, a BIM strategy can achieve high performances in terms of productivity, efficiency and quality of the working processes. In [127], authors proposed a procedure to integrate construction robotics into a job site by establishing a method of graph-based change analysis. It can account for the scheduling and sequencing changes caused by the robotics integration and how these changes ultimately propagate through the construction schedule. Wu et al. [128] presented a BIM-based framework to generate vertical transportation demands during the construction of high-rise buildings. Instead, Bruckmann et al. [129] addressed BIM as a base for motion planning, investigating workspace aspects and site layout for a cable-driven parallel robot.

Sensing the environment is the fundamental step in positioning, mapping, and navigating robots in construction operations. For this reason, developing newer and more accurate sensing technologies stimulated the introduction of new robotic devices in the building sector during the last decade. Construction sites are spatially complex and unstructured, and robots operating in such environments may be exposed to gradual change and unpredictable events. In [130], the authors introduced an external tripod-based measuring system, which was employed to investigate the potential of localizing a mobile fabrication unit with an external tracking strategy without fixed reference points around the robot to help constrain the pose, thus eliminating the need for a full enclosure. Instead, Liu et al. [131] proposed a mobile robot that could implement a floor-tiling task by adding a point laser measurement system guaranteeing good linearity of a row of tiles. Finally, Lee et al. [132] proposed a mobile robot embedded with infrared sensors to speed up the cleaning maintenance of high-rise building façade.

The rest of the document presents an overview of the different types of robotic and automated systems used in the construction industry, considering the main processes that could be of interest to a cable-driven parallel robot (*CDPR*) application. From this

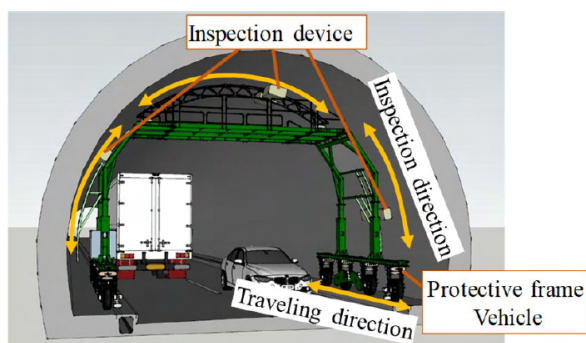
perspective, the significant advantages of this robotic architecture are (i) large workspace, (ii) high flexibility, (iii) high reconfigurability, and (iv) heavy loads concerning the workspace size.

These robotic and automated systems are varied, and there is no consensus regarding a defined categorization. The lines between categories are constantly moved or blurred by new technological developments. The categorization presented here intends to facilitate the understanding of a very complex and varied technology landscape and to provide the reader with a quick overview of the different types of systems. It is possible to distinguish two main fields of applications:

- Additive manufacturing (3D printing)
- Large-scale façade

It is clearly possible to identify many other different examples in literature [133], but this document seeks to highlight specific fields where the overmentioned peculiarities of CDPR architecture could improve productivity, safety and quality standards concerning possible competitors (e.g., drones, quadruped robots, climbing robots, manual workers).

However, some examples of applications cannot be classified into additive or façade processes but could be a cause for reflection about CDPR application. In [134], researchers proposed to implement drones as a way to address module transportation challenges and innovative logistics by lifting a module from below, similar to a pallet. This new method increased the system's flexibility but introduced limitations to the drones' possible payload and power supply. Kamimura and Nakamura [135] presented a tunnel-inspection system (Fig. A.1a). The inspection equipment was arranged at the upper part and both side parts; instead, the lower part consisted of a self-propelled portal frame secured space through which the vehicle could pass. Then, these inspection devices were moved to a predetermined position for inspection. Another large-scale application is described in [136]. The authors suggested a remote operation of the underwater excavators in order to improve the safety and productivity of underwater constructions. In conclusion, Pott [15] proposed a novel system for assembling parabolic reflector panels in a solar power plant. The architecture consisted of a large-scale cable robot with computer-controlled winches mounted on mobile towers (Fig. A.1b). It can guarantee a high workspace and heavy payloads attached to the mobile platform that was the robot end-effector.



(a) Tunnel inspection



(b) CDPR for solar power plant

Figure A.1: Large-scale robotic application

A.1 Additive Manufacturing

Three-dimensional (3D) printing, as one of the additive manufacturing technologies, is transforming the design and manufacture of products and components across various disciplines; however, architectural design and the construction industry have only recently begun to adopt these technologies for construction purposes. The potential advantages of 3D printing in the construction sector are significant.

One such advantage is freedom of form. With 3D concrete printing, very fine concrete structures are possible [137]. In traditional concrete pouring, the formwork determines the shape of the concrete. With concrete printing, builders can create shapes of round, convex or hollow forms. This will enable concrete buildings and structures with entirely new shapes. Another advantage is that 3D concrete printing reduces waste: the concrete is alloyed only where it is constructively needed. Traditionally poured concrete is solid and contains much more concrete than is constructively required. Developing 3D printable concrete, also known as mortar, reduces the carbon footprint and environmental impact. Another advantage is the ability to accommodate individual customer requirements. Unlike traditional design methods, parametric design uses algorithms to implement the effect of one custom part on an entire design. After all, a different design involves little cost. This saves time in the design process. In addition, the significant advantage is that 3D concrete printing allows for faster construction thanks to the high production speed of the automated process, reducing human error. Because of the quick-curing concrete, which sets in 3 minutes, it is possible to continue printing in one go without breaks, delivering affordable homes faster.

A growing number of companies are entering this market [22]. Founded in 2014, a U.S.-based company, Apis Cor, developed a 3D concrete printing robot to construct low-cost housing (<https://apis-cor.com/>). The crane-sized robot weighs about 2 tons, the rotating robotic arm has a swept area of 132 m² and approximately 100 m² of concrete can be printed in 24 h. In December 2016, Apis Cor, in cooperation with PIK Group, a leading company in the Russian housing construction market, printed a complete six-room, single-story house with an area of 38 m² in about a day at the company's test facility in the town of Stupino. The company also built the Dubai Municipality in UAE, which set the record to be the largest 3D-printed structure with a standing tall of 9.5 meters and an area of 640 m² (Fig. A.2). The construction was erected entirely on-site, with no additional assembly required.



Figure A.2: The largest 3D-printed structure in the world

An innovative Dutch start-up, MX3D, was founded in 2014 and has developed technology that extends 3D printing and fabrication to metals (<https://mx3d.com/>). The system uses a six-axis robotic arm from ABB to print metal parts by ejecting small amounts of molten metal through a welding nozzle at the robotic arm's end, which quickly solidifies. The system can also weld printed parts together. The printing speed is 1-3 kg per hour per nozzle, and the system can operate with most weldable metals such as stainless steel, aluminium, bronze and Inconel. To demonstrate the capabilities of the technology in a structural context, the company printed a steel pedestrian bridge that spans a canal in Amsterdam. The ultimate aim is to develop a robust metal printing machine suitable for on-site construction and heavy-duty industrial use outside a controlled environment. In theory, this could ultimately allow the robotic fabrication of all steel structures and components used in the construction sector.

Concurrently with companies and start-up projects, also from a scientific point of view, additive manufacturing processes brought interesting applications. In [138], the authors presented a new cable robot designed for use in a contour crafting system. Its geometry permitted translation-only motion and highly simplified kinematic equations. It actuated cable mounts that allow online reconfiguration of the cable robot to eliminate cable interference while maintaining full constraint of the end-effector (Fig. A.3). This system can be engineered to provide the ability to contour-craft large structures with the potential for being less expensive and more portable than existing robot concepts. The static equations were presented, including a discussion of how the redundancy of the manipulator can be used to maintain nonnegative tensions in all cables. The manipulator's workspace was investigated for a specific geometry, including the calculation of the maximum cable tension for various loading conditions. The workspace was determined to be potentially very large, with low maximum cable tensions for nearly all positions.

Another common application that was traced to additive manufacturing is brick-laying. It was first automated in the 1990s by Pritschow et al. [139], with the development of the BRONCO mobile robot. Following this approach, Dörfler et al. [140] theorized the "In Situ Fabricator" (*IF*). *IF* is designed to autonomously complete building tasks directly on a construction site. The level of autonomy intended for the robot is defined to contain all the facilities required for precisely manipulating building materials. In this way, human interaction with the robot is narrowed down to the specification of

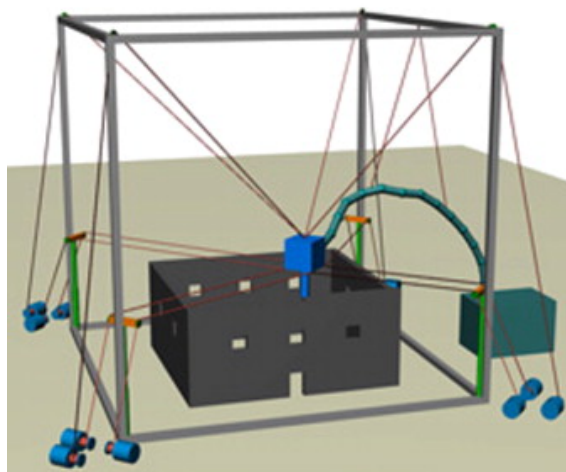


Figure A.3: Cable-Suspended Contour-Crafting Construction Robot

building tasks through high-level planning environments and dedicated interfaces. To achieve this, the robot is designed to be self-contained, with all components needed for construction on-board: mainly sensing, control hardware, and computing systems. Thanks to its sensing equipment, it should not depend on external referencing systems (e.g., Vicon, etc.).

On the other hand, the same process could be accomplished with a CDPR [141, 142]. In particular, Boumann et al. [65] introduced a cable robot that offered outstanding advantages in terms of workspace size, stiffness, modularity and mobility. The authors introduced the models, the optimization problem and the solution approach to optimize the trajectories for automated bricking. The results indicated that the choice of the cost functions and their weights significantly impact the trajectory and allow a tuning regarding preferences like transport time, stiffness and cable tension level. Collisions and paths outside the workspace could be effectively avoided.

Appendix B

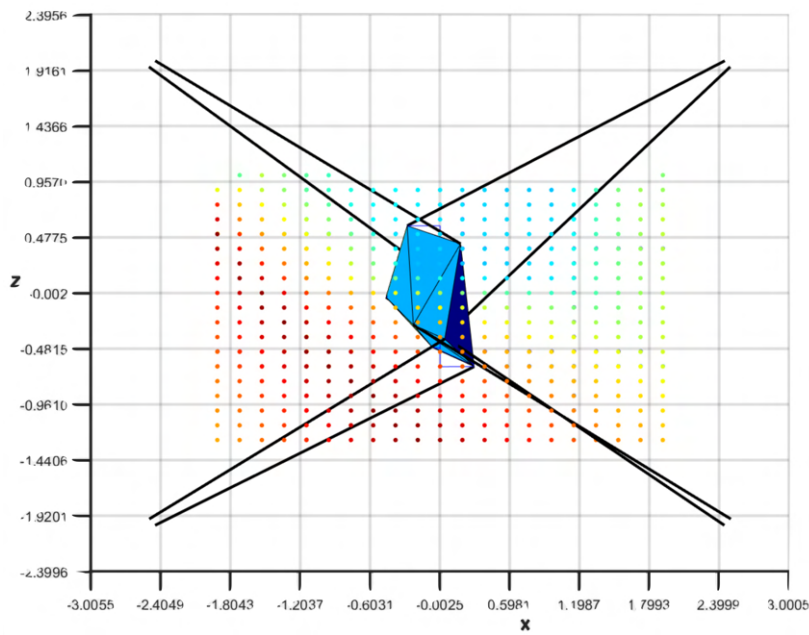
MATLAB Code for Cable Interference

```
1 %cable interference check
2 for i = 1:cdpr_p.n_cables
3     for j = i+1:cdpr_p.n_cables
4         AB = cdpr_p.cable(i).pos_OD_glob-...
5             cdpr_p.cable(j).pos_OD_glob;
6         n_norm = cross(cdpr_v.cable(i).pos_BA_glob,...
7             cdpr_v.cable(j).pos_BA_glob);
8         dist = (abs(n_norm'*AB))/(norm(n_norm));
9         if dist<0.008 %8 mm tolerance
10            condition = condition*0;
11        else
12            condition = condition*1;
13        end
14
15        if condition == 0 %interference possible points inside ...
16            or outside cable segment
17            a = cross(cdpr_v.cable(j).pos_BA_glob,n_norm);
18            b = cross(cdpr_v.cable(i).pos_BA_glob,n_norm);
19            t1 = (a'*(-AB))/(n_norm'*n_norm);
20            t2 = (b'*(-AB))/(n_norm'*n_norm);
21            point1 = cdpr_p.cable(i).pos_OD_glob+...
22                t1*cdpr_v.cable(i).pos_BA_glob;
23            point2 = cdpr_p.cable(j).pos_OD_glob+...
24                t2*cdpr_v.cable(j).pos_BA_glob;
25            L1 = norm(point1-cdpr_p.cable(i).pos_OD_glob);
26            L2 = norm(point2-cdpr_p.cable(j).pos_OD_glob);
27            toll = 0.01; %10 mm tolerance for shared EE anchor ...
28                point configuration
29            limit1 = cdpr_v.cable(i).complete_length-toll;
30            limit2 = cdpr_v.cable(j).complete_length-toll;
31            if L1 < limit1 && L2 < limit2
32                condition = 0;
33            else
34                condition = 1;
35            end
36        end
37    end
38 end
```

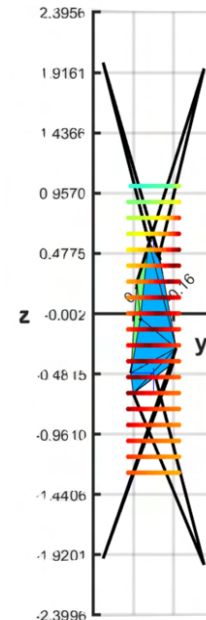

Appendix C

Details for the Workspace Solutions

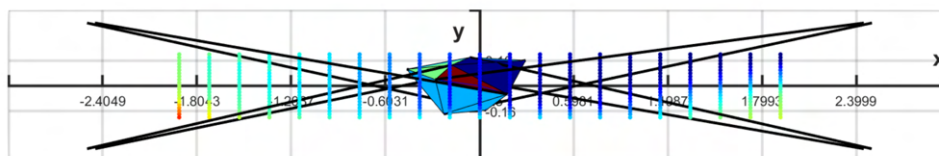
C.1 First *ga* Design



(a) Front view



(b) Lateral view



(c) Top view

Figure C.1: More detailed views, solution one

C.2 Second *ga* Design

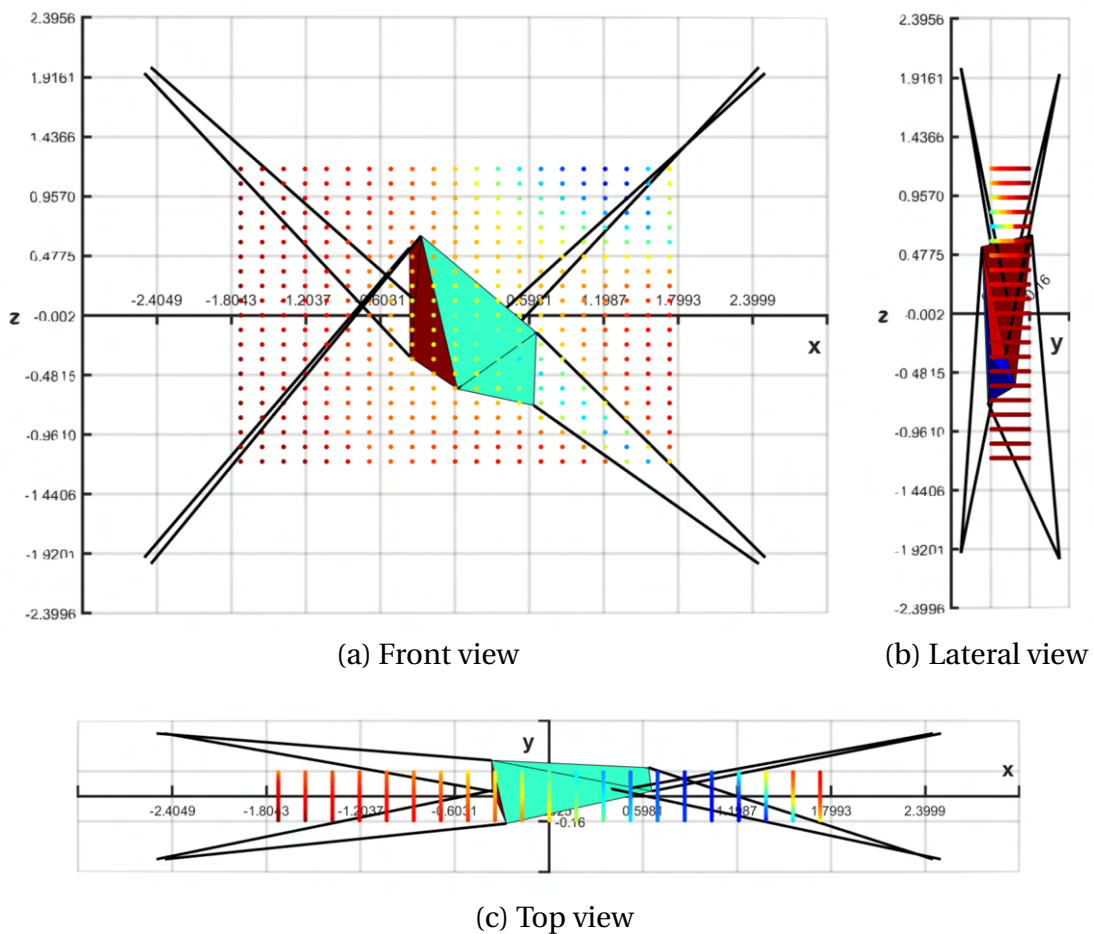


Figure C.2: More detailed views, solution two

C.3 Third *ga* Design

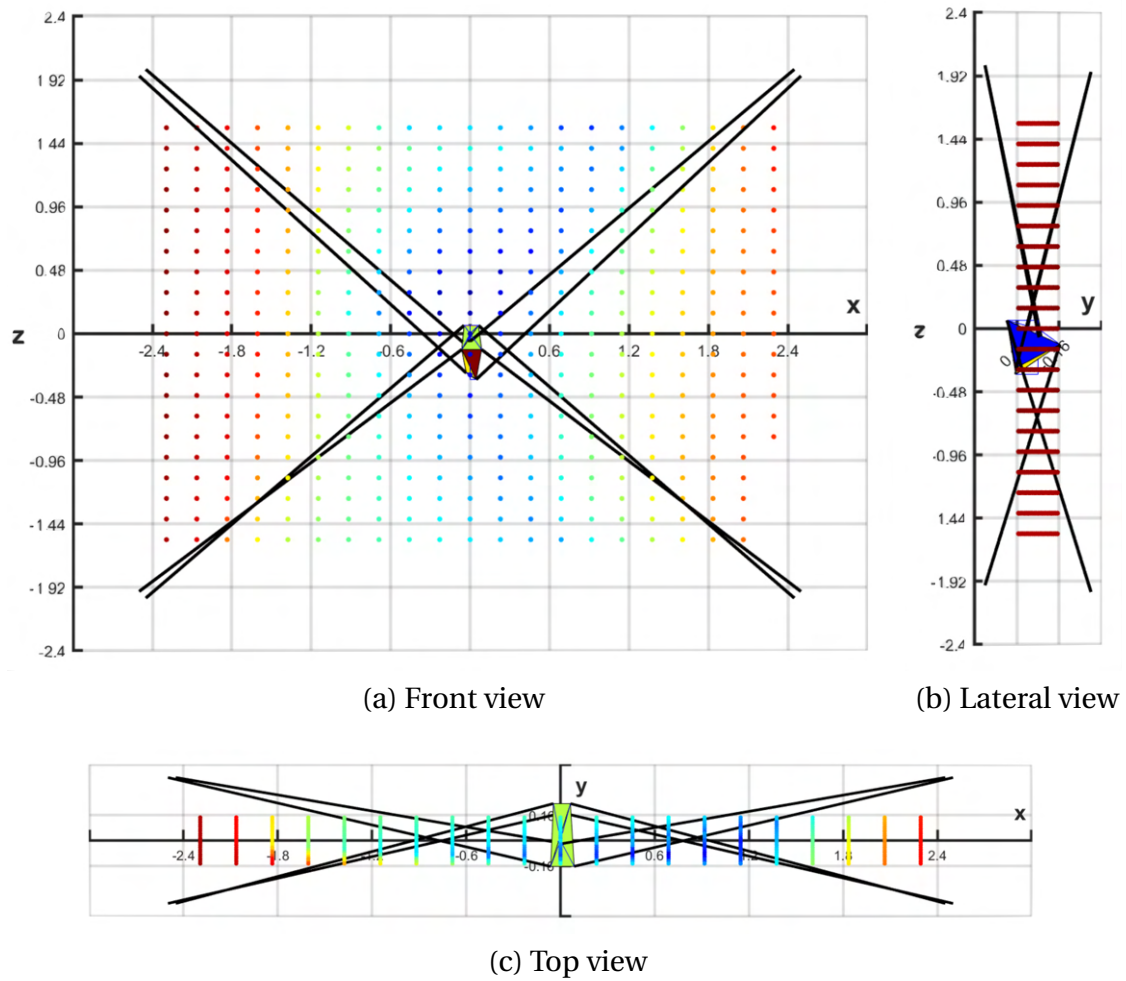


Figure C.3: More detailed views, solution three

C.4 Fourth *ga* Design

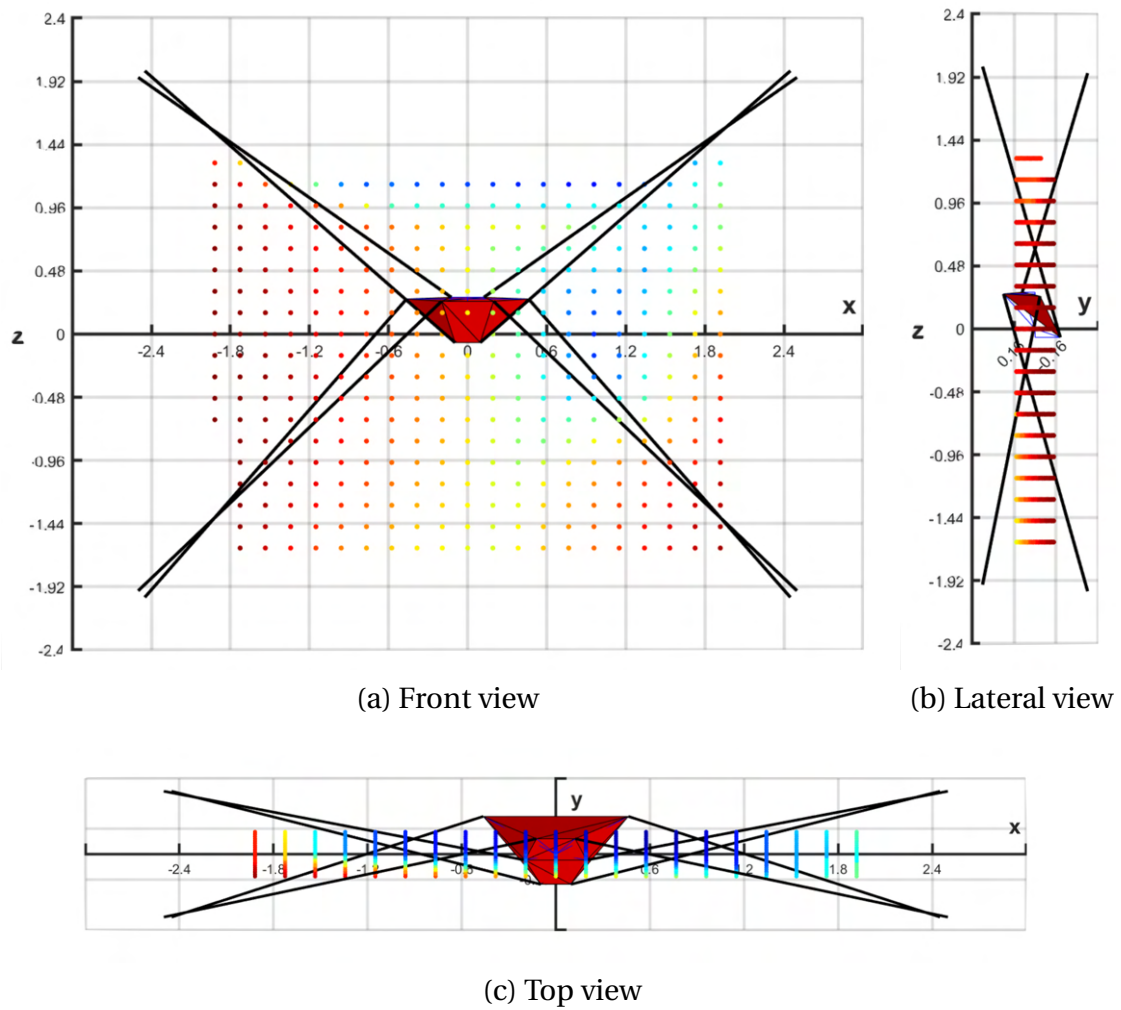


Figure C.4: More detailed views, solution four

C.5 Final Optimal Design

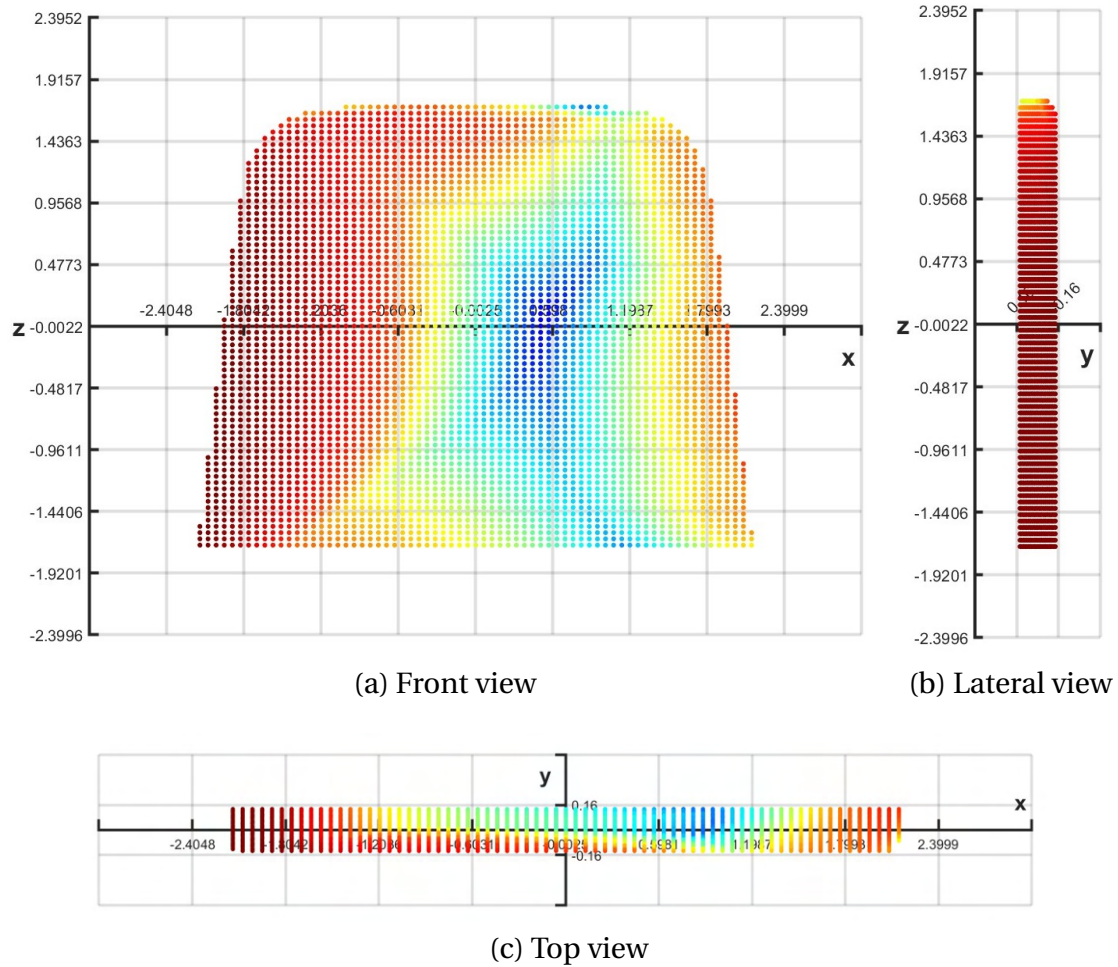


Figure C.5: More detailed views, final solution

Appendix D

Mechanical Transmission Design

In this final design chapter, the mobile platform winch unit is presented. In particular, the drum design is computed and the electric motor and gearbox are chosen, according to the power constraint implemented before. Once the cable and anchor points arrangement is derived, the maximum cable length wound up by the winch is calculated in the MATLAB simulation. This parameter represents an important feature of the drum design. Therefore, to choose the correct mechanical transmission between the cable and the motor, the transmission ratio and the applied loads should be estimated. The definition of the design parameters requires an iterative procedure because the choice of the motor and gearbox influences the drum of the winch and vice-versa.

D.1 Drum and Servo-motor Design

The drum of the winch unit represents a critical component because of its importance in the transmission of the torque and force from the electric motor to the cable. The drum is designed taking into account a safety factor of 1.5. The choice of this coefficient descends from technical reasons: (i) the weight of the drive unit should be as small as possible because of its direct installation into the mobile platform, and a low-security factor could lead to small components; (ii) the painting task does not represent a high-danger task that could lead to a human injury hazard.

The input data for this drum design is the maximum cable length, simulated and obtained in the previous chapter (see Table 4.1). To this end, the maximum cable length L_{max} that each drum can wind up is 6 m. The cable diameter d is 3 mm and for this reason, the drum helix pitch h_d is 4 mm. The maximum cable tension simulated is $T = 600$ N, so the design tension that accounts for the safety factor is:

$$T_{max} = T \times CS = 900 \quad [N] \quad (D.1)$$

The objective of this design is to find out the axial length of the drum L_d , directly influenced by the maximum cable length L_{max} and the pitch h_d , and the drum radius R_d , that is responsible for the torque M_{max} that the mechanical transmission must support because $M_{max} = T_{max} \times R_d$. The two design parameters L_d and R_d are dependent on each other: a drum with a small radius generates low torque to the motor but has a high axial size L_d , creating important bending moment for the structure; on the other hand, a compact axial drum has a high radius because of the wound up cable length L_{max} , leading to relevant torque to the gearbox and motor.

Another important design parameter directly related to the drum radius R_d is the cable exit velocity v_{out} , which is calculated by the drum angular velocity ω as:

$$v_{out} = \omega \times R_d \quad [m/s] \quad (D.2)$$

So, the drum radius could be interpreted as a transmission ratio because it influences both the force and the linear velocity of the exit cable, modifying the output power of the transmission.

In conclusion, the equations that are responsible for the drum design can be summarized as follows:

$$\begin{cases} L_d = h_d \times \frac{L_{max}}{2\pi R_d} \\ R_d = \frac{M_{max}}{T_{max}} \\ \rho = \frac{L_d}{2R_d} \end{cases} \quad (D.3)$$

The maximum torque M_{max} is the gearbox and servo-motor target torque. The adimensional geometry factor ρ is bound between 1.5 and 3, according to the common design procedure. The final design parameter estimation is limited by the gearbox and servo-motor choice.

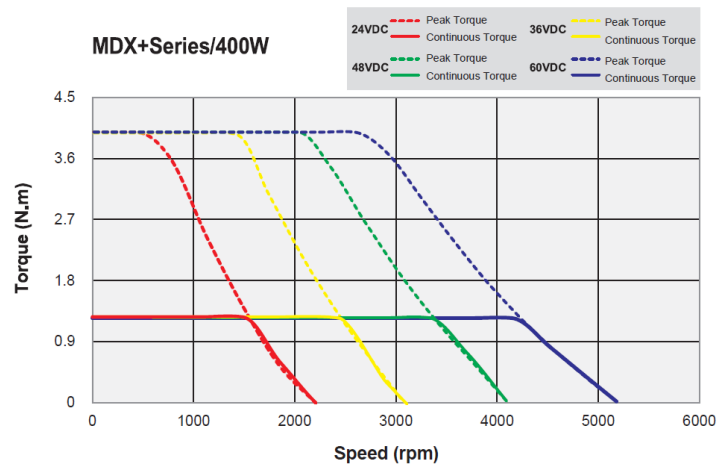
Moreover, the crucial constraint for the servo-motor choice is the weight. Inside the platform, eight different motors must be located and with them the corresponding gearboxes. Due to the presence of the safety brake, the smallest integrated servo motor that is selected for this application is the MDX Moons' MDXR62G5BECA000 (Fig. D.1a). The integrated servo motor implements a delocalized Motion Control. The nominal supply voltage is 48 VDC, and the power rating at 3000 rpm is 400 W. The continuous motor torque M_{nom} is 1.27 Nm, with a peak torque of 3.8 Nm, as presented in the green speed-torque curve in Fig. D.1b. The motor weight is 2.3 kg.

Once the servo-motor has been selected, the gearbox is the last component to finish the transmission. The principal parameters are the gearbox transmission ratio τ_{gb} , its number of reduction phases and weight. The selected gearbox from MechaMotion has two reduction phases with a transmission ratio of 1:20. The maximum gearbox output torque is 44 Nm, and its weight is 1.4 kg.

It is now possible to calculate the maximum torque M_{max} that the gearbox must



(a) MDX Moons' motor



(b) Motor speed-torque curve

Figure D.1: Integrated servo motor by Moons'

ensure, which in nominal condition is:

$$M_{max} = \frac{M_{nom}}{\tau_{gb}} = 1.27 \times 20 = 24.5 \quad [Nm] \quad (D.4)$$

This parameter allows us to solve the linear system D.3. The final drum radius is $R_d = 28$ mm and the axial length $L_d = 140$ mm, with a shape factor of $\rho = 2.5$. On the other hand, the total weight of the servo-motor and gearbox is 3.7 kg for each servo-winch. In nominal conditions, the cable velocity is:

$$v_{out} = \frac{\pi n}{30} \times \tau_{gb} \times R_d = 0.44 \quad [m/s] \quad (D.5)$$

So the output power at the cable, where the tension is calculated with a safety factor of 1.5, is $P_{out} = 400$ W as the motor power, neglecting the friction losses inside the mechanical transmission.

Greetings

Giunto al termine di questo lavoro vorrei soffermarmi un istante per ringraziare tutte le persone che con entusiasmo, dedizione e grande professionalità mi hanno aiutato a raggiungere questo traguardo importante per la mia carriera, sia come studente che come persona.

Un ringraziamento speciale va al mio relatore di tesi, il professore Edoardo Idà, che mi ha seguito ed aiutato durante tutto questo ultimo anno di studi e non solo. Il suo approccio al mondo della ricerca ed innovazione scientifica è stato di grande ispirazione per me. Inoltre, voglio ringraziare i miei correlatori. In primis il professore Marco Carricato per avermi dato l'opportunità di poter lavorare ad un progetto importante che ha rappresentato una sfida decisamente stimolante nel mio percorso accademico. Quindi voglio ringraziare l'ingegner Federico Zaccaria per i preziosi consigli nel mondo della progettazione, per l'enorme aiuto con i disegni finali del progetto, e più in generale per i suoi consigli su come affrontare problemi ingegneristici rilevanti.

Voglio ringraziare la mia famiglia. I miei genitori e mio fratello che mi hanno stimolato a dare il meglio di me, sin dal primo giorno, e che hanno sempre rappresentato un punto di riferimento importante verso cui rivolgermi nei momenti di indecisione. Grazie ad Alice, che è cresciuta con me in questo splendido percorso universitario, dai primi spaventosi esami alla consegna di questa tesi, grazie per aver sempre creduto in me ancora prima che lo facessi io, spero di avervi dato solo un po' di quello che tu hai dato a me. Grazie a mio zio Vincenzo, a cui dedico in particolare questa tesi, perché mi hai trasmesso la tua contagiosa curiosità e voglia di scoprire. Grazie ai miei nonni, Carla e Antonio, per i vostri preziosi consigli e l'affetto che mi avete sempre dimostrato. Grazie ai miei nonni che non ci sono più, Francesco ed Elga, perché nel mio cuore avete sempre un posto importante e i vostri ricordi rappresentano per me un grande tesoro, so che sareste fieri di me. Voglio infine ringraziare i miei zii di Pescara, Enrico e Mimma, per essere sempre con me nei momenti importanti come questo, posso sempre contare su di voi.

Ci sono tante persone che vorrei ringraziare e in queste poche righe ne potrò citare solo alcune ma tutti e tutte voi, che siete con me per questa laurea, siete importanti. Un grazie speciale ai miei amici del cuore, Briga, Peppo e Morris. Ripenso alle serate che abbiamo fatto dal primo anno e a tutti i momenti fantastici che abbiamo condiviso, questo percorso universitario non sarebbe stato lo stesso senza di voi. Grazie ai miei amici che sono con me da sempre, Lori e Cam, siamo cresciuti insieme ed è bellissimo condividere con voi questo traguardo. Quindi voglio ringraziare tutte le splendide persone che hanno reso indimenticabili questi anni, compagni di studi e non solo: grazie a Sisco, Mario, Tome, Gigi, Diego, Matte e Filo. Infine volevo ringraziare un caro amico con cui so che posso sempre scherzare e soprattutto su cui posso sempre contare, grazie Gus.

List of Figures

| | | |
|------|---|----|
| 1.1 | CDPR simple architecture | 7 |
| 1.2 | All possible motion patterns, where R is the rotational and T is the translational EE degree of freedom | 10 |
| 1.3 | CDPR architecture for production engineering | 11 |
| 1.4 | CDPR architecture for handling and logistics | 12 |
| 1.5 | Examples of gondola robot for cleaning task | 14 |
| 1.6 | Applications of cables | 15 |
| 1.7 | CDPR architecture for painting and cleaning | 16 |
| 1.8 | Differnet robotic architecture for maintenance task | 17 |
| 1.9 | Mobile platform for green maintenance | 18 |
| 1.10 | Hephaestus CDPR | 21 |
| 2.1 | Different reconfigurable CDPRs performing continuous reconfiguration | 25 |
| 2.2 | Zhou's alternative design for planar CDPRs | 26 |
| 2.3 | Discrete reconfigurable CDPR | 26 |
| 2.4 | Reconfigurable mobile platform to allow motions | 27 |
| 2.5 | SkyBAAM system test: internal and external experiments | 28 |
| 2.6 | NIMS RD system developed for permanent installation | 29 |
| 2.7 | Preliminary concept of deployable EE | 30 |
| 2.8 | RBOT9 prototype | 31 |
| 3.1 | Smooth drum connected to a motor | 34 |
| 3.2 | Rototranslating servo-winch architectures | 35 |
| 3.3 | Spooling-helper servo-winch architecture | 36 |
| 3.4 | Ball-spline servo-winch architecture | 37 |
| 3.5 | The extruded aluminium frame | 38 |
| 3.6 | Example of guiding system and sensors | 39 |
| 3.7 | Frame translating motor solution | 40 |
| 3.8 | Two-grooving drum servo-winch | 40 |
| 3.9 | EE Spooling-helper motor solution | 41 |
| 3.10 | Spooling-helper winch | 42 |
| 3.11 | Eight EE motors solution | 42 |
| 3.12 | Four motors in the EE | 43 |
| 4.1 | Engineering design optimisation process | 48 |
| 4.2 | Basic optimisation problem | 49 |
| 4.3 | Example of first-order necessary condition satisfied | 50 |
| 4.4 | Example of zig-zagging gradient descent for a two-dimensional problem | 52 |
| 4.5 | Initial population distribution | 53 |

| | |
|--|----|
| 4.6 | 54 |
| 4.7 | 54 |
| 4.8 | 55 |
| 4.9 Genetic algorithm application | 55 |
| 4.10 Two-dimensional convex polygon of feasible cable tensions | 57 |
| 4.11 Two special cable interference conditions | 59 |
| 4.12 First <i>ga</i> design | 60 |
| 4.13 Second <i>ga</i> design | 61 |
| 4.14 Third <i>ga</i> design | 62 |
| 4.15 Fourth <i>ga</i> design | 63 |
| 4.16 Two special EE cable configurations | 63 |
| 4.17 Optimised solution | 64 |
| 4.18 Final workspace | 65 |
| 5.1 Final design solution | 67 |
| 5.2 Actuation installed into the EE mobile platform | 68 |
| A.1 Large-scale robotic application | 75 |
| A.2 The largest 3D-printed structure in the world | 76 |
| A.3 Cable-Suspended Contour-Crafting Construction Robot | 77 |
| C.1 More detailed views, solution one | 81 |
| C.2 More detailed views, solution two | 82 |
| C.3 More detailed views, solution three | 83 |
| C.4 More detailed views, solution four | 84 |
| C.5 More detailed views, final solution | 85 |
| D.1 Integrated servo motor by Moons' | 88 |

Bibliography

- [1] A. Ming and T. Higuchi, "Study on multiple degree-of-freedom positioning mechanism using wires. i: Concept, design and control," *International Journal of the Japan Society for Precision Engineering*, vol. 28, no. 2, pp. 131–138, 1994.
- [2] J.-P. Merlet, *Parallel robots*, vol. 74. Springer, 2012.
- [3] M. Hiller, S. Fang, S. Mielczarek, R. Verhoeven, and D. Franitza, "Design, analysis and realization of tendon-based parallel manipulators," *Mechanism and Machine Theory*, vol. 40, no. 4, pp. 429–445, 2005.
- [4] V. Mattioni, E. Idà, and M. Carricato, "Force-distribution sensitivity to cable-tension errors in overconstrained cable-driven parallel robots," *Mechanism and Machine Theory*, vol. 175, p. 104940, 2022.
- [5] C. Gosselin and M. Grenier, "On the determination of the force distribution in overconstrained cable-driven parallel mechanisms," *Meccanica*, vol. 46, no. 1, pp. 3–15, 2011.
- [6] K. Müller, C. Reichert, and T. Bruckmann, "Analysis of a real-time capable cable force computation method," in *Cable-Driven Parallel Robots* (A. Pott and T. Bruckmann, eds.), (Cham), pp. 227–238, Springer International Publishing, 2015.
- [7] A. Pott, "An improved force distribution algorithm for over-constrained cable-driven parallel robots," in *Computational Kinematics* (E. Thomas and A. Perez Gracia, eds.), (Dordrecht), pp. 139–146, Springer Netherlands, 2014.
- [8] M. Gouttefarde, J. Lamaury, C. Reichert, and T. Bruckmann, "A versatile tension distribution algorithm for n -dof parallel robots driven by $n + 2$ cables," *IEEE Transactions on Robotics*, vol. 31, pp. 1444–1457, Dec 2015.
- [9] R. Verhoeven, M. Hiller, and S. Tadokoro, "Workspace, stiffness, singularities and classification of tendon-driven stewart platforms," in *Advances in robot kinematics: Analysis and Control*, pp. 105–114, Springer, 1998.
- [10] S.-R. Oh and S. Agrawal, "Cable-suspended planar parallel robots with redundant cables: controllers with positive cable tensions," in *2003 IEEE International Conference on Robotics and Automation (Cat. No.03CH37422)*, vol. 3, pp. 3023–3028 vol.3, Sep. 2003.
- [11] M. Hassan and A. Khajepour, "Minimization of Bounded Cable Tensions in Cable-Based Parallel Manipulators," in *International Design Engineering Technical Conferences and Computers and Information in Engineering Conference*,

- vol. Volume 8: 31st Mechanisms and Robotics Conference, Parts A and B, pp. 991–999, 09 2007.
- [12] J. Lamaury and M. Gouttefarde, “A tension distribution method with improved computational efficiency,” in *Cable-Driven Parallel Robots* (T. Bruckmann and A. Pott, eds.), pp. 71–85, Berlin, Heidelberg: Springer Berlin Heidelberg, 2013.
- [13] L. Mikelsons, T. Bruckmann, M. Hiller, and D. Schramm, “A real-time capable force calculation algorithm for redundant tendon-based parallel manipulators,” in *2008 IEEE International Conference on Robotics and Automation*, pp. 3869–3874, May 2008.
- [14] R. L. Williams II, M. Xin, and P. Bosscher, “Contour-crafting-cartesian-cable robot system: dynamics and controller design,” in *Proc. of the ASME 2008 International Design Engineering Technical Conferences, DETC 2008*, (Brooklyn, New York, USA), pp. 39 – 45, 2008.
- [15] A. Pott, C. Meyer, and A. Verl, “Large-scale assembly of solar power plants with parallel cable robots,” in *ISR 2010 (41st International Symposium on Robotics) and ROBOTIK 2010 (6th German Conference on Robotics)*, pp. 1–6, VDE, 2010.
- [16] V. Mattioni, E. Ida’, and M. Carricato, “Design of a planar cable-driven parallel robot for non-contact tasks,” *Applied Sciences*, vol. 11, no. 20, 2021.
- [17] S. Kawamura, W. Choe, S. Tanaka, and H. Kino, “Development of an ultrahigh speed robot falcon using parallel wire drive systems,” *Journal of the Robotics Society of Japan*, vol. 15, no. 1, pp. 82–89, 1997.
- [18] T. Bruckmann, W. Lalo, K. Nguyen, and B. Salah, “Development of a storage retrieval machine for high racks using a wire robot,” in *ASME 2012 International Design Engineering Technical Conferences and Computers and Information in Engineering Conference*, pp. 771–780, American Society of Mechanical Engineers, 2012.
- [19] T. Bruckmann, C. Reichert, and H. Ji, “Energy consumption reduction of a cable-driven storage and retrieval system,” in *Advances in Robot Kinematics 2018* (J. Lenarcic and V. Parenti-Castelli, eds.), (Cham), pp. 383–391, Springer International Publishing, 2019.
- [20] J.-p. Merlet and D. Daney, “A portable, modular parallel wire crane for rescue operations,” in *Robotics and Automation (ICRA), 2010 IEEE International Conference on*, pp. 2834–2839, IEEE, 2010.
- [21] C. Bauer, “Device and method for detecting the inventory of a selling and/or storing device, and a storage-managing system equipped with said device,” 2012.
- [22] R. Bogue, “What are the prospects for robots in the construction industry?,” *Industrial Robot: An International Journal*, vol. 45, pp. 1–6, Jan. 2018.
- [23] S. Cai, Z. Ma, M. Skibniewski, J. Guo, and L. Yun, “Application of automation and robotics technology in high-rise building construction: An overview,” in *Proceedings of the 35th International Symposium on Automation and Robotics in*

- Construction (ISARC)* (J. Teizer, ed.), (Taipei, Taiwan), pp. 309–316, International Association for Automation and Robotics in Construction (IAARC), July 2018.
- [24] M. Gharbia, A. Y. Chang-Richards, and R. Zhong, “Robotic technologies in concrete building construction: A systematic review,” in *Proceedings of the 36th International Symposium on Automation and Robotics in Construction (ISARC)* (M. Al-Hussein, ed.), (Banff, Canada), pp. 10–19, International Association for Automation and Robotics in Construction (IAARC), May 2019.
- [25] J. M. Davila Delgado, L. Oyedele, A. Ajayi, L. Akanbi, O. Akinade, M. Bilal, and H. Owolabi, “Robotics and automated systems in construction: Understanding industry-specific challenges for adoption,” *Journal of Building Engineering*, vol. 26, p. 100868, 2019.
- [26] T. Lipecki, P. Jamińska-Gadomska, and E. Błazik-Borowa, “Wind load on façade scaffolding without protective cover – eurocode and in-situ measurement approaches,” *Journal of Building Engineering*, vol. 42, p. 102516, 2021.
- [27] E. Paquet and B. Furet, “Stiffness study of a robotic system working on vertical building surfaces in construction field,” in *Proceedings of the 38th International Symposium on Automation and Robotics in Construction (ISARC)* (C. Feng, T. Linner, I. Brilakis, D. Castro, P.-H. Chen, Y. Cho, J. Du, S. Ergan, B. Garcia de Soto, J. Gasparík, F. Habbal, A. Hammad, K. Iturralde, T. Bock, S. Kwon, Z. Lafhaj, N. Li, C.-J. Liang, B. Mantha, M. S. Ng, D. Hall, M. Pan, W. Pan, F. Rahimian, B. Raphael, A. Sattineni, C. Schlette, I. Shabtai, X. Shen, P. Tang, J. Teizer, Y. Turkan, E. Valero, and Z. Zhu, eds.), (Dubai, UAE), pp. 805–810, International Association for Automation and Robotics in Construction (IAARC), November 2021.
- [28] B. Guo, Y. M. Goh, E. Scheepbouwer, and Y. Zou, *An ontology of control measures for fall from height in the construction industry*. Taipei, Taiwan: International Association for Automation and Robotics in Construction (IAARC), July 2018.
- [29] J.-B. Izard, M. Gouttefarde, C. Baradat, D. Culla, and D. Sallé, “Integration of a parallel cable-driven robot on an existing building façade,” in *Cable-Driven Parallel Robots* (T. Bruckmann and A. Pott, eds.), pp. 149–164, Berlin, Heidelberg: Springer Berlin Heidelberg, 2013.
- [30] K. E. Larsen, F. Lattke, S. Ott, and S. Winter, “Surveying and digital workflow in energy performance retrofit projects using prefabricated elements,” *Automation in Construction*, vol. 20, no. 8, pp. 999–1011, 2011.
- [31] J. O’Donnell, L. Truong-Hong, N. Boyle, E. Corry, J. Cao, and D. F. Laefer, “Lidar point-cloud mapping of building façades for building energy performance simulation,” *Automation in Construction*, vol. 107, p. 102905, 2019.
- [32] J. K. Lee, J. H. Ryu, and D. J. Lee, “An experimental study of automatic cleaning tool and robot for facade in high-rise buildings,” in *28th International Symposium on Automation and Robotics in Construction (ISARC 2011)* (S. Kwon, ed.), (Seoul, Korea), pp. 1453–1458, International Association for Automation and Robotics in Construction (IAARC), June 2011.

- [33] T. Seo, Y. Jeon, C. Park, and J. Kim, "Survey on glass and façade-cleaning robots: Climbing mechanisms, cleaning methods, and applications," *International Journal of Precision Engineering and Manufacturing-Green Technology*, vol. 6, no. 2, pp. 367–376, 2019.
- [34] J. Hong, T. Kim, H. Chae, G. Park, J. Lee, J. Kim, H. S. Kim, and T. Seo, "Design of window-cleaning robotic manipulator with compliant adaptation capability," *IEEE/ASME Transactions on Mechatronics*, vol. 25, no. 4, pp. 1878–1885, 2020.
- [35] W. Pan, R. Li, and T. Bock, "Design and synthesis of the localization system for the on-site construction robot," in *Proceedings of the 37th International Symposium on Automation and Robotics in Construction (ISARC)* (T. K. "Osumi Hisashi", "Furuya Hiroshi", ed.), (Kitakyushu, Japan), pp. 1501–1507, International Association for Automation and Robotics in Construction (IAARC), October 2020.
- [36] H. Fawzy, H. El Sherif, and A. Khamis, "Robotic façade cleaning system for high-rise building," in *2019 14th International Conference on Computer Engineering and Systems (ICCES)*, pp. 282–287, 2019.
- [37] H. Chae, Y. Moon, K. Lee, S. Park, H. S. Kim, and T. Seo, "A tethered façade cleaning robot based on a dual rope windlass climbing mechanism: Design and experiments," *IEEE/ASME Transactions on Mechatronics*, vol. 27, no. 4, pp. 1982–1989, 2022.
- [38] K. H. J. Voss, V. van der Wijk, and J. L. Herder, "Investigation of a cable-driven parallel mechanism for interaction with a variety of surfaces, applied to the cleaning of free-form buildings," in *Latest Advances in Robot Kinematics* (J. Lenarcic and M. Husty, eds.), (Dordrecht), pp. 261–268, Springer Netherlands, 2012.
- [39] Z. Shao, G. Xie, Z. Zhang, and L. Wang, "Design and analysis of the cable-driven parallel robot for cleaning exterior wall of buildings," *International Journal of Advanced Robotic Systems*, vol. 18, no. 1, p. 1729881421990313, 2021.
- [40] L. Gang-feng, Z. Ying-yong, L. Chang-le, and Y. Ji-hong, "Design and optimization of spraying robot arm for hull blocks," in *2015 IEEE International Conference on Robotics and Biomimetics (ROBIO)*, pp. 2615–2620, 2015.
- [41] A. Jayaraj and H. N. Divakar, "Robotics in construction industry," *IOP Conference Series: Materials Science and Engineering*, vol. 376, p. 012114, jun 2018.
- [42] T. Kitahara, K. Satou, and J. Onodera, "Marking robot in cooperation with three-dimensional measuring instruments," in *Proceedings of the 35th International Symposium on Automation and Robotics in Construction (ISARC)* (J. Teizer, ed.), (Taipei, Taiwan), pp. 292–299, International Association for Automation and Robotics in Construction (IAARC), July 2018.
- [43] Y. S. C. Darwin Tat Ming Lau, "System and method for building façade cleaning and painting with a dual cable-driven robot," June 2021.

- [44] D. Panyaa, J. Seo, H. Park, W. Lee, and S. Choo, "A study of kinetic façade modelling performance using virtual reality," in *Proceedings of the 36th International Symposium on Automation and Robotics in Construction (ISARC)* (M. Al-Hussein, ed.), (Banff, Canada), pp. 356–359, International Association for Automation and Robotics in Construction (IAARC), May 2019.
- [45] S. Cai, Z. Ma, and J. Guo, "Analysis on the implementation mechanism of an inspection robot for glass curtain walls in high-rise buildings," in *Proceedings of the 37th International Symposium on Automation and Robotics in Construction (ISARC)* (T. K. "Osumi Hisashi", "Furuya Hiroshi", ed.), (Kitakyushu, Japan), pp. 1556–1561, International Association for Automation and Robotics in Construction (IAARC), October 2020.
- [46] Y. Hou, L. Soibelman, R. Volk, and M. Chen, "Factors affecting the performance of 3d thermal mapping for energy audits in a district by using infrared thermography (irt) mounted on unmanned aircraft systems (uas)," in *Proceedings of the 36th International Symposium on Automation and Robotics in Construction (ISARC)* (M. Al-Hussein, ed.), (Banff, Canada), pp. 266–273, International Association for Automation and Robotics in Construction (IAARC), May 2019.
- [47] P. Ko, S. A. Prieto, and B. García de Soto, "Abecis: an automated building exterior crack inspection system using uavs, open-source deep learning and photogrammetry," in *Proceedings of the 38th International Symposium on Automation and Robotics in Construction (ISARC)* (C. Feng, T. Linner, I. Brilakis, D. Castro, P.-H. Chen, Y. Cho, J. Du, S. Ergan, B. Garcia de Soto, J. Gasparík, F. Habbal, A. Hammad, K. Iturralde, T. Bock, S. Kwon, Z. Lafhaj, N. Li, C.-J. Liang, B. Mantha, M. S. Ng, D. Hall, M. Pan, W. Pan, F. Rahimian, B. Raphael, A. Sattineni, C. Schlette, I. Shabtai, X. Shen, P. Tang, J. Teizer, Y. Turkan, E. Valero, and Z. Zhu, eds.), (Dubai, UAE), pp. 637–644, International Association for Automation and Robotics in Construction (IAARC), November 2021.
- [48] X. Xu, D. Lu, B. Sher, S. Kim, A. Rathod, S. Ergan, and C. Feng, "Conceptual design of a robotic building envelope assessment system for energy efficiency," in *Proceedings of the 38th International Symposium on Automation and Robotics in Construction (ISARC)* (C. Feng, T. Linner, I. Brilakis, D. Castro, P.-H. Chen, Y. Cho, J. Du, S. Ergan, B. Garcia de Soto, J. Gasparík, F. Habbal, A. Hammad, K. Iturralde, T. Bock, S. Kwon, Z. Lafhaj, N. Li, C.-J. Liang, B. Mantha, M. S. Ng, D. Hall, M. Pan, W. Pan, F. Rahimian, B. Raphael, A. Sattineni, C. Schlette, I. Shabtai, X. Shen, P. Tang, J. Teizer, Y. Turkan, E. Valero, and Z. Zhu, eds.), (Dubai, UAE), pp. 653–660, International Association for Automation and Robotics in Construction (IAARC), November 2021.
- [49] S. M. Moon, D. H. Hong, S. W. Kim, and S. R. Park, "Development of building-façade maintenance robot with docking station based on vertical climbing mechanism," in *28th International Symposium on Automation and Robotics in Construction (ISARC 2011)* (S. Kwon, ed.), (Seoul, Korea), pp. 1221–1222, International Association for Automation and Robotics in Construction (IAARC), June 2011.

- [50] S.-M. Moon, D. Hong, S.-W. Kim, and S. Park, "Building wall maintenance robot based on built-in guide rail," in *2012 IEEE International Conference on Industrial Technology*, pp. 498–503, 2012.
- [51] K. H. Koh, M. Farhan, K. P. C. Yeung, D. C. H. Tang, M. P. Y. Lau, P. K. Cheung, and K. W. C. Lai, "Teleoperated service robotic system for on-site surface rust removal and protection of high-rise exterior gas pipes," *Automation in Construction*, vol. 125, p. 103609, 2021.
- [52] S. Schröder, "Under constrained cable-driven parallel robot for vertical green maintenance," in *Cable-Driven Parallel Robots* (M. Gouttefarde, T. Bruckmann, and A. Pott, eds.), (Cham), pp. 389–400, Springer International Publishing, 2021.
- [53] EU, "Directive (eu) 2018/844 of the european parliament and of the council of 30 may 2018: amending directive 2010/31/eu on the energy performance of buildings and directive 2012/27/eu on energy efficiency," May 2018.
- [54] E. Lublasser, T. Adams, A. Vollpracht, and S. Brell-Cokcan, "Robotic application of foam concrete onto bare wall elements - analysis, concept and robotic experiments," *Automation in Construction*, vol. 89, pp. 299–306, 2018.
- [55] D. A. Pohoryles, D. A. Bournas, F. Da Porto, A. Caprino, G. Santarsiero, and T. Triantafyllou, "Integrated seismic and energy retrofitting of existing buildings: A state-of-the-art review," *Journal of Building Engineering*, vol. 61, p. 105274, 2022.
- [56] K. Iturralde, T. Linner, and T. Bock, "Comparison of automated and robotic support bodies for building facade upgrading," in *Proceedings of the 32nd International Symposium on Automation and Robotics in Construction and Mining (ISARC 2015)* (M. Malaska and R. Heikkilä, eds.), (Oulu, Finland), pp. 1–8, International Association for Automation and Robotics in Construction (IAARC), June 2015.
- [57] K. Iturralde, T. Linner, and T. Bock, "First monitoring and analysis of the manufacturing and installation process of timber based 2d modules for accomplishing a future robotic building envelope upgrading," in *Proceedings of the 34th International Symposium on Automation and Robotics in Construction (ISARC)* (M.-Y. N. T. U. o. S. Cheng, Technology), H.-M. N. T. U. o. S. Chen, Technology), K. C. N. T. U. o. S. Chiu, and Technology), eds.), (Taipei, Taiwan), pp. 65–73, Tribun EU, s.r.o., Brno, July 2017.
- [58] K. Iturralde and T. Bock, "Integrated, automated and robotic process for building upgrading with prefabricated modules," in *Proceedings of the 35th International Symposium on Automation and Robotics in Construction (ISARC)* (J. Teizer, ed.), (Taipei, Taiwan), pp. 340–347, International Association for Automation and Robotics in Construction (IAARC), July 2018.
- [59] B. Johns, M. Arashpour, and E. Abdi, "Curtain wall installation for high-rise buildings: Critical review of current automation solutions and opportunities," in *Proceedings of the 37th International Symposium on Automation and Robotics in Construction (ISARC)* (T. K. Osumi Hisashi, Furuya Hiroshi, ed.), (Kitakyushu, Japan), pp. 393–400, International Association for Automation and Robotics in Construction (IAARC), October 2020.

-
- [60] H. Hussein, J. C. Santos, and M. Gouttefarde, "Geometric optimization of a large scale cdpr operating on a building facade," in *2018 IEEE/RSJ International Conference on Intelligent Robots and Systems (IROS), "International Conference on Intelligent Robots and Systems"*, pp. 5117–5124, Oct 2018.
- [61] H. Hussein, J. C. Santos, J.-B. Izard, and M. Gouttefarde, "Smallest maximum cable tension determination for cable-driven parallel robots," *IEEE Transactions on Robotics*, vol. 37, no. 4, pp. 1186–1205, 2021.
- [62] M. Taghavi, K. Iturralde, and T. Bock, "Cable-driven parallel robot for curtain wall modules automatic installation," in *Proceedings of the 35th International Symposium on Automation and Robotics in Construction (ISARC)* (J. Teizer, ed.), (Taipei, Taiwan), pp. 396–403, International Association for Automation and Robotics in Construction (IAARC), July 2018.
- [63] K. Iturralde, M. Feucht, D. Illner, R. Hu, W. Pan, T. Linner, T. Bock, I. Eskudero, M. Rodriguez, J. Gorrotxategi, J. Izard, J. Astudillo, J. Cavalcanti Santos, M. Gouttefarde, M. Fabritius, C. Martin, T. Henninge, S. Nornes, Y. Jacobsen, A. Pracucci, J. Cañada, J. Jimenez-Vicaria, R. Alonso, and L. Elia, "Cable-driven parallel robot for curtain wall module installation," *Automation in Construction*, vol. 138, p. 104235, 2022.
- [64] K. Iturralde, W. Pan, T. Linner, T. Bock, E. Gasparri, A. Brambilla, G. Lobaccaro, F. Goia, A. Andaloro, and A. Sangiorgio, "19 - automation and robotic technologies in the construction context: research experiences in prefabricated façade modules," in *Rethinking Building Skins*, pp. 475–493, Woodhead Publishing, 2022.
- [65] R. Boumann, P. Lemmen, R. Heidel, and T. Bruckmann, "Optimization of trajectories for cable robots on automated construction sites," in *Proceedings of the 37th International Symposium on Automation and Robotics in Construction (ISARC)* (T. K. "Osumi Hisashi", "Furuya Hiroshi", ed.), (Kitakyushu, Japan), pp. 465–472, International Association for Automation and Robotics in Construction (IAARC), October 2020.
- [66] S. Perreault, P. Cardou, C. M. Gosselin, and M. J.-D. Otis, "Geometric determination of the interference-free constant-orientation workspace of parallel cable-driven mechanisms," *J. Mechanisms Robotics*, vol. 2, July 2010.
- [67] M. M. Aref and H. D. Taghirad, "Geometrical workspace analysis of a cable-driven redundant parallel manipulator: Kntu cdrpm," in *2008 IEEE/RSJ International Conference on Intelligent Robots and Systems, "International Conference on Intelligent Robots and Systems"*, pp. 1958–1963, Sep. 2008.
- [68] K. Youssef and M. J.-D. Otis, "Reconfigurable fully constrained cable driven parallel mechanism for avoiding interference between cables," *Mechanism and Machine Theory*, vol. 148, p. 103781, 2020.
- [69] E. Khoshbin, K. Youssef, R. Meziane, and M. J.-D. Otis, "Reconfigurable fully constrained cable-driven parallel mechanism for avoiding collision between cables with human," *Robotica*, vol. 40, no. 12, p. 4405–4430, 2022.

- [70] J. Bettega, G. Boschetti, G. Piva, D. Richiedei, and A. Trevisani, "Reconfiguration strategy for fully actuated translational cable-suspended parallel robots," *Frontiers in Robotics and AI*, vol. 10, 2023.
- [71] D. Q. Nguyen, M. Gouttefarde, O. Company, and F. Pierrot, "On the analysis of large-dimension reconfigurable suspended cable-driven parallel robots," in *2014 IEEE International Conference on Robotics and Automation (ICRA), (ICRA) OR "International Conference on Robotics and Automation"*, pp. 5728–5735, May 2014.
- [72] G. Abbasnejad and M. Tale-Masouleh, "Optimal wrench-closure configuration of spatial reconfigurable cable-driven parallel robots," *Proceedings of the Institution of Mechanical Engineers, Part C: Journal of Mechanical Engineering Science*, vol. 0, no. 0, p. 0954406220976166, 2020.
- [73] M. Gouttefarde, D. Daney, and J.-P. Merlet, "Interval-analysis-based determination of the wrench-feasible workspace of parallel cable-driven robots," *IEEE Transactions on Robotics*, vol. 27, pp. 1–13, Feb 2011.
- [74] G. Boschetti and A. Trevisani, "Performance evaluation for cable direct driven robot," in *ASME 2014 12th Biennial Conference on Engineering Systems Design and Analysis*, July 2014.
- [75] A. Raman, I. Walker, V. Krovi, and M. Schmid, "Cable failure tolerant control and planning in a planar reconfigurable cable driven parallel robot," *Frontiers in Robotics and AI*, vol. 10, 2023.
- [76] H. Xiong, H. Cao, W. Zeng, J. Huang, X. Diao, W. Lu, and Y. Lou, "Real-Time Reconfiguration Planning for the Dynamic Control of Reconfigurable Cable-Driven Parallel Robots," *Journal of Mechanisms and Robotics*, vol. 14, p. 060913, 09 2022.
- [77] L. Gagliardini, S. Caro, M. Gouttefarde, and A. Girin, "Discrete reconfiguration planning for cable-driven parallel robots," *Mechanism and Machine Theory*, vol. 100, pp. 313–337, 2016.
- [78] H. Tan, L. Nurahmi, B. Pramujati, and S. Caro, "On the reconfiguration of cable-driven parallel robots with multiple mobile cranes," in *2020 5th International Conference on Robotics and Automation Engineering (ICRAE)*, pp. 126–130, 2020.
- [79] T. Rasheed, P. Long, and S. Caro, "Wrench-feasible workspace of mobile cable-driven parallel robots," *J. Mechanisms Robotics, "J. Mechanisms Robotics" OR "Journal of Mechanisms and Robotics", J. Mechanisms Robotics OR Journal of Mechanisms and Robotics, (J. Mechanisms Robotics) OR (Journal of Mechanisms and Robotics)*, vol. 12, Jan. 2020.
- [80] M. Anson, A. Alamdari, and V. Krovi, "Orientation Workspace and Stiffness Optimization of Cable-Driven Parallel Manipulators With Base Mobility," *Journal of Mechanisms and Robotics*, vol. 9, 03 2017. 031011.

-
- [81] A. Raman, M. Schmid, and V. Krovi, "Stiffness Modulation for a Planar Mobile Cable-Driven Parallel Manipulators via Structural Reconfiguration," in *International Design Engineering Technical Conferences and Computers and Information in Engineering Conference*, vol. Volume 10: 44th Mechanisms and Robotics Conference (MR), 08 2020. V010T10A054.
- [82] S. Qian, B. Zi, D. Wang, and Y. Li, "Development of modular cable-driven parallel robotic systems," *IEEE Access*, vol. 7, pp. 5541–5553, 2019.
- [83] T. Zhao, B. Zi, S. Qian, Z. Yin, and D. Zhang, "Typical configuration analysis of a modular reconfigurable cable-driven parallel robot," *International Journal of Advanced Robotic Systems*, vol. 16, no. 2, p. 1729881419834756, 2019.
- [84] X. Wang, Y. Li, B. Zi, Q. Wu, and J. Zhao, "Obstacle avoidance planning and experimental study of reconfigurable cable-driven parallel robot based on deep reinforcement learning," in *Intelligent Robotics and Applications* (H. Liu, Z. Yin, L. Liu, L. Jiang, G. Gu, X. Wu, and W. Ren, eds.), (Cham), pp. 541–551, Springer International Publishing, 2022.
- [85] C. Masone, H. H. Bühlhoff, and P. Stegagno, "Cooperative transportation of a payload using quadrotors: A reconfigurable cable-driven parallel robot," in *2016 IEEE/RSJ International Conference on Intelligent Robots and Systems (IROS), "International Conference on Intelligent Robots and Systems"*, pp. 1623–1630, Oct 2016.
- [86] D. Six, A. Chriette, S. Briot, and P. Martinet, "Dynamic modeling and trajectory tracking controller of a novel flying parallel robot," *IFAC-PapersOnLine*, vol. 50, no. 1, pp. 2241–2246, 2017. 20th IFAC World Congress.
- [87] M. Manubens, D. Devaurs, L. Ros, and J. Cortes, "Motion planning for 6-d manipulation with aerial towed-cable systems," in *Robotics: Science and Systems IX* (D. F. Paul Newman and D. Hsu, eds.), (Berlin, Germany), pp. 28–35, 2013.
- [88] Q. Jiang and V. Kumar, "The inverse kinematics of cooperative transport with multiple aerial robots," *IEEE Transactions on Robotics*, vol. 29, no. 1, pp. 136–145, 2013.
- [89] R. Bostelman, A. Jacoff, F. Proctor, T. Kramer, and A. Wavering, "Cable-based reconfigurable machines for large scale manufacturing," in *Proceedings of the 2000 Japan-USA Symposium on Flexible Automation*, pp. 23–26, Citeseer, 2000.
- [90] J.-B. Izard, M. Gouttefarde, M. Michelin, O. Tempier, and C. Baradat, "A reconfigurable robot for cable-driven parallel robotic research and industrial scenario proofing," in *Cable-Driven Parallel Robots* (T. Bruckmann and A. Pott, eds.), pp. 135–148, Berlin, Heidelberg: Springer Berlin Heidelberg, 2013.
- [91] G. Rosati, D. Zanotto, and S. K. Agrawal, "On the design of adaptive cable-driven systems," *ASME Journal of Mechanisms and Robotics*, vol. 3, no. 2, pp. 021004/1–13, 2011.
- [92] X. Zhou, C. P. Tang, and V. Krovi, "Analysis framework for cooperating mobile cable robots," in *2012 IEEE International Conference on Robotics and Automation*, pp. 3128–3133, May 2012.

- [93] X. Zhou, S. kook Jun, and V. Krovi, "Stiffness modulation exploiting configuration redundancy in mobile cable robots," in *2014 IEEE International Conference on Robotics and Automation*, pp. 5934–5939, May 2014.
- [94] L. Gagliardini, S. Caro, M. Gouttefarde, P. Wenger, and A. Girin, "A reconfigurable cable-driven parallel robot for sandblasting and painting of large structures," in *Cable-Driven Parallel Robots* (A. Pott and T. Bruckmann, eds.), (Cham), pp. 275–291, Springer International Publishing, 2015.
- [95] A. Rodriguez-Barroso, R. Saltaren, G. A. Portilla, J. S. Cely, and M. Carpio, "Cable-driven parallel robot with reconfigurable end effector controlled with a compliant actuator," *Sensors*, vol. 18, no. 9, 2018.
- [96] R. Wang, S. Li, and Y. Li, "A suspended cable-driven parallel robot with articulated reconfigurable moving platform for schonflies motions," *IEEE/ASME Transactions on Mechatronics*, pp. 1–12, 2022.
- [97] P. C. Chesser, P. L. Wang, J. E. Vaughan, R. F. Lind, and B. K. Post, "Kinematics of a Cable-Driven Robotic Platform for Large-Scale Additive Manufacturing," *Journal of Mechanisms and Robotics*, vol. 14, 09 2021. 021010.
- [98] S. A. Khalilpour, A. Bourbour, R. Khorrambakht, S. Kariminasab, and H. D. Taghirad, "Forward kinematics resolution of a deployable cable robot," in *2017 5th RSI International Conference on Robotics and Mechatronics (ICRoM)*, pp. 27–32, 2017.
- [99] S. A. Khalilpour, R. Khorrambakht, H. D. Taghirad, and P. Cardou, "Wave based control of a deployable cable driven robot," in *2018 6th RSI International Conference on Robotics and Mechatronics (ICRoM)*, pp. 166–171, Oct 2018.
- [100] S. A. Khalilpour, R. Khorrambakht, M. J. Harandi, H. D. Taghirad, and P. Cardou, "Cascade terminal sliding mode control of a deployable cable driven robot," in *2019 6th International Conference on Control, Instrumentation and Automation (ICCA)*, pp. 1–6, 2019.
- [101] R. Khorrambakht, H. Damirchi, S. A. Khalilpour, and H. D. Taghirad, "A calibration framework for deployable cable driven parallel robots with flexible cables," in *2019 7th International Conference on Robotics and Mechatronics (ICRoM)*, pp. 552–557, 2019.
- [102] S. A. Khalilpour, R. Khorrambakht, H. Damirchi, H. D. Taghirad, and P. Cardou, "Tip-trajectory tracking control of a deployable cable-driven robot via output redefinition," *Multibody System Dynamics*, vol. 52, no. 1, pp. 31–58, 2021.
- [103] S. A. Khalilpour, A. Hassani, R. Khorambakht, A. Zahedi, A. Bataleblu, and H. D. Taghirad, "Joint space control of a deployable cable driven parallel robot with redundant actuators," in *2022 30th International Conference on Electrical Engineering (ICEE)*, pp. 748–754, 2022.
- [104] C. C. Cheah and X. Li, *Task-space sensory feedback control of robot manipulators*, vol. 73. Springer, 2015.

-
- [105] B. L. Jordan, M. A. Batalin, and W. J. Kaiser, "Nims rd: A rapidly deployable cable based robot," in *Proceedings 2007 IEEE International Conference on Robotics and Automation*, pp. 144–150, 2007.
- [106] P. H. Borgstrom, M. J. Stealey, M. A. Batalin, and W. J. Kaiser, "Nims3d: A novel rapidly deployable robot for 3-dimensional applications," in *2006 IEEE/RSJ International Conference on Intelligent Robots and Systems*, pp. 3628–3635, 2006.
- [107] E. Idà, D. Marian, and M. Carricato, "A deployable cable-driven parallel robot with large rotational capabilities for laser-scanning applications," *IEEE Robotics and Automation Letters*, vol. 5, no. 3, pp. 4140–4147, 2020.
- [108] D. S. Monich, I. I. Borisov, E. S. Skosarev, and S. A. Kolyubin, "Development of light-weight and rapidly deployable cable-driven robot," in *2019 IEEE International Conference on Mechatronics (ICM)*, vol. 1, pp. 622–627, 2019.
- [109] P. Bosscher, R. L. Williams, and M. Tummino, "A concept for rapidly-deployable cable robot search and rescue systems," in *ASME 2005 International Design Engineering Technical Conferences and Computers and Information in Engineering Conference*, pp. 589–598, American Society of Mechanical Engineers, 2005.
- [110] O. Saber, "A Spatial Translational Cable Robot," *Journal of Mechanisms and Robotics*, vol. 7, p. 031006, 08 2015.
- [111] J. Albus, R. Bostelman, and N. Dagalakis, "The nist robocrane," *Journal of National Institute of Standards and Technology*, vol. 97, no. 3, 1992.
- [112] R. L. Williams, "Novel cable-suspended robocrane support," *Industrial Robot: An International Journal*, vol. 32, pp. 326–333, Jan. 2005.
- [113] J. S. Albus, R. V. Bostelman, and A. S. Jacoff, "Modular suspended manipulator," May 2003.
- [114] M. Thaler and A. Sarlah, "System for Moving a Platform and a Useful Load in Space by Using Cables and Drums Arranged on the Platform," Aug. 2016.
- [115] P. J. Bennett, G. Cook, M. R. Jones, K. Ashenayi, M. F. Henry, and A. Macdonald, "Aerial Camera System," Sept. 2012.
- [116] F. Vachon, "Cable robot," Nov. 2019.
- [117] E. G. Dousis, I. Z. Emiris, T. E. Lilas, and A. V. Tomazos, "System for the Cleaning and Inspection of Containers and Tanks in Commercial Ships with Use of Robot Wire Ropes," Jan. 2021.
- [118] H. Trigui and A. Al-Hannabi, "Cable suspended robot for industrial plants," Mar. 2023.
- [119] R. Heidel, R. Boumann, T. Bruckmann, and P. Lemmen, "Rekonfigurierbares Seilrobotersystem," Apr. 2023.
- [120] E. Idà and V. Mattioni, "Cable-driven parallel robot actuators: State of the art and novel servo-winch concept," 2022.

- [121] R. Zhang, J. Wu, and Y. Wang, “Stability analysis of a novel mobile spray-painting robot for touch-up painting in vehicle repair plant,” *Journal of Mechanical Science and Technology*, vol. 36, no. 5, pp. 2571–2584, 2022.
- [122] G. A. I. Carra, A. Y. R. E. Argiolas, A. Y. R. E. Bellissima, M. Y. R. E. Niccolini, and .-. Y. R. E. Ragaglia, Matteo, “Robotics in the construction industry: State of the art and future opportunities,” in *Proceedings of the 35th International Symposium on Automation and Robotics in Construction (ISARC)* (J. Teizer, ed.), (Taipei, Taiwan), pp. 866–873, International Association for Automation and Robotics in Construction (IAARC), July 2018.
- [123] J.-I. Jäkel, S. Rahnema, and K. Klemt-Albert, “Construction robotics excellence model: A framework to overcome existing barriers for the implementation of robotics in the construction industry,” in *Proceedings of the 39th International Symposium on Automation and Robotics in Construction* (T. Linner, B. García de Soto, R. Hu, I. Brilakis, T. Bock, W. Pan, A. Carbonari, D. Castro, H. Mesa, C. Feng, M. Fischer, C. Brosque, V. Gonzalez, D. Hall, M. S. Ng, V. Kamat, C.-J. Liang, Z. Lafhaj, W. Pan, M. Pan, and Z. Zhu, eds.), pp. 605–613, International Association for Automation and Robotics in Construction (IAARC), July 2022.
- [124] R. Hu, K. Iturralde, T. Linner, C. Zhao, W. Pan, A. Pracucci, and T. Bock, “A simple framework for the cost–benefit analysis of single-task construction robots based on a case study of a cable-driven facade installation robot,” *Buildings*, vol. 11, no. 1, 2021.
- [125] T. Bock, “The future of construction automation: Technological disruption and the upcoming ubiquity of robotics,” *Automation in Construction*, vol. 59, pp. 113–121, 2015.
- [126] B. Xiao, C. Chen, and X. Yin, “Recent advancements of robotics in construction,” *Automation in Construction*, vol. 144, p. 104591, 2022.
- [127] T. Beauchat, Y. Hu, R. M. Leicht, and C. Suanico, “Analyzing schedule dependency and sequencing changes for robotic construction using graph analysis,” *Journal of Computing in Civil Engineering*, vol. 37, no. 1, p. 04022043, 2023.
- [128] K. Wu, B. Garcia de Soto, B. T. Adey, and F. Zhang, “Automatic generation of the vertical transportation demands during the construction of high-rise buildings using bim,” in *Proceedings of the 36th International Symposium on Automation and Robotics in Construction (ISARC)* (M. Al-Hussein, ed.), (Banff, Canada), pp. 99–106, International Association for Automation and Robotics in Construction (IAARC), May 2019.
- [129] T. Bruckmann, C. Reichert, M. Meik, P. Lemmen, A. Spengler, H. Mattern, and M. König, “Concept studies of automated construction using cable-driven parallel robots,” in *Cable-Driven Parallel Robots* (C. Gosselin, P. Cardou, T. Bruckmann, and A. Pott, eds.), (Cham), pp. 364–375, Springer International Publishing, 2018.
- [130] S. Ercan, S. Meier, F. Gramazio, and M. Kohler, “Automated localization of a mobile construction robot with an external measurement device,” in *Proceedings of*

- the 36th International Symposium on Automation and Robotics in Construction (ISARC)* (M. Al-Hussein, ed.), (Banff, Canada), pp. 929–936, International Association for Automation and Robotics in Construction (IAARC), May 2019.
- [131] T. Liu, H. Zhou, Y. Du, and J. Zhao, “Measuring and positioning system design of robotic floor-tiling,” in *Proceedings of the 36th International Symposium on Automation and Robotics in Construction (ISARC)* (M. Al-Hussein, ed.), (Banff, Canada), pp. 716–721, International Association for Automation and Robotics in Construction (IAARC), May 2019.
- [132] S. Lee, M.-S. Kang, and C.-S. Han, “Sensor based motion planning and estimation of highrise building façade maintenance robot,” *International Journal of Precision Engineering and Manufacturing*, vol. 13, no. 12, pp. 2127–2134, 2012.
- [133] Y. Tian, C. Chen, K. Sagoe-Crentsil, J. Zhang, and W. Duan, “Intelligent robotic systems for structural health monitoring: Applications and future trends,” *Automation in Construction*, vol. 139, p. 104273, 2022.
- [134] J. O. Choi and D. B. Kim, “A new uav-based module lifting and transporting method: Advantages and challenges,” in *Proceedings of the 36th International Symposium on Automation and Robotics in Construction (ISARC)* (M. Al-Hussein, ed.), (Banff, Canada), pp. 645–650, International Association for Automation and Robotics in Construction (IAARC), May 2019.
- [135] N. Kamimura and S. Nakamura, “Automatic traveling method for the self-propelled tunnel inspection system,” in *Proceedings of the 35th International Symposium on Automation and Robotics in Construction (ISARC)* (J. Teizer, ed.), (Taipei, Taiwan), pp. 194–198, International Association for Automation and Robotics in Construction (IAARC), July 2018.
- [136] T. Kita, T. Hirabayashi, A. Ueyama, H. Kinjo, N. Oshiro, and N. Kinjo, “Sea experiment on tele-operation system of underwater excavator,” in *Proceedings of the 37th International Symposium on Automation and Robotics in Construction (ISARC)* (T. K. "Osumi Hisashi", "Furuya Hiroshi", ed.), (Kitakyushu, Japan), pp. 118–125, International Association for Automation and Robotics in Construction (IAARC), October 2020.
- [137] M. Niemelä, A. Shi, S. Shirowzhan, S. Sepasgozar, and C. Liu, “3d printing architectural freeform elements: Challenges and opportunities in manufacturing for industry 4.0,” in *Proceedings of the 36th International Symposium on Automation and Robotics in Construction (ISARC)* (M. Al-Hussein, ed.), (Banff, Canada), pp. 1298–1304, International Association for Automation and Robotics in Construction (IAARC), May 2019.
- [138] P. Bosscher, R. L. Williams II, L. S. Bryson, and D. Castro-Lacouture, “Cable-suspended robotic contour crafting system,” *Automation in Construction*, vol. 17, no. 1, pp. 45–55, 2007.
- [139] G. Pritschow, M. Dalacker, J. Kurz, and J. Zeiher, “A mobile robot for on-site construction of masonry,” in *Proceedings of IEEE/RSJ International Conference on Intelligent Robots and Systems (IROS'94)*, vol. 3, pp. 1701–1707 vol.3, 1994.

- [140] K. Dörfler, T. Sandy, M. Giftthaler, F. Gramazio, M. Kohler, and J. Buchli, “Mobile robotic brickwork,” in *Robotic Fabrication in Architecture, Art and Design 2016* (D. Reinhardt, R. Saunders, and J. Burry, eds.), pp. 204–217, Cham: Springer International Publishing, 2016.
- [141] I. Vukorep, “Autonomous big-scale additive manufacturing using cable-driven robots,” in *Proceedings of the 34th International Symposium on Automation and Robotics in Construction (ISARC)* (K. C. N. T. U. o. S. Chiu and Technology), eds.), pp. 254–259, Tribun EU, s.r.o., Brno, 2017.
- [142] C. K. Karl and C. W. Ibbs, “Influence of automated building construction systems on vocational education and training,” in *Proceedings of the 35th International Symposium on Automation and Robotics in Construction (ISARC)* (J. Teizer, ed.), (Taipei, Taiwan), pp. 236–243, International Association for Automation and Robotics in Construction (IAARC), July 2018.